สังเคราะห์และวิเคราะห์เอกลักษณ์ของอะพาไทต์และวัฏภาคอื่นจากสารละลายแคลเซียม-เลด-ฟอสเฟต

นางสาวอรทัย สายสะอาด

SYNTHESIS AND CHARACTERIZATION OF APATITE AND OTHER PHASES FROM CALCIUM-LEAD-PHOSPHATE SOLUTIONS
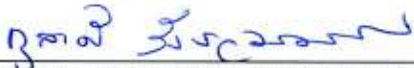
Oratai Saisa-ard

A Thesis Submitted in Partial Fulfillment of the Requirements for the

Degree of Doctor of Philosophy in Chemistry

Suranaree University of Technology

Academic Year 2011

SYNTHESIS AND CHARACTERIZATION OF APATITE AND OTHER PHASES FROM CALCIUM-LEAD-PHOSPHATE SOLUTIONS

Suranaree University of Technology has approved this thesis submitted in partial fulfillment of the requirements for the Degree of Doctor of Philosophy.

Thesis Examining Committee

_____

(Asst. Prof. Dr. Kunwadee Rangsriwatananon)
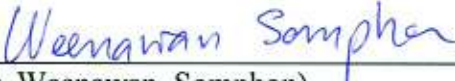
Chairperson

_____

(Assoc. Prof. Dr. Kenneth J. Haller)

Member (Thesis Advisor)

_____

(Prof. Dr. Adrian E. Flood)

Member

_____

(Asst. Prof. Dr. Sutham Srilomsak)

Member

_____

(Dr. Weenawan Somphon)

Member

_____   _____

(Prof. Dr. Sukit Limpijumnong)   (Assoc. Prof. Dr. Prapun Manyum)

Vice Rector for Academic Affairs   Dean of Institute of Science

อรทัย สายสะอาด : สังเคราะห์และวิเคราะห์เอกลักษณ์ของอะพาไทต์และวัฏภาคอื่นจาก สารละลายแคลเซียม-เลด-ฟอสเฟต (SYNTHESIS AND CHARACTERIZATION OF APATITE AND OTHER PHASES FROM CALCIUM-LEAD-PHOSPHATE SOLUTIONS) อาจารย์ที่ปรึกษา : รองศาสตราจารย์ ดร.เค็นเนท เจ. แฮลเลอร์, 130 หน้า.

งานวิจัยนี้ศึกษาอะพาไทต์และสารที่เกี่ยวข้องประกอบด้วยแคลเซียมไฮดรอกซีอะพาไทต์ (CaHAp) เลดไฮดรอกซีอะพาไทต์ (PbHAp) และสารแคลเซียม-ฟอสเฟต สารเลด-ฟอสเฟตอื่น และ สารแคลเซียม-เลด-ฟอสเฟต ผลจากการวิเคราะห์โครงสร้างของ PbHAp (โครงสร้างที่ตีพิมพ์แล้ว จากข้อมูลที่ได้จาก powder X-ray diffraction) พบว่ามีความคลาดเคลื่อนของค่าผลรวม bond valence จากค่าที่น่าจะเป็นของอะตอม P Pb(2) และ O(4) ในโครงสร้างของ PbHAp ซึ่งค่าของ ผลรวม bond valence ในโครงสร้างที่ตีพิมพ์แล้วดีขึ้นหลังจากการปรับอะตอม O(3) และ O(4) แต่ ค่าที่ได้ยังไม่ดีที่สุด จากผลที่ได้นี้สามารถชี้ได้ว่าแบบโครงสร้างของ PbHAp ที่ตีพิมพ์แล้วนี้อาจจะมี ความผิดพลาด

วิธีการตกผลึกด้วยเจล และวิธีรีฟลักซ์ ถูกใช้เพื่อเตรียม PbHAp ให้มีผลึกที่ใหญ่ขึ้น สาร ผลิตภัณฑ์ที่ได้จากวิธีการตกผลึกด้วยเจลระบุได้ว่ามีวัฏภาคของ PbHPO$_4$ Pb$_3$(PO$_4$)$_2$ และ PbHAp ซึ่ง งานนี้เป็นงานแรกที่สามารถเตรียม PbHAp การปรับปรุงการทดลองโดยเพิ่มชั้นของเจลบริสุทธิ์ อาจจะเป็นปัจจัยสำคัญที่ทำให้ได้ PbHAp ผลของ XRD SEM และโปรแกรม PHREEQC แสดงให้ เห็นว่ามีสารผลิตภัณฑ์หลายชนิดในระบบนี้ การปรากฏ PbHAp ในชั้นของเจลบริสุทธิ์แต่ไม่พบใน ชั้นของเจลฟอสเฟตอาจจะเนื่องมาจากการเกิด PbHAp ต้องการอัตราส่วนของ Pb^{2+}:PO$_4^{3-}$ สูงกว่า การเกิด Pb$_3$(PO$_4$)$_2$ (5:3 ต่อ 3:2) และผลจากการเพิ่มขึ้นของจำนวนไอออน PO$_4^{3-}$ ใกล้ๆ กับชั้นของ สารละลายเลดหลังจากการเพิ่มสารละลายเจลบริสุทธิ์ลงบนชั้นของเจลฟอสเฟต ค่า pH ของระบบนี้ ลดลงเนื่องมาจากการปรับสมดุลของไอออนเพื่อเปลี่ยน HPO$_4^{2-}$ ไปเป็น H$^+$ และ PO$_4^{3-}$ เมื่อเกิดการ ตกตะกอนของสารที่มี PO$_4^{3-}$ เป็นองค์ประกอบ

วิธีรีฟลักซ์ ถูกนำมาใช้เพื่อเพิ่มอัตราการละลายของ CaHAp และอัตราการตกผลึกของ PbHAp ในระบบ ซึ่งผลที่ได้แสดงให้เห็นว่าขนาดผลึกของสารผลิตภัณฑ์เพิ่มขึ้นเมื่อเพิ่มระยะเวลา การทำปฏิกิริยา ผลึกขนาดใหญ่ที่สุดที่เตรียมได้มีขนาดใหญ่กว่าผลึกที่ได้จากงานตีพิมพ์อื่นซึ่งมี วิธีการเตรียมใกล้เคียงกัน (วิธีการเขย่าเชิงกล) และมีขนาดใหญ่กว่าผลึกที่ได้จากวิธีการตกผลึกด้วย เจล ผลของ XRD และ EDX ยืนยันได้ว่าสารผลิตภัณฑ์ที่เป็นของแข็งนี้คือ สารอะพาไทต์และแสดง ถึงการผสมกันของวัฏภาค CaHAp และ PbHAp เนื่องจากความลำบากในการแยกสารผลิตภัณฑ์ PbHAp จากสารตั้งต้น

สารละลายของแข็งแคลเซียม-เลดไฮครอกซีอะพาไทต์ (Ca-PbHAp) ได้ถูกเตรียมขึ้นจากวิธีการตกตะกอนและผลของ XRD ชี้ให้เห็นว่ามี วัฏภาคของ CaHAp และ PbHAp เกิดขึ้น แต่ Ca-PbHAp ไม่เกิดในระบบนี้ ผลที่ได้นี้สอดคล้องกับการที่ไม่ปรากฏพฤติกรรมของสารละลายของแข็งตามกฎของ Vegard ผลจากการคำนวณโดยโปรแกรม PHREEQC ชี้ให้เห็นว่ามีวัฏภาคหลายชนิดของ แคลเซียม-ฟอสเฟต และ เลด-ฟอสเฟต อิ่มตัวยิ่งยวดในระบบ ซึ่งแสดงว่ามีสารผลิตภัณฑ์หลายตัวสามารถเกิดได้ในระบบนี้ อย่างไรก็ตาม สารเหล่านี้ไม่สามารถแสดงพีคที่ชัดเจนได้ใน XRD เนื่องจากเป็นสารผลิตภัณฑ์ส่วนน้อย

สาขาวิชาเคมี   ลายมือชื่อนักศึกษา_____

ปีการศึกษา 2554   ลายมือชื่ออาจารย์ที่ปรึกษา_____

ORATAI SAISA-ARD : SYNTHESIS AND CHARACTERIZATION OF
APATITE AND OTHER PHASES FROM CALCIUM-LEAD-PHOSPHATE
SOLUTIONS. THESIS ADVISOR : ASSOC. PROF. KENNETH J. HALLER,
Ph.D. 130 PP.

CALCIUM-PHOSPHATE/LEAD-PHOSPHATE/CALCIUM-LEAD-PHOSPHATE/
CALCIUM HYDROXYAPATITE/LEAD HYDROXYAPATITE/APATITE

Apatite and related materials including calcium hydroxyapatite (CaHAp), lead hydroxyapatite (PbHAp), and other calcium-phosphate, lead-phosphate, and calcium-lead-phosphate materials were studied in this work. Results from the structural analysis of PbHAp (published structure based on powder X-ray diffraction data) demonstrate discrepancy in the expected bond valence sum values of P, Pb(2), and O(4) atoms in the PbHAp structure. Modification of the O(3) and O(4) positions improve the bond valence sums of the published structure but they are still not optimal. These results suggest that there is probable error in the published PbHAp structure model.

Gel crystallization and reflux methods were utilized for preparation of larger PbHAp crystals. $PbHPO_4$, $Pb_3(PO_4)_2$, and PbHAp phases are identified in the gel crystallization product. The presence of PbHAp from this method is first reported in this work. The experimental modification of adding a pure gel layer may be an important factor for obtaining PbHAp material. XRD, SEM, and PHREEQC results show multiple product phases in the system, but the presence of PbHAp in the pure gel layer and not in the PO_4^{3-} gel layer may be attributed to the higher Pb^{2+}:PO_4^{3}

ratio (5:3 vs 3:2) required for the PbHAp phase relative to the $Pb_3(PO_4)_2$ phase and the increment of PO_4^{3-} ion concentrations near the lead solution after placing the pure gel solution on the PO_4^{3-} gel layer. The pH of the system decreases as crystallization occurs due to the speciation equilibrium converting HPO_4^{2-} to H^+ and PO_4^{3-} as PO_4^{3-} containing species precipitate.

Reflux method was used to increase CaHAp dissolution rate and consequently PbHAp crystallization rate in the system and results show product crystal size increased with increasing reaction time. The largest crystal size from this work is larger than has been reported in previous work with similar methodology. XRD and EDX results confirm solid products are apatite materials and show mixed phases of CaHAp and PbHAp due to the difficulty in separation of the PbHAp product from the reaction substrate. Larger PbHAp crystals were obtained from the reflux method than from the gel crystallization method.

Calcium-lead hydroxyapatite solid solution (Ca-PbHAp) materials were prepared by a precipitation method. XRD results suggest the CaHAp and PbHAp phases are formed but Ca-PbHAp is not formed in this system. These results are consistent with the absence of Vegard's law behavior. PHREEQC calculations show several calcium-phosphate and lead-phosphate phases are supersaturated, suggesting multiple products can be formed in this system. However, these phases do not appear clearly in the XRD pattern because they are minor products.

School of Chemistry

Academic Year 2011

Student's Signature _____

Advisor's Signature _____

ACKNOWLEDGEMENTS

Finally, I would like to express my thankfulness to my parents, my brother, and my sister for every support throughout the long time of my study, and without whose love and understanding this work would not have been possible.

Oratai Saisa-ard

CONTENTS

CONTENTS (Continued)

CONTENTS (Continued)

CONTENTS (Continued)

CONTENTS (Continued)

CONTENTS (Continued)

LIST OF TABLES

LIST OF TABLES (Continued)

LIST OF FIGURES

LIST OF FIGURES (Continued)

LIST OF FIGURES (Continued)

LIST OF ABBREVIATIONS

%	percentage
% w/v	percentage weight by volume
α	interaxial (lattice) angle between **b** and **c**
β	interaxial (lattice) angle between **c** and **a**
γ	interaxial (lattice) angle between **a** and **b**
γ^+	activity coefficients of cations
γ^-	activity coefficients of anions
ΔG	Gibbs free energy
λ	wavelength
μg	microgram
μm	micrometer
μmol	micromole
θ	Bragg angle or diffraction angle
υ_1	symmetric stretching
υ_2	bending
υ_3	asymmetric stretching
υ_4	bending
°	degree
°C	degree celsius
$\angle_{A-B-C}$	interatomic angles
Å	angstrom

LIST OF ABBREVIATIONS (Continued)

a	**a** basis vector of the direct lattice
a	The lengths of the **a** basis vector
aq	aqueous
AR	analytical reagent
ATSDR	Agency for Toxic Substances and Disease Registry
a.u.	atomic unit
b	broad (IR analysis)
b	**b** basis vector of the direct lattice
b	constant used in bond valence calculations
	The lengths of the **b** basis vector
c	**c** basis vector of the direct lattice
c	The lengths of the **c** basis vector
Ca-CdHAp	calcium-cadmium hydroxyapatite solid solution
CaHAp	calcium hydroxyapatite
Ca-PbHAp	calcium-lead hydroxyapatite solid solution
Ca-SrHAp	calcium-strontium hydroxyapatite solid solution
CDC	Centers for Disease Control and Prevention
cif	crystallographic information file
cm^{-1}	wavenumber (per centimeter)
d	the perpendicular spacing of the lattice planes
D	density
d_{A-B}	interatomic distance between atoms A and B

LIST OF ABBREVIATIONS (Continued)

DI   deionized water

dL   deciliter

EBLL   elevated blood-lead level

EDX   Energy dispersive X-ray fluorescence

EPA   Environmental Protection Agency

FTIR   Fourier transform infrared

g   gram

h   hour

IAP   ion activity product

ICDD   International Center for Diffraction Data

ICSD   Inorganic Crystal Structure Database

JCPDS   Joint Committee on Powder Diffraction Standards

K_a acid dissociation constants

K_{eq} equilibrium constant

K_{sp} solubility product constants

kV   kilovolt

L   liter

M   molar

m   medium

m^3 cubic meter

mA   milliampere

mg   milligram

min   minute

LIST OF ABBREVIATIONS (Continued)

mL	milliliter
mm	millimeter
mmol	millimolar
n	the order of diffraction of X-rays
NIOSH	National Institute for Occupational Safety and Health
nm	nanometer
OSHA	Occupational Safety and Health Administration
PbHAp	lead hydroxyapatite
Pb-SrHAp	lead-strontium hydroxyapatite solid solution
R	ideal gas constant
	discrepancy index
R_o	constant used in bond valence calculations
R_{ij}	observed bond length between atoms i and j
s	strong (IR analysis)
s	solid
SEM	Scanning electron microscopy
sh	shoulder (IR analysis)
SI	Saturation index
s_{ij}	partial bond valence between atoms i and j
T	temperature
T_d	tetrahedral
TEM	Transmission electron microscope
U.S.	United State of America

LIST OF ABBREVIATIONS (Continued)

v	very (IR analysis)
V	cell volume of the direct lattice
v.u.	valence unit
w	weak (IR analysis)
WDX	wavelength dispersive X-ray fluorescence
WHO	World Health Organization
wt %	weight percentage
x	Fractional x coordinate
X	Cartesian X coordinate
XRD	X-ray diffraction
y	Fractional y coordinate
Y	Cartesian Y coordinate
z	Fractional z coordinate
Z	Cartesian Z coordinate
	number of formula units in one unit cell
Z_j	bond valence sum for a given atom or ion

CHAPTER I

INTRODUCTION

1.1 Lead

Lead is a toxic heavy metal which can be released into the environment and contaminate the human food chain. The U.S. Centers for Disease Control and Prevention (CDC) currently designates a blood-lead level of 10 µg/dL (0.48 µmol/L) or higher as abnormal and requiring follow-up and intervention (Centers for Disease Control and Prevention, 2012). Blood-lead levels lower than 10 µg/dL can also affect cognitive development (Needleman, Schell, Bellinger, Leviton, and Allred, 1990). The Ministry of Public Health of Thailand designated the standard blood-lead level of 40 µg/dL (Ministry of Public Health of Thailand, 2001).

Lead source

In the past lead was used in several industries such as paint, gasoline, pipe, and solder. Because lead is responsible for potential health problems, the amount of lead used in paint, gasoline, pipe, and solder has been reduced in recent years. However, lead is still used in many industries, including construction, mining, burning fossil fuels, and manufacturing. Lead is often used to make batteries and other metal products and also used in the production of pottery and ceramics.

The source of lead exposure is ingestion of contaminated food and drinking water. Sources of lead contaminated drinking water are untreated natural drinking water from ground water or surface water and drinking water from lead-soldered

joints or leaded pipes in water distribution systems or individual houses. Lead may also enter foods if they are put into improperly glazed pottery or ceramic dishes.

Another potential source of exposure is occupation. Potentially high levels of lead may occur in the following industries: lead smelting and refining industries, battery manufacturing plants, steel welding or cutting operations, construction, rubber products and plastics industries, printing industry, firing ranges, radiator repair shops, and other industries requiring flame soldering of lead solder.

In the U.S. the standard for airborne lead in the workplace is set at less than 100 $\mu g/m^3$ by the National Institute for Occupational Safety and Health, NIOSH (2003). In Thailand the standard for airborne lead in the workplace set by the Ministry of Interior of Thailand (Ministry of Interior of Thailand, 1972) is 200 $\mu g/m^3$ which is higher than the U.S.

The lead levels in normal human and environmental samples in the U.S. and Thailand are listed in Tables 1.1 and 1.2, respectively.

Table 1.1 Lead standards for biological systems and the environment in the U.S.

Occurrence	Lead level	Reference
Lead in biological system		
- Blood (μg/dL)	10	Centers for Disease Control and Prevention, 2012
Lead in environment		
- Airborne (μg/m^3)	< 100	National Institute for Occupational Safety and Health, 2003
	50	Occupational Safety and Health Administration, 2011
- Air (μg/m^3)	1.5	Environmental Protection Agency, 2006
- Drinking water (μg/dL)	1.5	Environmental Protection Agency, 1991
- Ground water (μg/dL)	0.5-3	Agency for Toxic Substances and Disease Registry, 2007
- Soil (μg/g)	10-30	Agency for Toxic Substances and Disease Registry, 2007

Table 1.2 Lead standards for biological systems and the environment in Thailand.

Occurrence	Lead level	Reference
Lead in biological system		
- Blood (µg/dL)	40	Ministry of Public Health of Thailand, 2001
Lead in environment		
- Air borne (µg/m³)	< 200	Ministry of Interior of Thailand, 1972
- Air (µg/m³)	≤ 1.5	National Environmental Board, 1995
- Drinking water (µg/dL)	5	Ministry of Industry of Thailand, 1968
- Soil (µg/g)	400[1] 700[2]	National Environmental Board, 1992a
- Surface water (µg/dL)	5	National Environmental Board, 1992b

[1]Soil quality standard for habitat and agriculture

[2]Soil quality standard for other purpose

Health effects of lead exposure

Humans are at risk of being exposed to lead, by breathing it in, ingesting it, or coming in contact with it. Lead accumulated by humans over time is deposited in bone, a long term storage site for lead, with a half-life of about 20 years (Rabinowitz, Wetherill, and Kopple, 1976). Lead can affect almost every organ and system in the human body, especially the nervous system, of both adults and children. Lead may causes weakness in fingers, wrists, and ankles. It also may cause small increases in blood pressure, particularly in middle-aged and older people and decreased heme biosynthesis, elevated hearing threshold, and depressed serum levels of vitamin D (Warniment, 2010). Exposure to high lead levels can damage the brain and kidneys and ultimately cause death as reported by the Agency for Toxic Substances and Disease Registry, ASTDR (2007). Long-term exposure to lead decreased performance in some tests. High bone-lead levels indicate long-term exposure and are related to bone diseases like osteoporosis. There are several reports on the effects of lead on bone formation such as reduction of bone formation activity in dogs with blood-lead levels between 50 and 80 µg/dL (Anderson and Danylchuk, 1977), in rabbits with high dose lead exposure (Hass, Landerholm, and Hemmens, 1967), and in Egyptian vultures with bone-lead levels more than 20 µg/g (Gangoso et al., 2009). Blood-lead and bone-lead concentrations corresponding to human health effects are summarized in Table 1.3 (Agency for Toxic Substances and Disease Registry, 2007).

Table 1.3 Blood-lead and bone-lead concentrations corresponding to human health effects.

Age	Effect	Blood-lead levels (µg/dL)	Bone-lead levels (g/g)
Children	Depressed ALAD	< 5[1]	ND
Children	Neurodevelopmental effects	< 10[1]	ND
Children	Sexual maturaion	< 10[1]	ND
Children	Depressed vitamin D	> 15	ND
Children	Elevated EP	> 15	ND
Children	Depressed NCV	> 30	ND
Children	Depressed hemoglobin	> 40	ND
Children	Colic	> 60	ND
Adults (elderly)	Neurobehavioral effects	> 4	> 30
Adults	Depressed ALAD	< 5[1]	ND
Adults	Depressed GFR	< 10[1]	> 10
Adults	Elevated blood pressure	< 10[1]	> 10
Adults	Elevated EP (females)	> 20	ND
Adults	Enzymuria/proteinuria	> 30	ND
Adults	Peripheral neuropathy	> 40	ND
Adults	Neurobehavioral effects	> 40	ND
Adults	Altered thyroid hormone	> 40	ND
Adults	Reduced fertility	> 40	ND
Adults	Depressed hemoglobin	> 50	ND

ALAD = δ-aminolevulinic acid dehydrate; EP = erythrocyte protoporphyrin; GFR = glomerular filtration rate; NCV = nerve conduction velocity; ND = no data

[1]Some subjects can be affected at this level. An absolutely safe level is not known.

Lead poisoning in Thailand

The World Health Organization (WHO) has reported lead contamination of resources in Thailand (World Health Organization, 2008). Sources of lead contamination are generated from human activities such as mining and industry, and

may contribute to ingested lead in normal human life activities such as drinking tap water. Industries release lead waste contamination to the environment from industrial production processes, such as metal mixture, bullet, and X-ray protection building (World Health Organization, 2008). Lead waste from industries may contaminate the environment and food chain resulting in lead exposure in human.

Lead contamination of surface water in Thailand is found in mining and industrial areas such as Bannang Sata district in Yala province, Pattani River in Pattani province, and Thong Pha Phum district in Kanchanaburi province. The largest manmade contamination is from lead mining in Thong Pha Phum district, Sangkla Buri district, and Si Sawat district in Kanchanaburi province. Klity steam is a large steam in Kanchanaburi province which is near the lead mining in Thong Pha Phum district, Sangkla Buri district, and Si Sawat district (World Health Organization, 2008).

In 1998 people are in trouble with the consumption of water taken from Klity stream. The pollution control department has been monitoring lead contamination of the 8-kilometer-long Klity steam by sampling water, sediment, and aquatic animals. Results show lead contamination of surface waters are in the range of 17-40 µg/dL, much higher than the Thai standard of 5 µg/dL. Lead levels in sediments are in the range of 38.9-65.8 µg/g, 20-100 times higher than the area without mining. Lead levels in fish are ten times higher than the allowable food standard of 1 µg/g (Ministry of Public Health of Thailand, 1986). Therefore, aquatic animals, such as fish, shrimp, shell, and crab in Klity stream are not suitable for consumption (World Health Organization, 2008).

Several central and local departments of the Ministry of Public Health (Department of Health, Department of Medical Services, Division of Epidemiology, and Provincial Health Office) have set up mobile units to investigate and study the health impacts on villagers who live downstream in Klity Lang Village where the highest lead contamination levels were found. In the preliminary study the blood-lead level from 3 groups of villagers, young children (0-6 years), schoolchildren (7-15 years), and teenagers and adults ($\geq$ 16 years) were in the range of 10-44 µg/dL, 21-33 µg/dL, and 9-41 µg/dL, respectively. For young children and schoolchildren, almost all blood-lead levels were higher than the CDC standard of 10 µg/dL. In adults, there were 3 people with blood-lead levels higher than 40 µg/dL.

The U.S. CDC informs the Ministry of Public Health, Thailand that up to 13 % of Burmese refugee children who were transferred to the U.S. during 2007-2009 have elevated blood-lead levels, EBLL, (blood lead level > 10 µg/dL). Most of them lived in Umphang district, Tak province. A study on 213 3-7 year old Thai children with average age of 54.54 $\pm$ 12.41 months indicates an average blood-lead level of 7.71 $\pm$ 4.62 µg/dL (range = 3-25 µg/dL). Fifty-seven of these Thai children (26 %) had blood-lead level at 10 µg/dL or more. Analysis controlling other factors, indicates only gender and source of drinking water are risk factors. Specially, male children have 2.8 times higher risk than female children. Children who drink tap water and canal water have 15 and 72 times higher risk, respectively, than children drinking bottle water. Tap water in this area comes directly from natural waters in the mountains via pipes with no standard process performed for converting the natural water to drinking water. The results of this study show 1 of 4 Thai children in

Umphang district, Tak province who live near the Burmese refugee camps have EBLL (Neesanan *et al.*, 2011).

A study on 296 children with an average age 1.66 ± 1.39 years old in four communities, 2 in Bangkok (Klong Toei and Siriraj) and 2 in Kanchanaburi province (Thong Pha Phum and Paholpolpayuhasena) shows 8.1% of children with EBLL. The risk factors for EBLL were the presence of peeling paint inside or outside the house, eating paint chips, and the geographic location of children. Again, the results indicate that the source of drinking water is a risk factor which has an impact on EBLL (Chomchai, Padungtod, and Chomchai, 2005).

A study on 245-282 workers in a battery manufacturing plant in Bangkok, Thailand during 1998-2002 indicates the workers were exposed to lead in sections such as casting, spreading, forming, polishing, assembly, and special battery production. Workers have geometric average of blood-lead level increased from 17.9 µg/dL to 22.3 µg/dL during 4 years but no workers had blood-lead level 60 µg/dL or more in 2002. Factors of sex, age, and duration of work were considered in this work. The results found average blood-lead level in males of 23.3 µg/dL and in females of 12.6 µg/dL. However, age and duration of work did not have significant effect on the average blood-lead level of workers. The correlation between blood-lead level and airborne lead level was also studied. High airborne lead level was detected in all sections, especially, in the forming and polishing sections. These sections had airborne lead levels higher than the standard level set by the Ministry of Interior of Thailand (200 µg/m^3). However, this study did not find airborne lead level to have a significant effect on average blood-lead level of workers (Lormphongs *et al.*, 2003).

A further study of lead poisoning on 132 workers at the assembly section in the same battery manufacturing plant in Bangkok, Thailand in 2002 shows a high average blood-lead level of 32.7 µg/dL. After occupational health education and training to workers and managers, the average blood-lead level was reduced to 22.4 µg/dL, although the airborne lead level in the workplace remained unchanged from previous values. Airborne lead level in the workplace was between 0.026-0.603 mg/m^3, eight samples (36.3 %) were more than the standard level of 200 µg/m^3 set by the Ministry of Interior of Thailand (Lormphongs *et al.*, 2004).

1.2 Apatite materials

Apatite is the name of a mineral supergroup. The chemical formula of apatite is $M(1)_2M(2)_3(TO_4)_3X$. M(1) and M(2) are monovalent, divalent, and trivalent cations, such as Na^+, K^+, Ca^{2+}, Sr^{2+}, Ba^{2+}, Cd^{2+}, Pb^{2+}, Al^{3+}, Bi^{3+}, Y^{3+}, or La^{3+}; TO_4 is a divalent, trivalent, or tetravalent anion, such as SO_4^{2-}, PO_4^{3-}, VO_4^{3-}, AsO_4^{3-}, or SiO_4^{4-}; and X is a monovalent anion, such as OH^-, F^-, or Cl^-. Other anions, including CO_3^{2-} and NO_3^- may also occur in the TO_4 sites.

Classes of apatite materials

The apatite supergroup can be divided into five groups, based on crystal-chemical arguments (Pasero *et al.*, 2010);

Apatite group: hexagonal and pseudo-hexagonal phosphates, arsenates, and vanadates containing the same cation at both the M(1) and M(2) sites, such as $Ca_5(PO_4)_3(OH)$, $Ca_5(PO_4)_3F$, $Pb_5(PO_4)_3Cl$, $Ba_5(PO_4)_3Cl$, or $Pb_5(PO_4)_3(OH)$.

Hedyphane group: hexagonal and pseudo-hexagonal phosphates, arsenates, and sulfates containing different cations at the M(1) and M(2) sites, such as $Ca_2Pb_3(AsO_4)_3Cl$, $Ca_2Pb_3(AsO_4)_3OH$, $Ca_2Sr_3(PO_4)_3F$, or $Mn_2Ca_3(PO_4)_3Cl$.

Belovite group: hexagonal and trigonal phosphates with the M(1) site split into M(1) and M(1') sites containing different cations, such as $SrCaCa_3(PO_4)_3F$, $NaCeSr_3(PO_4)_3F$, or $NaCeBa_3(PO_4)_3F_{0.5}Cl_{0.5}$.

Britholite group: hexagonal and pseudo-hexagonal silicates, typically with partially ordered M(1) and M(2) cations, such as $(Ce,Ca)_5(SiO_4)_3(OH)$, $(Y,Ca)_5(SiO_4)_3(OH)$, or $(Y,Ca)_5(SiO_4)_3F$.

Ellestadite group: hexagonal and pseudo-hexagonal sulfato-silicates with the ideal ratio for charge balance of $(SiO_4)^{4-}:(SO_4)^{2-}$ 1:1, such as $Ca_5(SiO_4)_{1.5}(SO_4)_{1.5}(OH)$, $Pb_5(SiO_4)_{1.5}(SO_4)_{1.5}Cl$, or $Pb_5(SiO_4)_{1.5}(SO_4)_{1.5}(OH)$.

Characteristics of apatite materials

One interesting characteristic of apatites is their susceptibility to ionic substitution in both anionic and cationic sites. Divalent cations with ionic radii about 1 Å can form apatites such as Ca^{2+}, Ba^{2+}, Cd^{2+}, and Pb^{2+}, with free ionic radii 0.99, 1.13, 0.97, and 1.35 Å, respectively (Narasaraju and Phebe, 1996). It should be noted that the ionic radii in bound states is larger than the free ion radii and depends on the coordination number of the ion. For example, with coordination number 7, Ca^{2+} = 1.20 Å and Pb^{2+} = 1.37 Å, and with coordination number 9, Ca^{2+} = 1.32 Å and Pb^{2+} = 1.49 Å (Bruckner, Lusvardi, Menabue, and Saladini, 1995). Among the anionic substituents, the monovalent anions (OH^-) can be replaced by F^-, Cl^-, and a variety of other monovalent anions, while trivalent anions (PO_4^{3-}) can be replaced by AsO_4^{3-}

and VO_4^{3-}, the anionic radii of these being 1.68, 1.32, and 1.81, and 1.10, 1.18, and 1.22 Å, respectively (Narasaraju and Phebe, 1996). All structures within the apatite group are isostructural. However, there are two series within the group, the apatite series and the pyromorphite series. Pyromorphite is lead chlorophosphate, $Pb_5(PO_4)_3Cl$, and the principal cation in the pyromorphite series is lead. Examples of apatites and pyromorphites, their empirical formula, and their lattice constants are given in Table 1.4.

Table 1.4 Name, formula, and lattice constants of selected apatites.

Series	Name	Empirical formula	Lattice constants (Å)	
			a	c
Apatite	Barium hydroxyapatite	$Ba_5(PO_4)_3(OH)$	10.19	7.70
	Cadmium arsenic chloroapatite	$Cd_5(AsO_4)_3Cl$	10.07	7.26
	Cadmium hydroxyapatite	$Cd_5(PO_4)_3(OH)$	9.01	6.61
	Cadmium chloroapatite	$Cd_5(PO_4)_3Cl$	9.62	6.49
	Calcium hydroxyapatite	$Ca_5(PO_4)_3(OH)$	9.42	6.88
	Chlorapatite	$Ca_5(PO_4)_3Cl$	9.63	6.78
	Fermorite	$Ca_5(AsO_4)_6F$	9.75	6.92
	Fluorapatite	$Ca_5(PO_4)_3F$	9.35	6.58
	Hydroxyvanadinite	$Ca_5(VO_4)_3(OH)$	9.82	6.98
	Lead hydroxyapatite	$Pb_5(PO_4)_3(OH)$	9.90	7.29
	Magnesium hydroxyapatite	$Mg_5(PO_4)_3(OH)$	9.30	6.89
	Strontium hydroxyapatite	$Sr_5(PO_4)_3(OH)$	9.76	7.28
Pyromorphite	Pyromorphite	$Pb_5(PO_4)_3Cl$	9.95	7.32
	Vanadinite	$Pb_5(VO_4)_3Cl$	10.47	7.43
	Mimetite	$Pb_5(AsO_4)_3Cl$	10.36	7.52

A distinguishing characteristic of the two series is that, while members within one series can readily form solid solutions with other members of the same series,

they in general do not easily form solid solutions with members of the other series
(Berry and Mason, 1959).

Structural aspects of apatites

Apatite structures belong to space group $P6_3/m$ with the general formula
$M(1)_2M(2)_3(TO_4)_3X$. Figure 1.1 shows a representation of the symmetry properties of
space group $P6_3/m$. The Wycoff special positions[1] relevant to apatite structure are
indicated on the diagram. The f positions are on 3-fold rotation axes at 1/3, 2/3, z and
2/3, 1/3, z and the h positions are on mirror planes at $z = 1/4$ and $z = 3/4$.
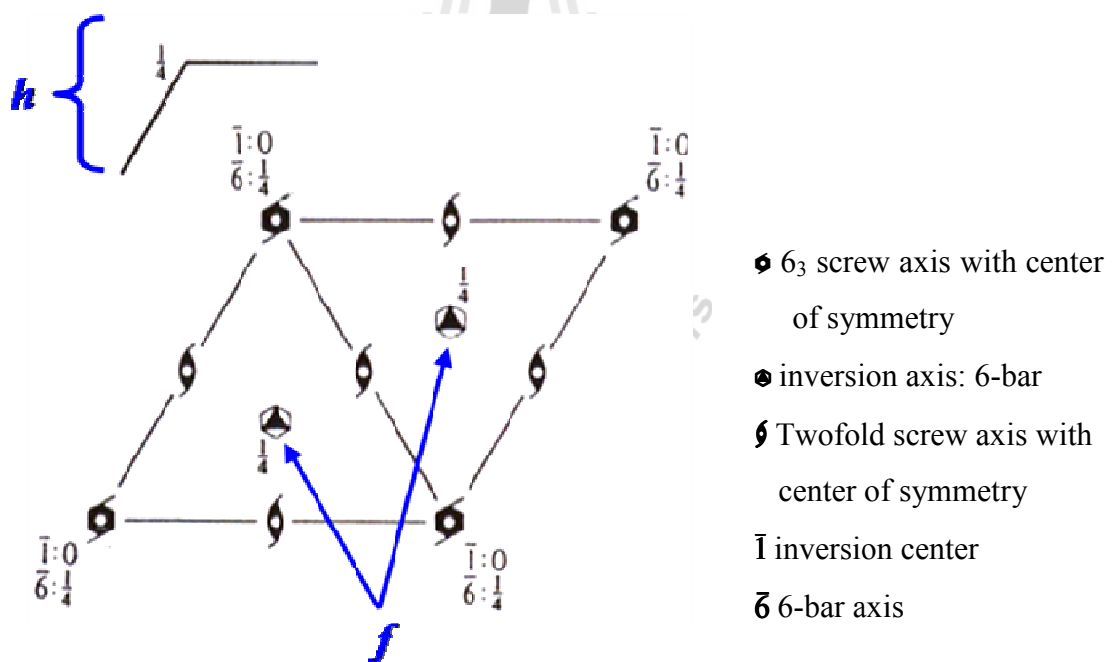
Figure 1.1 Representation of the symmetry properties of space group $P6_3/m$ projected
on the *ab* plane. Wycoff positions, f and h, relevant to apatite structure are
indicated on the diagram (Hahn, 1996).

---

[1] Wycoff positions are represented by letters, starting with a for the most symmetric special position in
the space group under consideration, and continuing in alphabetical order until the general position is
reached.

The CaHAp structure (Figure 1.2) consists of five Ca^{2+} ions, three PO_4^{3-} ions, and one OH^- ion. Two Ca^{2+} ions in the M(1) positions are located on f sites with 3 symmetry. Three Ca^{2+} ions in the M(2) positions, three P atoms, and six phosphate O atoms are located on h sites with m symmetry. The other six phosphate O atoms are located on general positions, pairwise related by the mirror plane through the P atoms. The hydroxyl O is disordered along the 3 axis near the 6-bar site with the hydrogen atom further disordered about the 3 axis.
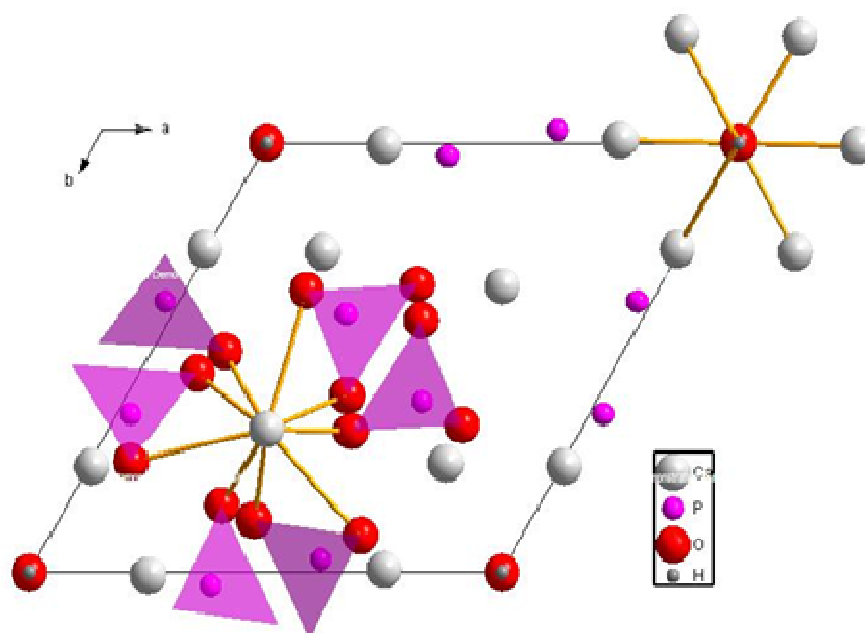
Figure 1.2 Representation of Ca, O, and P atoms in apatite structures projected on the *ab* plane. The polyhedra represent phosphate groups in the structure.

The Ca^{2+} ions at the f sites are coordinated with nine O atoms (six shorter bonds define a twisted trigonal prism and the three longer bonds extend through the prism faces). The Ca^{2+} ions at the h sites are coordinated with seven O atoms; six O atoms from PO_4^{3-} groups and one O atom from the OH^- group. The PO_4^{3-} groups project as

pairs of triangles about the 2_1 axes in Figure 1.2. The OH$^-$ ions are disordered along the 3 axis. The coordination environments of the distinct f and h Ca^{2+} sites are different, consequently the ionic size of Ca^{2+} in these two positions are different. Thus, the ability to substitute other cations for Ca^{2+} at the two positions should also be different.

Applications of apatite materials

Apatites have been studied in several applications including as material for removal and immobilization of heavy metals from contaminated water (Admassu and Breese, 1999; Smičiklas, Onjia, Raičević, Janacković, and Mitrić, 2008), as support material for catalyst reactions (Mori *et al.*, 2002; Mori, Hara, Mizugaki, Ebitani, and Kaneda, 2003), and as biomaterial for artificial bones and teeth (Walsh and Tanaka, 2001).

1.3 Calcium-phosphate in mammalian hard tissues

Mammalian hard tissues such as teeth and bones are composed primarily of calcium-phosphates (Ca-P), including calcium hydroxyapatite (CaHAp) and other calcium-phosphate materials such as calcium hydrogen phosphate dihydrate (CHPD), calcium hydrogen phosphate (CHP), octacalcium phosphate (OCP), and calcium phosphate (CP). Natural teeth consist of three parts; enamel, dentine, and cementum with weight percents of CaHAp of 95, 75, and 35, respectively (Narasaraju and Phebe, 1996). There are two main parts of bone; inorganic (69 wt %) and organic (20 wt %) parts (Shi, 2005). The inorganic part contains calcium-phosphate, magnesium,

sodium, potassium, fluoride, and chloride while the organic part contains primarily matrix proteins (mostly collagen) and noncollagenous proteins (*i.e.* proteoglycans).

Bone also contains water (10 wt %) and other components such as polysaccharides and lipids in small quantities as shown in Figure 1.3.

Inorganic fraction 69 wt %
(Ca-P, Mg, Na, K, F, Cl)

Organic fraction 20 wt %
(matrix and
noncollagenous proteins)

Water 10 wt %

Other 1 wt %
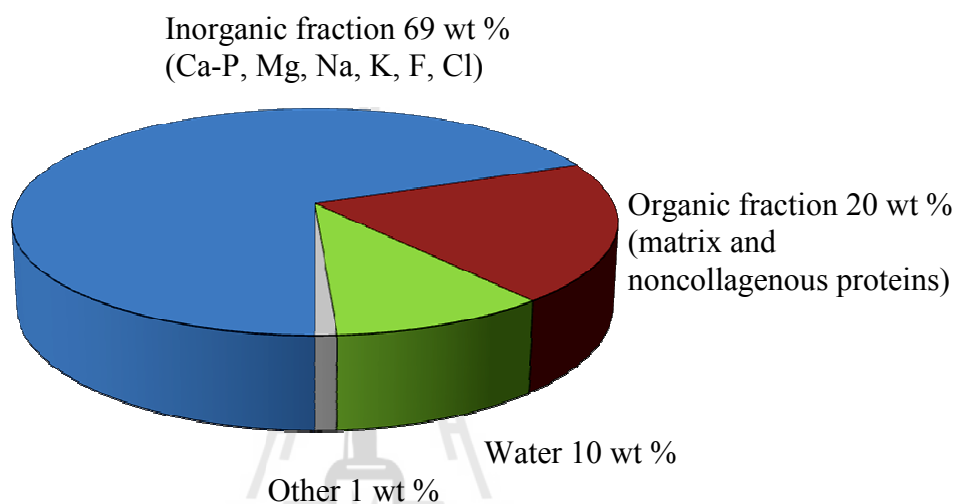
Figure 1.3 Composition of bone (LeGeros, 1991).

Calcium hydroxyapatite

Pure calcium hydroxyapatite ($Ca_5(PO_4)_3(OH)$) does not occur in biological systems and biological apatites have been described as calcium-deficient or nonstochiometric, carbonate apatites, fluorapatite, fluorhydroxyapatite, chlorapatite, and chlorhydroxyapatite.

Calcium-deficient apatites, such as $Ca_{5-x}Na_{2x}(PO_4)_3(OH)$, are apatites with less than five calcium ions to three phosphates.

Carbonate apatites are apatites which contain carbonate ions in the structure. They are classified into A-type and B-type carbonate apatites depending on the substitution site. Substitution of hydroxide ions gives A-type carbonate apatites while

substitution of phosphate ions gives B-type carbonate apatites. Carbonate apatites occur in bone, enamel, and dentin at about 7.4, 5.6, and 3.5 wt %, respectively, and are mostly B-type carbonate apatites with different amounts of carbonate incorporated into the lattice.

Chlorhydroxyapatite, and fluorhydroxyapatite are apatites with hydroxide ions substituted by chloride or fluoride ions, respectively. Total substitution results in chlorapatite or fluorapatite. Chloride and fluoride ions occur in biological hard tissues such as bone (0.13 wt % and 0.03 wt %), enamel (0.30 wt % and 0.01 wt %), and dentin (0.01 wt % and 0.06 wt %).

Amorphous calcium phosphate

Amorphous calcium phosphate ($Ca_3(PO_4)_2$) containing magnesium (Mg^{2+}), carbonate (CO_3^{2-}), or pyrophosphate ($P_2O_7^{4-}$) ions has been reported to occur in pathological calcifications.

Calcium hydrogen phosphate

Anhydrous calcium hydrogen phosphate ($CaHPO_4$) and calcium hydrogen phosphate dihydrate ($CaHPO_4 \cdot 2H_2O$) occur in biological systems. $CaHPO_4$ is speculated to form in carious lesions in the enamel while $CaHPO_4 \cdot 2H_2O$ occurs in pathological calcifications. It is also proposed as a precursor of calcium hydroxyapatite.

Octacalcium phosphate pentahydrate

Octacalcium phosphate pentahydrate ($2Ca_4H(PO_4)_3 \cdot 5H_2O$) occurs in pathological calcifications, and is also proposed as a precursor of calcium hydroxyapatite.

Calcium phosphate

Calcium phosphate ($Ca_3(PO_4)_2$) occurs in dental and urinary calculi, salivary stones, and arthritic cartilage.

The occurrence of calcium-phosphate materials in biological systems is summarized in Table 1.5.
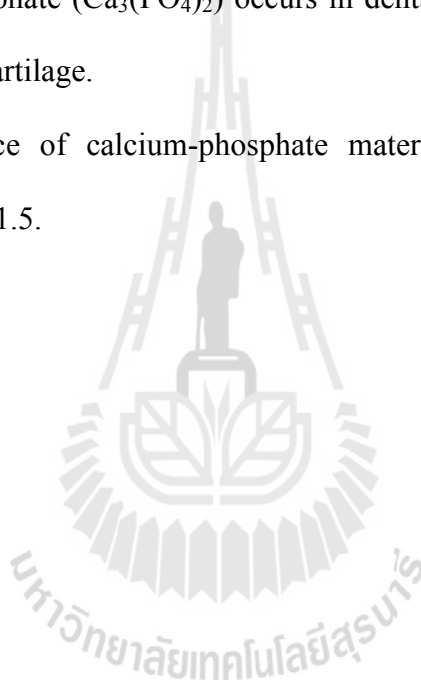
Table 1.5 Occurrence of calcium-phosphate materials in biological systems, empirical formula, and stochiometric Ca to P ratio.

Compound	Empirical formula	Ca/P	Occurrence
Calcium hydrogen phosphate dihydrate[1], CHPD	$CaHPO_4 \cdot 2H_2O$	1.0	urinary calculi, crystalluria
Calcium hydrogen phosphate[2], CHP	$CaHPO_4$	1.0	urinary calculi, crystalluria, decomposed bones
Calcium pyrophosphate dihydrate, CPPD	$Ca_2P_2O_7 \cdot 2H_2O$	1.0	psuedo-gout deposits in synovium fluids
Octacalcium phosphate pentahydrate, OCP	$2Ca_4H(PO_4)_3 \cdot 5H_2O$	1.33	dental and urinary calculi
Calcium phosphate[3], CP	$Ca_3(PO_4)_2$	1.5	dental and urinary calculi, salivary stones, arthritic cartilage
Amorphous calcium hydroxyapatite , ACaHAp	$Ca_5(PO_4)_3(OH)$	1.67	pathological calcifications
Calcium hydroxyapatite, CaHAp	$Ca_5(PO_4)_3(OH)$	1.67	enamel, dentine, bone, dental calculi, urinary calculi

[1]Also called dicalcium phosphate dehydrate (DCPD) or brushite (LeGeros, 1991)

[2]Also called dicalcium phosphate (DCP) or monetite (LeGeros, 1991)

[3]Also called Tricalcium phosphate (TCP) (LeGeros, 1991)

1.4 Solid solutions

Many minerals including apatite materials occur as solid solutions. West (1984) defines a "solid solution as solid state phenomena wherein the composition of a material varies significantly within the framework of the same overall crystal structure". When the ion exchange reaction in CaHAp is complete, another apatite

member in the apatite or pyromorphite series, depending on the ions substituted, has formed. Incomplete or partial substitution in the CaHAp structure may result in the formation of hydroxyapatite solid solution. Some examples of hydroxyapatite solid solutions are magnesium-calcium hydroxyapatite, strontium-lead hydroxyapatite, calcium phosphate fluorhydroxylapatite (Patel, 1980; Zhu, *et al.*, 2007; Rodriquez-Lorenzo, Hart, and Gross, 2003), and calcium phsosphate-arsenate hydroxyapatite (Mahapatra, Mahapatra, and Mishra, 1989).

Vegard's law is often used when characterizing homogeneous solid solution phases and other materials resulting from coprecipitation of insoluble materials. The law states that, unit cell parameters change linearly with composition as seen in Figure 1.4a.
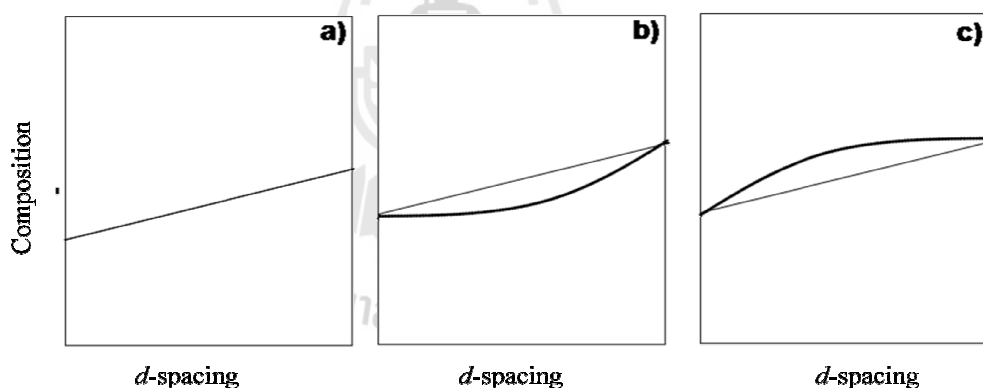
Figure 1.4 Vegard's law behavior. a) ideal solid solution, b) negative deviations, and c) positive deviations (West, 1984).

However, the law often holds approximately, and accurate measurements reveal both negative (Figure 1.4b) and positive (Figure 1.4c) deviations from linearity (West, 1984).

The potential for nonideal behavior, similar to nonideal behavior of normal solutions, suggests caution should be used when assuming a material is a solid

solution and that its properties are the weighted average of the pure component end points of the assumed solid solution.

1.5 Lead-phosphate materials

Lead-phosphate (Pb-P) materials such as lead hydroxyapatite, PbHAp, $(Pb_5(PO_4)_3(OH))$, lead hydrogen phosphate $(PbHPO_4)$, lead nitrate phosphate monohydrate $(Pb_2(NO_3)(PO_4) \cdot H_2O)$[1], and lead phosphate $(Pb_3(PO_4)_2)$ are interesting materials due to their structure and properties. PbHAp is a material of biological interest because of the similarity to CaHAp. $PbHPO_4$ and $Pb_2(NO_3)(PO_4) \cdot H_2O$ show dielectric, piezoelectric, and optical properties which are useful in transducers and memory devices. $Pb_3(PO_4)_2$ is a ferroelastic material with a phase transition near 180 °C. The phase is changed from α-phase ($C2/c$ ferroelastic phase) at below 180 °C to β-phase ($R\bar{3}m$ prototypic phase) at above 180 °C (Guimaraes, 1979; Decker, Petersen, and Debray, 1979). Growth of $PbHPO_4$ and $Pb_2(NO_3)(PO_4) \cdot H_2O$ in silica hydrogel, tetramethoxysilane gel, cross-linked polyacylamide gel, agar gel, and gelatin, all beginning from $Pb(NO_3)_2$ and H_3PO_4, but with different concentrations of reactants and gel medium, and different techniques has been reported (Březina, Havránková, and Dušek, 1976; Desai and Ramana, 1990; Vivekanandan, Selvasekarapandian, and Kolandaivel, 1995; Mayer and Woermann, 1996; Desai and Ramana, 1988; Robert and Lefaucheux, 1988). A summary of the crystallization of lead and phosphate containing materials in gel systems is given in Table 1.6.

---

[1]This formula is often reported as double formula, $Pb_4(NO_3)_2(PO_4)_2 \cdot 2H_2O$

Table 1.6 Summary of gel crystallization reports of lead hydrogen phosphate and lead nitrate phosphate dihydrate materials.

Gel medium	Technique	Products	Reference
Polyacylamide, poly(2-hydroxyl ethylacrylate), sodium metasilicate, agar, gelatin	Double diffusion	$PbHPO_4$ and $Pb_2(NO_3)(PO_4) \cdot H_2O$	Březina *et al.*, 1976
Sodium metasilicate	Single diffusion	$PbHPO_4$ and $Pb_2(NO_3)(PO_4) \cdot H_2O$	Desai *et al.*, 1988
Tetramethoxysilane	Double diffusion	$PbHPO_4$ and $Pb_2(NO_3)(PO_4) \cdot H_2O$	Robert *et al.*, 1988
Silica gel	Single diffusion	$PbHPO_4$	Desai *et al.*, 1990
Sodium metasilicate	Single diffusion	$Pb_2(NO_3)(PO_4) \cdot H_2O$	Vivekanandan *et al.*, 1995
Methoxysilane	Single diffusion	$PbHPO_4$ and $Pb_2(NO_3)(PO_4) \cdot H_2O$	Mayer *et al.*, 1996

However, the preparation of PbHAp material by gel crystallization methods or the appearance of this material in a gel system has not been reported (Březina, Havránková, and Dušek, 1976; Desai and Ramana, 1990; Vivekanandan, Selvasekarapandian, and Kolandaivel, 1995; Mayer and Woermann, 1996; Desai and Ramana, 1988; Robert and Lefaucheux, 1988).

The formula of $Pb_2(NO_3)(PO_4) \cdot H_2O$ compound in Table 1.6 was reported as a double formula ($Pb_4(NO_3)_2(PO_4)_2 \cdot 2H_2O$) in the literature. Březina, Havránková, and Dušek (1976) first reported the nonempirical $Pb_4(NO_3)_2(PO_4)_2 \cdot 2H_2O$ compound as a double formula and their work was cited by Robert and Lefaucheux (1988) and Desai and Ramana (1988). Later works of Vivekanandan, Selvasekarapandian, and

Kolandaivel (1995) and Mayer and Woermann (1996) cited the Desai and Ramana (1988) and Robert and Lefaucheux (1988) papers and propagated the error.

Conventionally nonmolecular compounds are reported as empirical formula units using subscripts that do not contain common factors. The importance of this is discussed in Appendix A (pp. 108-109). The mistake of the formula affects reported values of physical constants such as the K_{sp} value. K_{sp} is calculated using the number of atoms in the formula as exponents leading to dramatic discrepancies. Discussion of the K_{sp} value problem from the wrong formula is given in Appendix A.

1.6 Dissolution equilibria aspects

The solubility of a pure phase compound to make an aqueous solution is the maximum amount of the compound that can be dissolved in a given quantity of pure water at a given temperature. For molecular compounds and reasonably soluble ionic compounds solubility is generally expressed as g/100 mL of saturated solution.

The dissolution of an ionic compound is generally represented by a chemical equilibrium, as for example, for dissolution of barium sulfate:

$$\text{BaSO}_4(s) \rightleftharpoons \text{Ba}^{2+}(aq) + \text{SO}_4^{2-}(aq) \qquad \ldots\ldots\ldots\ldots(1.1)$$

where s indicates solid phase material, and aq indicates the species in solvated form in the aqueous solution, and the double arrow indicates the process is at chemical equilibrium. The conventional mathematical description of this equilibrium is usually in terms of K_{eq}, the equilibrium constant expression:

$$K_{eq} = [Ba^{2+}(aq)][SO_4^{2-}(aq)] / [BaSO_4(s)] \quad \text{..............(1.2)}$$

where the square brackets denote molar concentrations. If we assume the activity of the pure solid in equilibrium with the saturated solution is equal to one this expression reduces to the solubility product, K_{sp}, expression:

$$K_{sp} = [Ba^{2+}(aq)][SO_4^{2-}(aq)] \quad \text{..............(1.3)}$$

a form that is correct for ideal (infinitely dilute) solutions. In a real (nonideal) solution, the species also interact with one another, changing their effective participation (activity) in the equilibrium reaction. Empirical corrections are introduced as coefficients to the molar concentrations to account for the decreased activities as follows:

$$K_{sp} = [Ba^{2+}(aq)]\gamma^{+}[SO_4^{2-}(aq)]\gamma^{-} \quad \text{..............(1.4)}$$

where γ^{+} and γ^{-} are the activity coefficients of cations and anions, respectively.

Analytical techniques, such as fluorescence spectroscopy, atomic absorption spectroscopy, or inductively-coupled plasma mass spectrometry, give total concentrations of the elemental species in the sample being analyzed. However, for equilibrium studies, the concentrations of the individual chemical (ionic) species present in the solution are required, but may be difficult to obtain experimentally. Additionally, concentrations of the individual chemical (ionic) species are affected by any additional ions in the solution (*i.e.* NaOH and HCl from adjusting pH) due to the

interactions among the competing ionic equilibria in the system. A previous study has discussed the effect of Na^+ cation and Cl^- anion on the barium-arsenate system (Dungkaew, 2010). The results of that showed that with high Cl^- concentration (pH = 10.5), $Ba_5(AsO_4)_3Cl$ precipitates, and if the pH of system is increased to pH = 12.5 by adding more NaOH, Na^+ concentration is increased and $NaBaAsO_4 \cdot 9H_2O$ precipitates.

Hence, K_{sp} calculations based on only the molar concentrations of a single ionic compound may be seriously in error. The solution to this problem will involve the careful consideration and correct inclusion of all relevant equilibrium phenomena. The PHREEQC speciation calculation program has been used to calculate the activity coefficients of ions in the system (Dungkaew, Haller, Flood, and Scamehorn, 2012). Calculation of the K_{sp} based on molar concentrations and activity coefficients could be more correct.

1.7 Characterization background

PHREEQC program

PHREEQC is a computer program for simulating chemical reactions and transport processes based on equilibrium chemistry of aqueous solutions interacting with solids and gases. It can be used as a speciation program to calculate saturation indices and distribution of aqueous species and competing equilibria that change the concentration of the species, effects of ionic strength (Parkhurst and Appelo, 1999).

The PHREEQC calculations are based on all known equilibria existing in the database. PHREEQC is distributed with a PHREEQC default internal database, and the Minteq, MinteqV4, and Wateq4f databases. Input data for the program consists of

properties and compositions of equilibrated solutions, including pH, temperature, and total concentrations of ions in the system.

Saturation index (SI) is calculated by the PHREEQC program based on input data. SI uses calculated activities to provide a good indicator of the potential solid phases in a system at its equilibrium state. SI is defined as Eq. (1.5):

$$SI = \log\left(\frac{IAP}{K_{sp}}\right) \qquad\qquad \text{.............(1.5)}$$

where IAP is the free ionic activity product and K_{sp} is the thermodynamic solubility product constant of a pure precipitate phase. SI relates to ΔG (Stumm and Morgan, 1996) as,

$$\Delta G = -2.303RT \log\left(\frac{IAP}{K_{sp}}\right) \qquad\qquad \text{.............(1.6)}$$

where R is the ideal gas constant, and T is the temperature. From Eq. (1.6), ΔG equals zero when IAP = K_{sp} corresponding to SI = 0 and the solution is in equilibrium; ΔG is negative when IAP > K_{sp} corresponding to SI > 0; the solution is supersaturated and precipitation can occur (unless a metastable supersaturated solution occurs). However, ΔG is positive when IAP < K_{sp} corresponding to SI < 0 and the solution is undersaturated so precipitation cannot occur.

Powder X-ray diffraction

XRD is a useful technique to characterize the crystallographic structure, crystallite size (grain size), and preferred orientation in polycrystalline or powdered solid samples. XRD is commonly used to identify unknown substances, by comparing diffraction data with a database maintained by the International Center for Diffraction Data (ICDD). It may also be used to characterize heterogeneous solid mixtures to determine relative abundance of crystalline compounds. XRD can provide structural information of unknown materials by Rietveld refinement method.

XRD patterns are typically plotted as the intensity of the diffracted X-rays versus the angle 2θ. The diffracted X-ray beam is considered as "reflection" from a lattice plane as described by Bragg's Law (Eq. 1.7):

$$n\lambda = 2d \sin \theta \qquad\qquad …………..(1.7)$$

where *n* is the order of diffraction of X-rays, λ is wavelength, *d* is the perpendicular spacing of the lattice planes, and θ is the diffraction angle as shown in Figure 1.5.

For constructive
interference,
$2d (\sin \theta) = n\lambda$
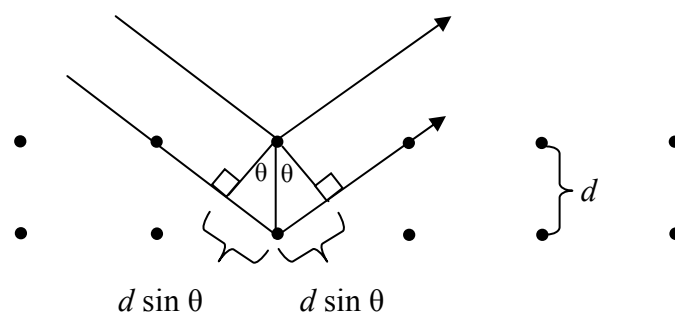
Figure 1.5 The incident and reflected beams relative to the planes.

Peaks will appear in the diffraction pattern at 2θ values when constructive interference is at a maximum. By measuring the 2θ values for each diffraction peak, we can calculate the *d*-spacing (the distance between the diffracting planes) for each diffraction peak. The data analysis software has a program for automatically calculating the *d*-spacing for all of the peaks in the diffraction pattern.

The number of observed peaks is related to the symmetry of the unit cell. The *d*-spacings of the observed peaks are related to the repeating distances between planes of atoms in the structure and the intensities of the peaks are related to the kinds of atoms and their arrangements within the unit cell. The scattering intensities for the diffracted beams are directly related to the number of electrons in the atom. Hence, light atoms scatter X-rays weakly, while heavy atoms scatter X-rays more effectively. These three features of a diffraction pattern (the number of peaks, the positions of the peaks, and the intensities of the peaks) define a unique, fingerprint XRD pattern for every crystalline material.

A unit cell contains basis vectors of the direct lattice **a**, **b**, and **c**. The lengths of the basis vectors **a**, **b**, and **c** are *a*, *b*, and *c*, respectively and the interaxial (lattice) angles between **b** and **c, c** and **a**, and **a** and **b** are α, β, and γ, respectively (Hahn, 1996).

Fourier transform infrared spectroscopy

Fourier transform infrared spectroscopy (FT-IR) is a technique for characterizing and identifying functional groups in organic molecules. The characterization is achieved by comparison with the spectra in databases and assigning each peak to the vibration of a specific functional group.

Principle of the FTIR technique is based on the interaction between the radiation and the sample. When infrared light interacts with a sample, materials are excited to a higher energy state. A material adsorbs only selected frequencies (energies) of the infrared radiation which match the energy differences between orbitals in the material. Therefore, vibrational modes of different chemical interactions can be detected and allow the identification of different materials The energy of an interaction is changed in an 8 to 40 kJ/mole range corresponding to the stretching and bending vibrational frequencies of the bonds in material (Pavia, Lampman, and Kriz, 1996).

As mentioned, infrared light matches the vibrational frequencies of the interactions. In order for a vibration to be "IR active", it is necessary for a change in the dipole moment during absorption of the infrared light. For example hydrochloric acid, HCl, when HCl vibrates along the bond, the chlorine takes on a slightly more negative charge, and the hydrogen takes on a slightly more positive charge.

Consequently, a change in dipole moment of the HCl molecule occurs. In some molecules, such as O_2, N_2, H_2, F_2, and Cl_2 there is no induced dipole moment and they are "IR-inactive". These compounds require use of other techniques to study interaction strengths such as Raman spectroscopy.

There are three regions of the infrared spectrum; the near-, mid- and far-infrared. The far-infrared is approximated in 400-10 cm^{-1} range, has low energy and may be used for rotational spectroscopy. The mid-infrared in 4000-400 cm^{-1} range may be used to study the fundamental vibrations and associated rotational-vibrational structure. The higher energy near-IR (14000-4000 cm^{-1}) can excite overtone or harmonic vibrations.

Electron microscopy

Scanning electron microscopy (SEM) and transmission electron microscopy (TEM) are techniques capable of providing structural information over a wide range of magnification. SEM is useful for studying morphology and surface features of samples which have size up to 10 μm, because of the depth focus of SEM instruments, the resulting picture is obtained with a three dimensional appearance. For TEM technique, samples should be thinner than 2000 Å because electrons interact strongly with matter and are completely absorbed by thick particles. The range of various techniques used to observe the morphology of samples are given in Figure 1.6 (West, 1984).

SEM

TEM

Optical microscope

Naked eye

1 Å	10 Å	100 Å	1000 Å	1 µm	10 µm	100 µm	1 mm
			0.1 µm			0.1 mm	
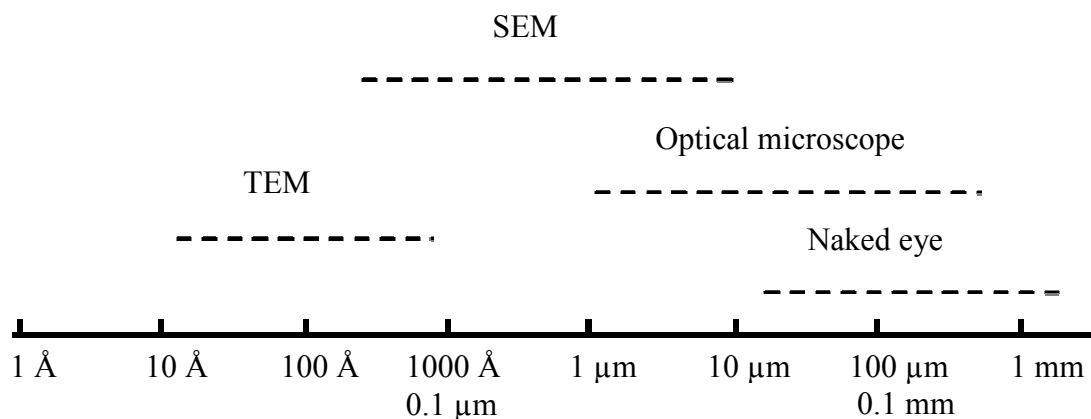
Figure 1.6 The range of various techniques used to observe the morphology of samples.

SEM operates from a source of electrons focused in vacuum into a fine probe that is modulated over the surface of the specimen. The electron beam passes through scan coils and objective lens that deflect it horizontally and vertically so the beam scans the surface of the sample. As the electrons penetrate the surface, a number of interactions occur that can result in the emission of electrons or photons from or through the surface. A reasonable fraction of the electrons emitted can be collected by appropriate detectors, and the output can be used to modulate the brightness of a cathode ray tube (CRT) whose x- and y-inputs are driven synchronously with the x-y voltages modulating the electron beam. In this way an image is produced on the CRT; every point that the beam strikes on the sample is mapped directly onto a corresponding point on the screen. The operation of TEM is similar to SEM and requires an ultra high vacuum and a high voltage.

X-ray fluorescence spectroscopy

When a sample is bombarded with high energy electrons many things can happen, including generation of X-rays. These X-rays are characteristic emission spectra of the elements present in the sample. Analysis of the emitted radiation can use either wavelength dispersive X-ray fluorescence (WDX) or energy dispersive X-ray fluorescence (EDX) to identify the elements in the sample. These techniques are useful for quantitative and qualitative analysis. However, these techniques can determine only elements heavier than and including fluorine. Lighter elements do not give suitable X-ray spectra.

Optical/polarizing microscopy

An optical or polarizing microscope is an optical measuring instrument for the detailed examination of specimens. The basic components of the microscope are shown in Figure 1.7 and 1.8. The source may give either white or monochromatic light. The light shines on the polarizer and only that component which vibrates parallel to the polarizer is permitted to pass through. The resulting polarized light passes through the sample. There are two variants of the analyzer position. In one the transmitted light is picked up by the objective lens, and the analyzer may be placed in or out of the path of light inside of the microscope (West, 1984).

Eyepiece lens

↑

Analyzer

↑

Objective lens

↑

Sample

↑

Polarizer

↑

Light source
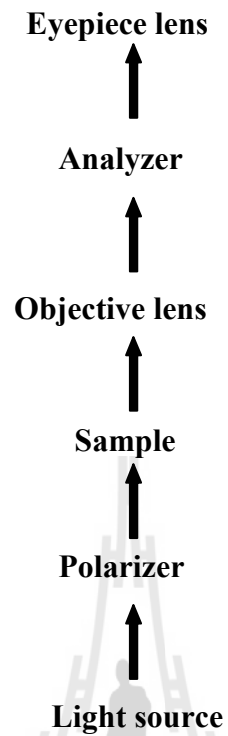
Figure 1.7 Basic components of a polarizing microscope.

In the second variant the analyzer is placed below the objective lens, exterior to the body of the microscope (Figure 1.7). Objective or eyepiece lenses may be available for different magnifications and/or the body of the microscope may include a zoom function, often called a power body.

Eyepiece lens

↑

Objective lens

↑

Analyzer

↑

Sample

↑

Polarizer

↑

Light source
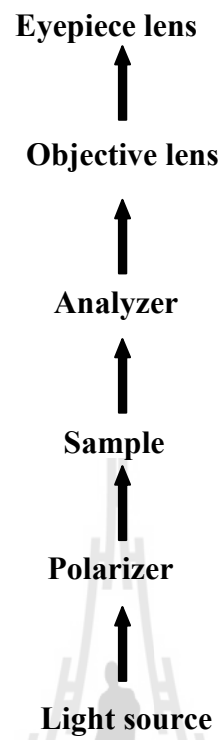
Figure 1.8 Alternative arrangement of the basic components of a polarizing microscope.

1.8 References

Admassu, W. and Breese, T. (1999). Feasibility of using natural fishbone apatite as a substitute for hydroxyapatite in remediating aqueous heavy metal. **J. Hazard. Mater.** B69: 187-196.

Agency for Toxic Substances and Disease Registry (2007). **Toxicological profile for lead.** Agency for Toxic Substances and Disease Registry. Atlanta GA:U.S. <http://www.atsdr.cdc.gov/toxprofiles/tp.asp?id=96&tid=22>, accessed on 16 May 2012.

Anderson, C. and Danylchuk, K. D. (1977). The effect of chronic low level lead intoxication on the Haversian remodeling system in dogs. **Lab. Invest.** 37: 466-469.

Berry, L. G. and Mason, B. (1959). **Mineralogy: Concepts, Descriptions, Determinations**. San Francisco, USA: W. H. Freeman.

Bruckner, S., Lusvardi, G., Menabue, L. and Saladini, M. (1995). Crystal structure of lead hydroxyapatite from powder X-ray diffraction data. **Inorg. Chim. Acta** 236: 209-212.

Březina, B., Havránková, M., and Dušek, K. (1976). The growth of $PbHPO_4$ and $Pb_4(NO_3)_2(PO_4)_2 \cdot 2H_2O$ in gels. **J. Cryst. Growth** 34: 248-252.

Centers for Disease Control and Prevention (2012). **Lead: Topic home.** Centers for Disease Control and Prevention. <http://www.cdc.gov/lead/>, accessed on 16 May 2012.

Chomchai, C., Padungtod, C., and Chomchai, S. (2005). Predictors of elevated blood level in Thai children: A pilot study using risk assessment questionnaire. **J. Med. Assoc. Thai.** 88: s53-s59.

Decker, D. L., Petersen, S., and Debray, D. (1979). Pressure-induced ferroelastic phase transition in $Pb_3(PO_4)_2$: A neutron-diffraction study **Phys. Rev., Section B** 19: 3552-3555.

Desai, C. C. and Ramana, M. S. V. (1988) Growth and properties of ferroelectric lead hydrogen phosphate and lead nitrate phosphate single crystals. **J. Cryst. Growth** 91: 126-134.

Desai, C. C. and Ramana, M. S. V. (1990). Nucleation density and electrolytic growth of lead hydrogen phosphate single crystals in silica gels. **J. Cryst. Growth** 102: 191-196.

Dungkaew, W. (2010). **Arsenate Precipitation from Polyelectrolyte-arsenate Complex Solutions.** Ph.D. Thesis, Suranaree University of Technology, Thailand.

Dungkaew, W., Haller, K. J., Flood, A. E., and Scamehorn, J. F. (2012). Phase precipitation boundary and dissolution study of barium arsenate compounds. **J. Phys. Chem., Section B.** (in preparation).

Environmental Protection Agency. (1991). **Lead and copper rule.** U.S. Environmental Protection Agency. <http://water.epa.gov/lawsregs/ rulesregs/sdwa/lcr/index.cfm#2006>, accessed on 16 May 2012.

Environmental Protection Agency. (2006). **Air quality criteria for lead.** U.S. Environmental Protection Agency. <http://cfpub.epa.gov/ ncea/cfm/recordisplaycfm?deid=158823>, accessed on 16 May 2012.

Gangoso, L., Álvarez-Lloret, P., Rodríguez-Navarro, A., Mateo, R., Hiraldo, F., and Donázar, J. A. (2009). Long-term effects of lead poisoning on bone

mineralization in vultures exposed to ammunition sources. **Environ. Pollut.** 157: 569-574.

Guimaraes, D. M. C. (1979). Ferroelastic transformations in lead orthophosphate and its structure as a function of temperature. **Acta Crystallogr., Section A** 35: A108-A114.

Hahn, T. (1996). **International Tables for Crystallography**, Volume A (4th ed.). Dordrecht, Holland: Kluwer Academic Publishers.

Hass, G. M., Landerholm, W., and Hemmens, A. (1967). Inhibition of intercellular matrix synthesis during ingestion of inorganic lead. **Amer. J. Pathol.** 50: 815-845.

LeGeros, R. Z. (1991). **Calcium Phosphates in Oral Biology and Medicine** (1st ed.). San Francisco, USA: Karger.

Lormphongs, S., Miyashita, K., Morioka, I., Chaikittiporn, C., Miyai, N., and Yamamoto, H. (2003). Lead exposure and blood lead level of workers in a battery manufacturing plant in Thailand. **Ind. Health** 41: 348-353.

Lormphongs, S., Morioka, I., Miyai, N., Yamamoto, H., Chaikittiporn, C., Thiramanus, T., and Miyashita, K. (2004). Occupation health education and collaboration for reducing the risk of lead poisoning of workers in a battery manufacturing plant in Thailand. **Ind. Health** 42: 440-445.

Mahapatra, P. P., Mahapatra, L. M., and Mishra, B. (1989). Physicochemical studies on solid solutions of calcium phosphorus arsenic hydroxyapatites. **Bull. Chem. Soc. Jpn.** 62: 3272-3277.

Mayer, K. and Woermann, D. (1996). Influence of a polycrystalline precipitation

zone on the growth of single crystals using a gel method: Growth of single crystals of PbHPO$_4$. **J. Cryst. Growth** 169: 317-324.

Ministry of Industry of Thailand (1968). **Industrial products standards: Drinking water quality standard.** Ministry of Industry of Thailand. <http://www.pcd.go.th/info_serv/en_reg_std_water01.html#s1>, accessed on 16 May 2012.

Ministry of Interior of Thailand (1972). **Safety in workplace.** Ministry of Interior of Thailand. <http://medinfo2.psu.ac.th/commed/occmed/images/TIS18001/tisp4/law%20Chem/images/law/1.environchem.pdf>, accessed on 16 May 2012.

Ministry of Public Health of Thailand (1986). **Standard of food is contaminated.** Ministry of Public Health of Thailand. <http://iodinethailand.fda.moph.go.th/food_54/data/announ_moph/P98.pdf>, accessed on 16 May 2012.

Ministry of Public Health of Thailand (2001). **Report of Environment: Health and environment.** Ministry of Public Health of Thailand. <http://www.onep.go.th/download/soe44dl.html>, accessed on 16 May 2012.

Mori, K., Yamaguchi, K., Hara, T., Mizugaki, T., Ebitani, K., and Kaneda, K. (2002). Controlled synthesis of hydroxyapatite-supported palladium complexes as highly efficient heterogeneous catalysts. **J. Am. Chem. Soc.** 124; 11572-11573.

Mori, K., Hara, T., Mizugaki, T., Ebitani, K., and Kaneda, K. (2003). Hydroxyapatite-bound cationic ruthenium complexes as novel heterogeneous Lewis acid catalysts for Diels-Alder and aldol reactions. **J. Am. Chem. Soc.** 125; 11460-11461.

Narasaraju, T. S. B. and Phebe, D. E. (1996). Some physico-chemical aspects of hydroxylapatite. **J. Mater. Sci.** 31: 1-21.

National Environmental Board (1992a). **Enhancement and conservation of national environmental quality: Soil quality standard**. National Environmental Board. <http://www.pcd.go.th/info_serv/en_reg_ std_soil01.html#s2>, accessed on 16 May 2012.

National Environmental Board (1992b). **Enhancement and conservation of national environmental quality: Surface water quality standard.** National Environmental Board. <http://infofile.pcd.go.th/law/3_14_water.pdf?CFID= 8341280&CFTOKEN=83596715>, accessed on 16 May 2012.

National Environmental Board (1995). **Enhancement and conservation of national environmental quality: Air quality standard**. National Environmental Board. <http://infofile.pcd.go.th/law/2_36_air.pdf?CFID=8341280&CFTOKEN=8359 6715>, accessed on 16 May 2012.

National Institute for Occupational Safety and Health (2003). **Health hazard evaluation report: HETA#2001-0537-2897.** National Institute for Occupational Safety and Health. <http://www.cdc.gov/niosh/hhe/reports/pdfs /2001-0537-2897.pdf>, accessed on 16 May 2012.

Neesanan, N., Kasemsup, R., Ratanachuaeg, S., Kojaranjit, P., Sakulnoom, K., and Padungtod, C. (2011). Preliminary study on assessment of lead exposure in Thai children aged between 3-7 years old who live in Umphang district, Tak province. **J. Med. Assoc. Thai.** 94: s113-s120.

Needleman, H. L., Schell, A., Bellinger, D., Leviton, A., and Allred, E. N. (1990). The long-term effects of exposure to low doses of lead in childhood. **N. Engl. J. Med.** 322: 83-88.

Occupational Safety and Health Administration (2011). **Occupational safety and health standards: Lead**. Occupational Safety and Health Administration. <http://www.osha.gov/pls/oshaweb/owadisp.show_document?p_table=STAND ARDS&p_id=10030#1910.1025%28d%29>, accessed on 16 May 2012.

Parkhurst, D. L. and Appelo, C. A. J. (1999). **User's Guide to PHREEQC: A Computer Program for Speciation, Batch-reaction, One-dimensional Transport, and Inverse Geochemical Calculations**, Version 2, Water-Resources Investigations Report 99-4259, U.S. Geological Survey, Denver CO:U.S.

Pasero, M., Kampf, A. R., Ferraris, C., Pekov, I. V., Rakovan, J., and White, T. J. (2010). Nomenclature of the apatite supergroup minerals. **Eur. J. Mineral.** 22: 163-179.

Patel, P. N. (1980). Magnesium calcium hydroxylapatite solid solution. **J. Inorg. Nucl. Chem.** 42: 1129-1132.

Pavia, D. L., Lampman, G. M., and Kriz, G. S. (1996). **Introduction to Spectroscopy; a Guide for Students of Organic Chemistry** (2nd ed.). USA: Harcourt Brance & Company.

Rabinowitz, M. B., Wetherill, G. W., and Kopple, J. D. (1976). Kinetic analysis of lead metabolism in healthy humans. **J. Clin. Invest.** 58: 260-270.

Rodríguez-Lorenzo, L. M., Hart, J. N., and Gross, K. A. (2003). Influence of fluorine in the synthesis of apatites. Synthesis of solid solutions of hydroxyl-fluorapatite. **Biomaterials** 24: 3777-3785.

Robert, M. C. and Lefaucheux, F. (1988). A comparative study of gel grown and space grown lead hydrogen phosphate crystals. **J. Cryst. Growth** 88: 499-510.

Shi, D. (2005). **Introduction to Biomaterials**. China: World Scientific.

Smičiklas, I., Onjia, A., Raičević, S., Janaćković, Đ., and Mitrić, M. (2008). Factors influencing the removal of divalent cations by hydroxyapatite. **J. Hazard. Mater.** 152: 876-884.

Stumm W. and Morgan J. J. (1996). **Aquatic Chemistry** (3rd ed.). New York, NY: John Wiley & Sons.

Vivekanandan, K., Selvasekarapandian, S., and Kolandaivel, P. (1995). Raman and FT-IR studies of $Pb_4(NO_3)_2(PO_4)_2 \cdot 2H_2O$. **Mater. Chem. Phys.** 39: 284-289.

Walsh, D. and Tanaka, J. (2001). Preparation of a bone-like apatite foam cement. **J. Mater. Sci. Mater. Med.** 12: 339-343.

Warniment, C. (2010). Lead poisoning in children. **Am. Fam. Physician** 81: 751-757.

West, A. R. (1984). **Solid State Chemistry and Its Applications**. Singapore: John Wiley & Sons.

World Health Organization (2008). **National environment and health action plans.** World Health Organization. <http://www.searo.who.int/nen/Section23/Section1318/ Section1797_7718.htm>, accessed on 16 May 2012.

Zhu, K., Yanagisawa, K., Shimanouchi, R., Onda, A., Kajiyoshi, K., and Qiu, J. (2007). Hydrothermal synthesis and crystallographic study of Sr-Pb hydroxyapatite solid solution. **J. Ceram. Soc. Jpn**. 115: 873-876.

CHAPTER II

STRUCTUAL ANALYSIS OF CALCIUM AND LEAD

HYDROXYAPATITE[1]

2.1 Introduction

Apatite is a class of mineral including two series, apatite and pyromorphite series. Calcium hydroxyapatite, CaHAp ($Ca(1)_2Ca(2)_3(PO_4)_3OH$) is the prototype of the apatite class and of the apatite series. The structure belongs to space group $P6_3/m$ and is susceptible to ionic substitution in both anion and cation sites. Ca^{2+} can be replaced by various divalent cations such as Ba^{2+}, Mg^{2+}, Cd^{2+}, Sr^{2+}, or Pb^{2+} (Sugiyama *et al*., 1999; Yasukawa, Yokoyama, Kandori, and Ishikawa, 2007; Barinova, Lusvardi, Menabue, and Saladini, 1998), PO_4^{3-} can be replaced by AsO_4^{3-} or VO_4^{3-}, and OH^- can be replaced by F^- or Cl^- (Dong, White, Wei, and Laursen, 2002; Dai and Hughes, 1989). Apatites are important materials for environmental remediation, including applications in removal of heavy metals from contaminated water (Mavropoulous, Rossi, and Costa 2002; Mavropoulous, Rocha, Moreira, Rossi, and Soares, 2004; Admassu and Breese, 1999; Smičiklas, Onjia, Raičević, Janaćković, and Mitrić, 2008) and immobilization of toxic and/or radioactive ions (Krestou, Xenidis, and Panias, 2004). Apatites are also important, because CaHAp is the dominant component in mammalian hard tissues such as bones and teeth;

---

[1]Portions of this work have been published in the proceedings of the 35th Congress on Science and Technology of Thailand (Saisa-ard and Haller, 2009).

about 69 wt % and 95 wt %, respectively (Aoba, 1997). Divalent metal ions such as Pb^{2+} can substitute for Ca^{2+} ions of CaHAp. Complete substitution of Pb^{2+} ions into CaHAp results in lead hydroxyapatite (PbHAp) which is isostructural with CaHAp. The relationship of PbHAp to CaHAp and its link to bone disease is one reason the structure of PbHAp is of interest.

Bond valence calculation is a method which can be used to determine the apparent formal valence of each atom in an ionic crystal structure by calculating partial bond valences from the individual bond lengths, then summing all the components about each atom to obtain its total bond valence. It is common practice in the structure determination of ionic crystal structures to assess the correctness of the results from these bond valence sums. If the sum of the bond valences around each atom is close to the expected formal oxidation state, the structure is likely to be correct. However, if the bond valence sum for any atom deviates from the expected value by more than 0.1 valence unit (v.u.) the result must be examined critically and the discrepancy explained, or the structural error corrected (Brown, 1993).

Bond valence calculations have been used for structural analysis of PbHAp and CaHAp (Saisa-ard and Haller, 2009). Results show the bond valence sums for all atoms of CaHAp are acceptable, but the bond valence sums of P, Pb in the M(2) site, and O(4) (5.66, 1.55, and 0.67, respectively) in PbHAp are dramatically different from integral values. The discrepancies in the expected bond valence sum values of these atoms may come from several causes such as an incorrect origin choice or structure distortions. The results are not optimal and additional work is required, however, the result suggests that part of the error in the PbHAp structure is likely from the unusual (probably incorrect) distortion of the PO_4^{3-} group with the O(3)

atom moved closer to the O(1) and O(2) positions, resulting in a larger O(3)–P–O(3i) angle (larger by 4.3°) and effectively decreasing the P–O(3) and the Pb(2)–O(3) bond lengths but increasing the O(3) bond lengths to the Pb(1) in the M(1) site.

The public-domain bond-valence program (Brown, 1993) is easy to use. However, using the program to evaluate a series of isostructural compounds is unnecessarily tedious, and in assessing structures with deviant atoms, interatomic distances and angles are also useful. Therefore, part of this work was construction of a tool which calculates the bond valence components, the relevant bond valence sums, and relevant interatomic distances and angles for all the crystallographically unique atoms and structural parameters in the apatite structure. Evaluation of alternate models is facilitated by the instantaneous availability of the bond valences, bond lengths, and bond angles on modification of any coordinate or atom type. Use of the calculator is illustrated by the example of PbHAp which, as published from powder diffraction data, has some unusual bond lengths and angles as well as unexpected bond valence sums.

2.2 Theory

Bond valence

The concept of bond valence derives from the Pauling electrostatic valence model (Pauling, 1929). The bond valences are calculated from simple expressions using empirically derived constants. The partial bond valence, s_{ij}, between any pair of adjacent atoms is given by:

$$s_{ij} = \exp[(R_o - R_{ij})/b] \qquad \text{…………..(2.1)}$$

where the bond valence between adjacent atoms i and j is related to the observed bond length R_{ij}; R_o is a constant depending on the nature of the ij pair, and b is 0.37. The bond valence sum for a given atom or ion, z_j, is defined as the sum of all the individual bond valences as follows:

$$z_j = \Sigma s_{ij} \qquad \text{…………..(2.2)}$$

The atoms to be summed over are determined by the criteria that a) every part of the electron density of the crystal must belong to at least one atom, b) the division of the electron density must ensure a reasonable assignment of the charges in the crystal, and c) the division and charges are chosen to minimize the local multipole energies associated with nonspherical charge distributions in most crystals (Brown, 2002).

Geometry

Interatomic distance, d_{A-B}, and interatomic angles, $\angle_{A-B-C}$, can be calculated from Cartesian coordinates, (X, Y, Z), as follows:

$$d_{A-B} = \sqrt{(X_A - X_B)^2 + (Y_A - Y_B)^2 + (Z_A - Z_B)^2} \qquad \text{…………..(2.3)}$$

$$= \sqrt{\Delta X^2_{A-B} + \Delta Y^2_{A-B} + \Delta Z^2_{A-B}} \qquad \text{…………..(2.4)}$$

$$\angle_{\text{A–B–C}} = \arctan\left(\sqrt{1-c_{\text{A}}^{2}}\,/\,c_{\text{A}}\right) \qquad \dots\dots\dots\dots(2.5)$$

where $c_{\text{A}} = -\,(\Delta X_{\text{A–B}}\Delta X_{\text{B–C}} + \Delta Y_{\text{A–B}}\Delta Y_{\text{B–C}} + \Delta Z_{\text{A–B}}\Delta Z_{\text{B–C}})/(d_{\text{A–B}}d_{\text{B–C}})$ …………..(2.6)

Crystallographic data are normally presented as fractional coordinates referred to the crystallographic unit cell parameters a, b, c, α, β, γ, and the crystallographic space group. While this form may at first seem inconvenient, it preserves the power and convenience of the crystalline symmetry. Fractional triclinic coordinates (x, y, z) may be converted to Cartesian coordinates as follows:

$$X = xa + yb\cos\gamma + zc\cos\beta \qquad \dots\dots\dots\dots(2.7)$$

$$Y = yb\sin\gamma + z\{c(\cos\alpha - \cos\beta\cos\gamma)/\sin\gamma\} \qquad \dots\dots\dots\dots(2.8)$$

$$Z = zcW/\sin\gamma \qquad \dots\dots\dots\dots(2.9)$$

where $W = \sqrt{(1 - \cos^{2}\alpha - \cos^{2}\beta - \cos^{2}\gamma + 2\cos\alpha\cos\beta\cos\gamma)}$ …………(2.10)

In a conventional hexagonal crystal system, such as that of apatite, $a = b$, $\alpha = \beta = 90°$, and $\gamma = 120°$, leading to simplification of equations 2.7, 2.8, and 2.9.

$$X = a(x - y/2) \qquad \dots\dots\dots\dots(2.11)$$

$$Y = ya \ \frac{\sqrt{3}}{2} \qquad\qquad \ldots\ldots\ldots\ldots..(2.12)$$

$$Z = zc \qquad\qquad \ldots\ldots\ldots\ldots..(2.13)$$

2.3 Experimental

A spreadsheet was constructed in Excel (Microsoft Office Excel, 2003). The input section accepts values for the hexagonal fractional coordinates of the seven crystallographically unique atom positions, the lengths of the a and c axes, and the values of R_o for Pb–O, P–O, and O–H atom pair types. Equations as defined in section 2.2 above were entered into the following area to create two additional sections. The center section presents the calculated interatomic distances and interbond angles about the two crystallographically unique metal sites and the phosphate site, and the final section presents a summary table of the bonds combined with the bond valence sums for each crystallographically unique atom.

The crystallographic information file, *cif* file, for the PbHAp structure (Barinova, Lusvardi, Menabue, and Saladini, 1998) utilized in this work was obtained from supporting information available via the Inorganic Crystal Structure Database, ICSD (Inorganic Crystal Structure Database, 2008), ICSD code 87518. Crystal data and positional parameters of each atom of the PbHAp compound are given in Table 2.1.

Atomic positions, unit cell parameters, and the bond valence interaction parameters R_o were entered into the bond valence calculator and the structure was

adjusted to be more chemically reasonable by adding an H atom and changing the positions of O(3) and O(4) as discussed in the following section.

Table 2.1 Crystal data and fractional hexagonal coordinates for PbHAp.

Parameter	PbHAp
Empirical formula	$Pb_5(PO_4)_3OH$
Crystal system	hexagonal
Space group	$P6_3/m$
Cell parameters (Å)	
a,b	9.774(1)
c	7.291(1)
$V (Å^3)$	603.20
Z	2
Discrepancy index, R	0.0127

Atom	Fractional coordinate		
	x	y	z
Pb(1)	1/3	2/3	0.4973(1)
Pb(2)	0.2364(1)	0.2319(1)	1/4
P	0.4045(3)	0.0231(3)	1/4
O(1)	0.3256(8)	0.8415(8)	1/4
O(2)	0.5860(8)	0.1005(9)	1/4
O(3)	0.3541(6)	0.0613(6)	0.08132(8)
O(H)	0	0	0

2.4 Results and discussion

The metal atoms in apatite structures are located on two crystallographically different sites[1]: h sites, mirror planes at $z = 1/4$ and 3/4, and f sites, 3-fold axes at (1/3, 2/3, z) and (2/3, 1/3, z), as shown in Figure 2.1. Three P atoms and six phosphate O atoms are also located on h sites while the other six phosphate O atoms are located on general positions, pairwise related by the mirror planes through the P atoms. Three metal ions at the h sites are coordinated with seven O atoms (one O(1), one O(2), and four general O(3) atoms from PO_4^{3-} groups and one O atom from an OH^- group), and two metal ions at the f sites are coordinated with nine O atoms (six shorter bonds to three O(1) and three O(2) phosphate oxygen atoms on h sites define a twisted trigonal prism, and three longer bonds to O(3) atoms extend through the prism faces). The hydroxyl O positions are disordered along the 3-fold axis with the hydrogen atom further disordered into general positions about the 3-fold axis, consistent with hydrogen bonding to O(3) positions.

---

[1]Wycoff special positions are represented by letters, starting with a for the most symmetric special position in the space group under consideration, and continuing in alphabetical order until the general position is reached.
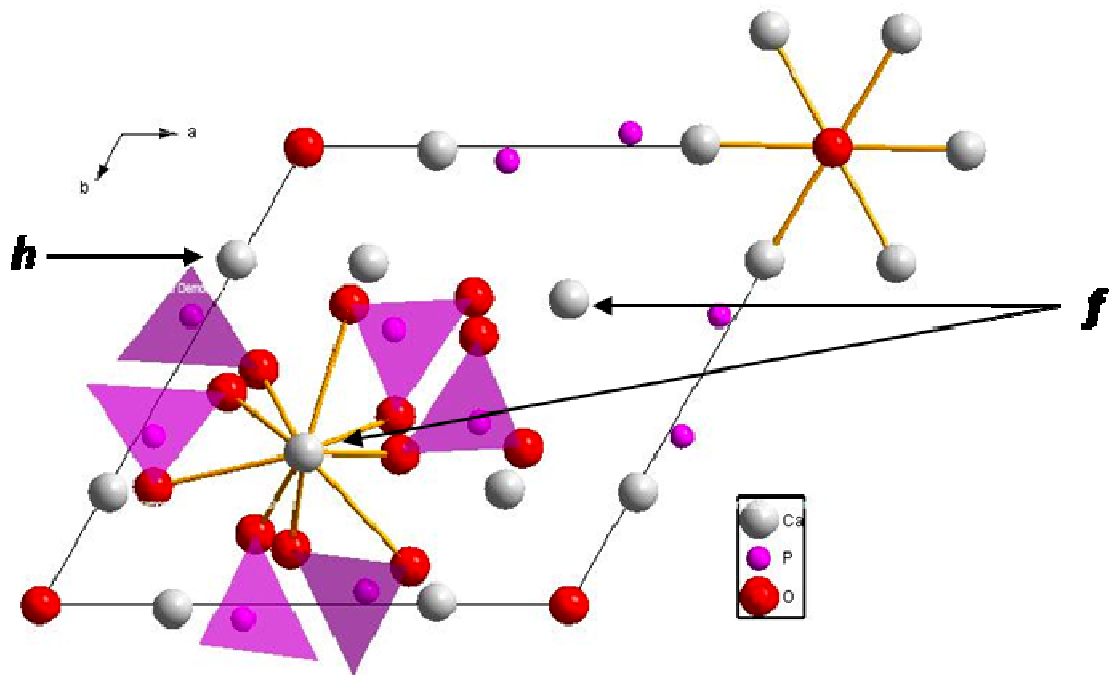
Figure 2.1 Representation of Ca, O, and P atoms in the CaHAp structure projected on the *ab* plane.

Calculated structural parameters and bond valence sums based on the published PbHAp structure are given in Table 2.2.

Table 2.2 Bond valence sums, bond lengths, and oxidation states for the unique atoms of PbHAp. The adjusted structural model has a modified O(3) atom position.

Atoms	Published structure		Adjusted structure		Formal oxidation state
	Bond length (Å)	Bond valence sum (v.u.)	Bond length* (Å)	Bond valence sum (v.u.)	
	P	5.66	P	4.90	+5
O(1)	1.542	2.02		2.02	−2
O(2)	1.542	2.08		2.08	−2
O(3)	1.442†	2.03	1.542†	1.69	−2
	Pb(1)	1.91	Pb(1)	1.96	+2
O(1)	2.511†	2.02		2.02	−2
O(2)	2.720†	2.08		2.08	−2
O(3)	2.893†	2.03	2.898†	1.69	−2
	Pb(2)	1.55	Pb(2)	1.62	+2
O(1)	2.921	2.02		2.02	−2
O(2)	2.391	2.08		2.08	−2
O(3)	2.745†	2.03	2.610†	1.69	−2
O(3i)	2.628†	2.03	2.703†	1.69	−2
O(4)	2.926	0.66		0.66	−2

*Only values which are modified are given.

†Bond lengths repeated by symmetry are not listed.

The general position, O(3), appeared to be misplaced based on rational values of P–O bond lengths. Specifically, the bond length of 1.442 Å is about 0.1 Å shorter than the other two P–O bond lengths which are in good agreement with structure correlation results (Burgi and Dunitz, 1994). Furthermore, the bond valence sum for P is 0.66 v.u. high, while that for Pb(2) is 0.45 v.u. low. The O(1)–P–O(2) angle of 110.82° is close to the ideal T_d angle of 109.54°. The positions of O(3) and its mirror related general counterpart were adjusted to give a geometrically idealized phosphate group with approximate T_d symmetry and d[P–O] = 1.542 Å (the two O(3) positions are constrained to be on the plane that bisects O(1)–P–O(2), with ideal T_d angles to both O(1) and O(2)). The adjusted bond lengths and bond valence sums are given in the right-hand section of Table 2.2.

The results after adjustment show the potential effect of the idealization of O(3) on the bond valence sums of P and Pb(2). The bond valence sum of P moves near to its expected oxidation state value. However, the bond valence sum of Pb(2) ion, while improved is still considerably below its expected oxidation state value.

The bond valence sum of the hydroxide oxygen atom, O(4), is also problematic. One obvious component of error in the bond valence sum of O(4) is the neglect of the hydrogen atom in the published structure. Including a hydrogen atom on the 3-fold axis 0.983 Å (Steiner, 2002) from O(4) increases the bond valence sum of O(4) to 1.55 v.u. A second component of error for O(4) is its location at $z = 0$ making its closest contact to a Pb(2) ion 2.926 Å. Adjusting the O(4) position along the 3-fold axis would move O(4) toward Pb(2), and away from Pb(2)′, thereby increasing the bond valence contribution to both Pb(2) and O(4). The O(4) atom was moved from (0, 0, 0) to (0, 0, 0.1200) producing the changes shown in Table 2.3.

Table 2.3 Bond valence sums, bond lengths, and oxidation states of atoms in the modified structural models.

Atom	Structure with adjusted O(3)		Further adjustment with hydroxide anion		Formal oxidation state
	Bond length (Å)	Bond valence sum (v.u.)	Bond length* (Å)	Bond valence sum (v.u.)	
	Pb(2)	1.62	Pb(2)	1.88	+2
O(1)	2.921	2.02		2.02	–2
O(2)	2.391	2.08		2.08	–2
O(3)	2.610†	1.69		1.69	–2
O(3i)	2.703†	1.69		1.69	–2
O(4)	2.926	0.66	2.477‡	2.07	–2
O(4)′	2.926	0.66	3.538‡	2.07	–2

*Only values which are modified are given.

†Bond lengths repeated by symmetry are not listed.

‡O(4) connects to six Pb(2) positions when O(4) is on the 3-bar site all contacts are equivalent, but on adjustment along the 3-fold, three contacts are short at 2.4773 Å and three are long at 3.5378 Å.

The bond valence sums of O(3) and Pb(2) after the modification still exhibit discrepancies in expected oxidation state values.

2.5 Conclusions

Results of modification of O(3) and O(4) atom positions in the PbHAp structure discussed here improved the internal agreement of the bond valence sums, but they are still not optimal. However, they do suggest that there is probable error in the published PbHAp structure model, and the alternative model formed with guidance of bond valence sums and geometric considerations would be a better

starting point for a new refinement against X-ray data. The ease of use of this tool makes it potentially useful for guiding constraints and restraints for apatite structural models during the refinement in data poor cases. It is also a useful tool for evaluation of any published apatite structure.
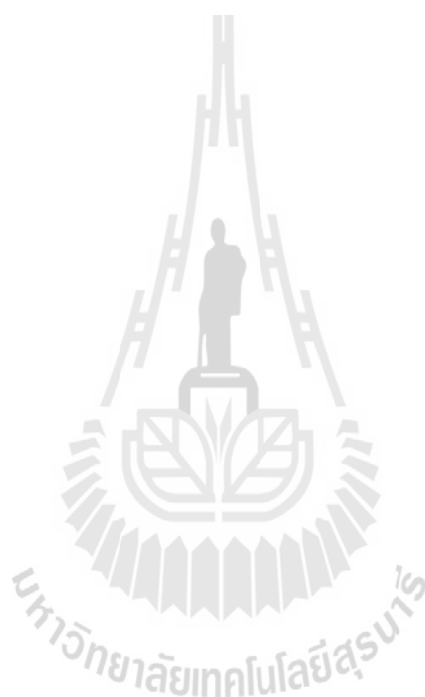
2.6 References

Admassu, W. and Breese, T. (1999). Feasibility of using natural fishbone apatite as a substitute for hydroxyapatite in remediating aqueous heavy metals. **J. Hazard. Mater.** B69: 187-196.

Aoba, T. (1997). The effect of fluoride on apatite structure and growth. **Crit. Rev. Oral Biol. Med.** 8: 136-153.

Barinova, A. V., Lusvardi, G., Menabue, L., and Saladini, M. (1998). Crystal structure of synthetic hydroxylpyromorphite $Pb_5(PO_4)_3(OH)$. **Kristallografiya** 43: 224-227.

Brown, I. D. (1993). **Instruction to Bond Valence Analysis Program**, Version 2, McMaster University.

Brown, I. D. (2002). **The Chemical Bond in Inorganic Chemistry: The Bond Valence Model**. Oxford: IUCr.

Burgi, H. B. and Dunitz, J. D. (1994). **Structure Correlation**. New York: Weinheim.

Dai, Y. and Hughes, M. J. (1989). Crystal structure refinements of vanadinite and pyromorphite. **Can. Mineral.** 27: 189-192.

Dong, Z., White, T. J., Wei, B., and Laursen, K. (2002). Model apatite systems for the stabilization of toxic metals: I. Calcium lead vanadate. **J. Am. Chem. Soc.** 85: 2515-2522.

Krestou, A., Xenidis, A., and Panias, D. (2004). Mechanism of aqueous uranium(VI) uptake by hydroxyapatite. **Miner. Eng.** 17: 373-381.

Mavropoulos, E., Rossi, A. M., and Costa, A. M. (2002). Studies on the mechanisms of lead immobilization by hydroxyapatite. **Environ. Sci. Technol.** 36: 1625-1629.

Mavropoulos, E., Rocha, C. C. N., Moreira, C. J., Rossi, M. A., and Soares, A. G. (2004). Characterization of phase evolution during lead immobilization by synthetic hydroxyapatite. **Mater. Charact.** 53: 71-78.

Microsoft (2003) Office Excel, SP3 part of Microsoft Office Professional Edition 2003, Microsoft Corporation, Redlands, Washington, USA.

Inorganic Crystal Structure Database <http://icsdweb.fiz-karlsruhe.de/>, accessed on 29 October 2008.

Pauling, L. (1929). The principles determining the structure of complex ionic crystals. **J. Am. Chem. Soc.** 51: 1010-1026.

Saisa-ard, O. and Haller, K. J. (2009). Structure analysis of calcium and lead hydroxyapatites. **Proceedings of the 35th Congress on Science and Technology of Thailand**. <http://www.scisoc.or.th/stt/35/sec_c/paper/STT35_C2_C0196.pdf>, accessed on 16 May 2012.

Smičiklas, I., Onjia, A., Raičević, S., Janaćković, Đ., and Mitrić, M. (2008). Factors influencing the removal of divalent cations by hydroxyapatite. **J. Hazard. Mater.** 152: 876-884.

Steiner, T. (2002). The hydrogen bond in the solid state. **Angew. Chem. Int. Ed.** 41: 48-76.

Sugiyama, S., Fukuda, N., Massumoto, H., Shigemoto, N., Hiraga, Y., and Moffat, J. B. (1999). Interdependence of anion and cation exchanges in calcium hydroxyapatite: Pb^{2+} and Cl^-. **J. Colloid Interface Sci.** 220: 324-328.

Yasukawa, A., Yokoyama, T., Kandori, K., and Ishikawa, T. (2007). Reaction of calcium hydroxyapatite with Cd^{2+} and Pb^{2+} ions. **Colloids Surf.** 238: 203-208.

CHAPTER III

PHASE CHARACTERIZATION AND SATURATION

MODELING OF CALCIUM-LEAD HYDROXYAPATITE

SOLID SOLUTION

3.1 Introduction

Structure of calcium hydroxyapatite, CaHAp $(Ca(1)_2Ca(2)_3(PO_4)_3(OH))$ contains four positions; $Ca^{2+}(1)$, $Ca^{2+}(2)$, PO_4^{3-}, and OH^- that can be replaced by other cations or anions as explained in chapter 1 (pp. 11-15). Its structure belongs to space group $P6_3/m$. There are two Wycoff positions, f and h, relevant to apatite structure. Ca(1) is located on f sites and coordinated with nine phosphate oxygen atoms while Ca(2) is located on h sites and coordinated with seven oxygen atoms (six phosphate oxygen atoms and one hydroxyl oxygen atom). Incomplete or partial substitution of Ca^{2+} by other cations may result in apatite solid solution materials. Studies of apatite solid solutions have been reported, including calcium-cadmium hydroxyapatite solid solution (Ca-CdHAp), calcium-strontium hydroxyapatite solid solution (Ca-SrHAp), calcium-lead hydroxyapatite solid solution (Ca-PbHAp), and lead-strontium hydroxyapatite solid solution (Pb-SrHAp) (Yaskawa, Higashijima, Kandori, and Ishikawa, 2005; Zhu, Yanagisawa, Shimanouchi, Onda, and Kajiyoshi, 2006; Zhu, Yanagisawa, Shimanouchi, Onda, Kajiyoshi, and Qiu, 2009). The preferential occupancy of alternate metal ions in the hydroxyapatite solid

solutions is in the M(2) sites due to two reasons. One is the arrangement of ions in the M(2) sites located on staggered triangles allows for the optimization of packing of larger ions, in contrast, the M(1) sites are located in the column and have strict alignment. Therefore, the substitution by larger cations such as Pb^{2+} (1.35 Å) and Sr^{2+} (1.13 Å) occurs preferentially in the M(2) positions. The second reason is based on the electronegativity of cation. If an increase in the electronegativity of the cation results in increased covalent character of the bond between the cation and the hydroxyl group (Rajagopal, Dhanabalan, Major, and Kulkarni, 1998). In the case of Cd^{2+} (0.97 Å) which is smaller than Ca^{2+} (0.99 Å) preferential position for substitution is still the M(2) position because the electronegativity of Cd^{2+} (1.7) is higher than that of Ca^{2+} (1.0) which favors bonding with the hydroxyl group at the M(2) position.

When studying solid solution materials, Vegard's law behavior confirms the formation of a solid solution by the relationship between composition and unit cell parameters. The law states that unit cell parameters change linearly with composition. When Vegard's law holds over the composition range studied the material is generally assumed to be a solid solution over that range. More detail of Vegard's law is given in the Chapter I (pp. 19-20).

The PHREEQC speciation calculation program is useful for prediction of possible phases in the system based on the equilibrium chemistry of an aqueous solution interacting with solids and gases. Saturation index (SI) calculations from PHREEQC indicate the superaturation state of an individual phase in the solution. SI is calculated for each phase made up of the ions in the solution as determined by speciation and other solution processes. When SI < 0 the solution is undersaturated,

when SI = 0 the solution is in equilibrium, and when SI > 0 the solution is supersaturated and precipitation is thermodynamically spontaneous. The PHREEQC program is described further in Chapter I, pp. 25-26.

Previous work (Dungkaew, Saisa-ard, and Haller, 2010) studied the phase characterization and saturation modeling of the calcium phosphate-arsenate apatite system. The study shows that arsenic removal efficiency is increased by adding phosphate to the system. The PHREEQC speciation program was used for simulation of saturated phases in the system, and the results suggest several calcium-arsenate phases are supersaturated in the system even without adding phosphate. However, when phosphate was added, the saturation index of CaHAp was considerably higher than those for arsenate containing phases, implying a considerably higher driving force for nucleation of phosphate containing apatite. The XRD result is consistent with the PHREEQC result and suggests arsenate ions are incorporated into the CaHAp structure as d-spacing in the CaHAp materials expand with higher percent arsenic incorporated into the solid products. When composition is plotted versus the d-spacing value of the solid products Vegard's law holds showing that the solid products are hydroxyapatite solid solution supporting the hypothesis that solid products can form calcium phosphate-arsenate hydroxyapatite solid solutions. These results support understanding of arsenate removal through calcium phosphate-arsenate precipitation. Therefore, characterization of solid products in the system is concerned.

The current chapter reports a study of Ca-PbHAp materials. Several other studies of Ca-PbHAp materials have been reported (Narasaraju, Singh, and Rao, 1972; Verbeeck, Lassuyt, Heijligers, Driessens, and Vrojijk, 1981; Yasukawa,

Kamiuchi, Yokoyama, and Ishikawa, 2002). However, the characterization of Ca-PbHAp solid product phase with prediction from the PHREEQC program has not been reported. A precipitation method was utilized for preparation of Ca-PbHAp materials in this chapter.

3.2 Experimental

Reagents

Reagents for preparation of CaHAp, PbHAp, and Ca-PbHAp

- Diammonium hydrogen phosphate, $(NH_4)_2HPO_4$ (Ajax Finechem, AR grade)

- Calcium nitrate tetrahydrate, $Ca(NO_3)_2 \cdot 4H_2O$ (Ajax Finechem, AR grade)

- Lead(II) nitrate, $Pb(NO_3)_2$ (Ajax Finechem, AR grade)

Reagents for adjusting pH

- Sodium hydroxide, NaOH (Eka Chemicals AB, AR grade)

All solutions in this experiment were prepared from deionized (DI) water.

Preparation of apatite material

CaHAp, PbHAp, and Ca-PbHAp materials were prepared by adding 20 mL of 0.6 M $(NH_4)_2HPO_4$ (pH adjusted to 10 with 1.0 M NaOH) into 20 mL of 1.0 M total metal solutions prepared from $Pb(NO_3)_2$ (natural pH = 6.44) and/or $Ca(NO_3)_2 \cdot 4H_2O$ (natural pH = 6.61), by dropwise addition. After addition of the $(NH_4)_2HPO_4$ solution, the suspension was stirred an additional 30 min and filtered. The solid materials were

dried at room temperature for 24 h and then heated at 600 ºC for 4 h. The molar ratios of Ca:Pb were controlled as 5Ca, 4Ca:1Pb, 3Ca:2Pb, 2Ca:3Pb, 1Ca:4Pb, and 5Pb.

Characterization

The precipitate products were characterized by Powder X-ray diffraction using a Bruker Analytical X-ray Systems model D5005 X-ray diffractometer equipped with a Cu Kα radiation source operating at 40 kV and 40 mA and the XRD Commander Executable analysis software (Bruker axs, 2011). XRD data were collected in the 2θ range 10-60° in steps of 0.02° and scan speed of 0.5 sec/step. Crystal morphologies were observed by scanning electron microscopy using a JSM 6400 electron microscope (JEOL, Japan). A plot of *d*-spacing as a function of composition was prepared to evaluate Vegard's law behavior. PHREEQC program (Parkhurst and Appelo, 1999) was used to calculate ion speciation and saturation indices of potential phases in the system. The database used in this work based on MinteqV4 database (Parkhurst and Appelo, 1999) which is distributed with the PHREEQC program.

3.3 Results and discussion

Morphologies of solid products were observed by SEM as shown in Figure 3.1. Ca_1Pb_4 shows plate-like crystal morphology (Figure 3.1(d)), while other products show aggregates of powdery products (Figure 3.1(a-c), (e-f)).

XRD patterns of the products from pure calcium, 5Ca (Figure 3.2(a)) and pure lead, 5Pb (Figure 3.2(f)) match with the XRD peak patterns of CaHAp (JCPDS 3-0742) and PbHAp (JCPDS 1-0924), respectively, in the JCPDS database (Figure 3.3).

These results indicate the solid products are apatite materials. The XRD peak patterns of products from mixing calcium and lead (4Ca:1Pb, 3Ca:2Pb, 2Ca:3Pb, and 1Ca:4Pb) do not match with the apatite phases in the JCPDS database as shown in Figure 3.2(b-e).
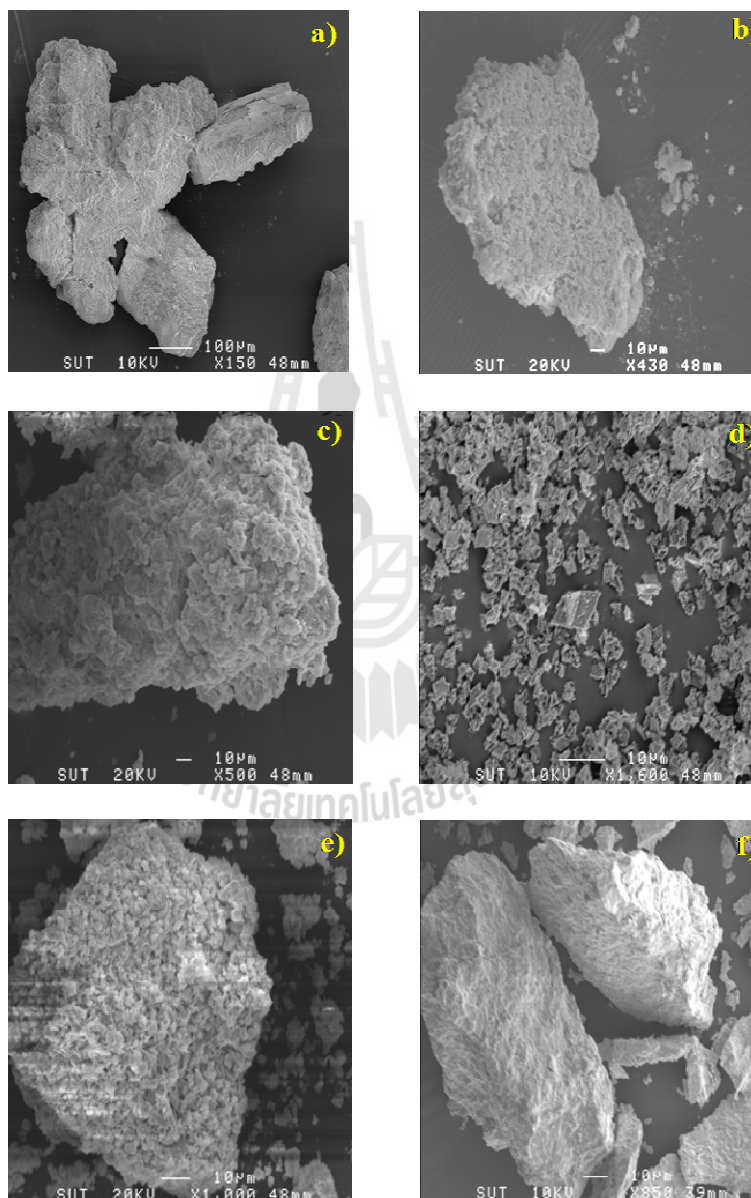
Figure 3.1 SEM images of solid products from precipitation of Ca-PbHAp. Molar ratio of Ca/Pb was varied as a) 5Ca, b) 4Ca:1Pb, c) 3Ca:2Pb, d) 2Ca:3Pb, e) 1Ca:4Pb, and f) 5Pb.
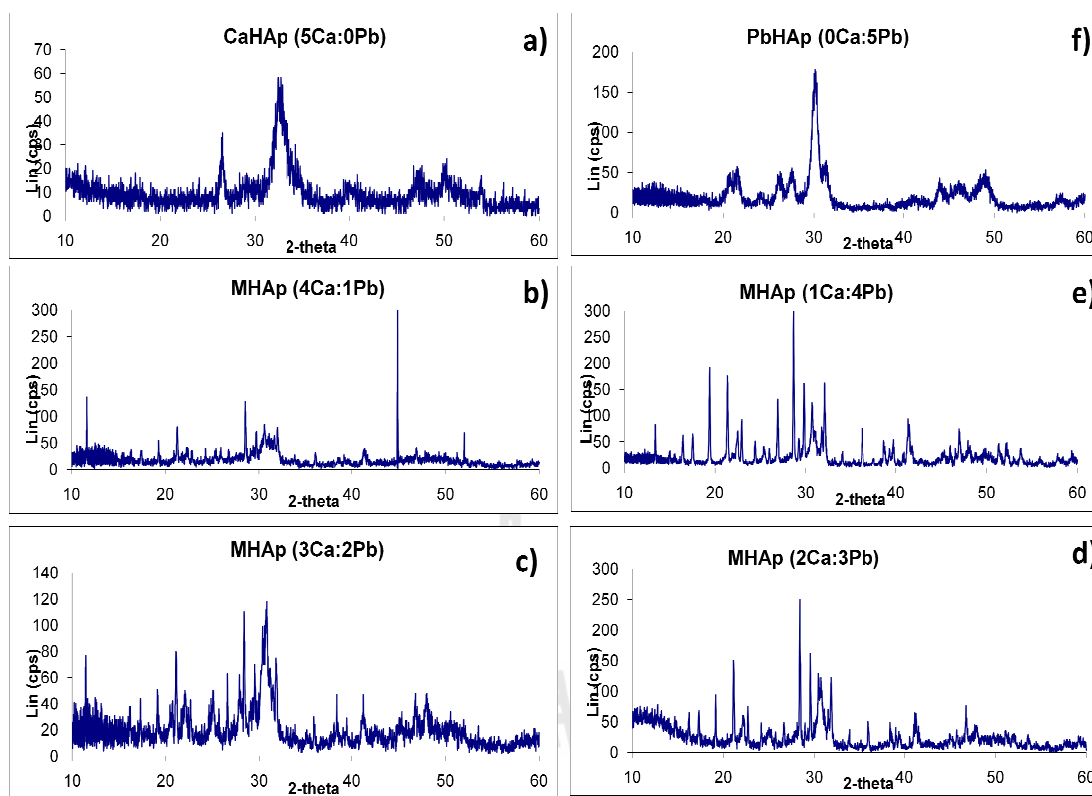
Figure 3.2 XRD patterns of solid products from precipitation of Ca-PbHAp. Molar ratio of Ca/Pb was varied as a) 5Ca, b) 4Ca:1Pb, c) 3Ca:2Pb, d) 2Ca:3Pb, e) 1Ca:4Pb, and f) 5Pb.
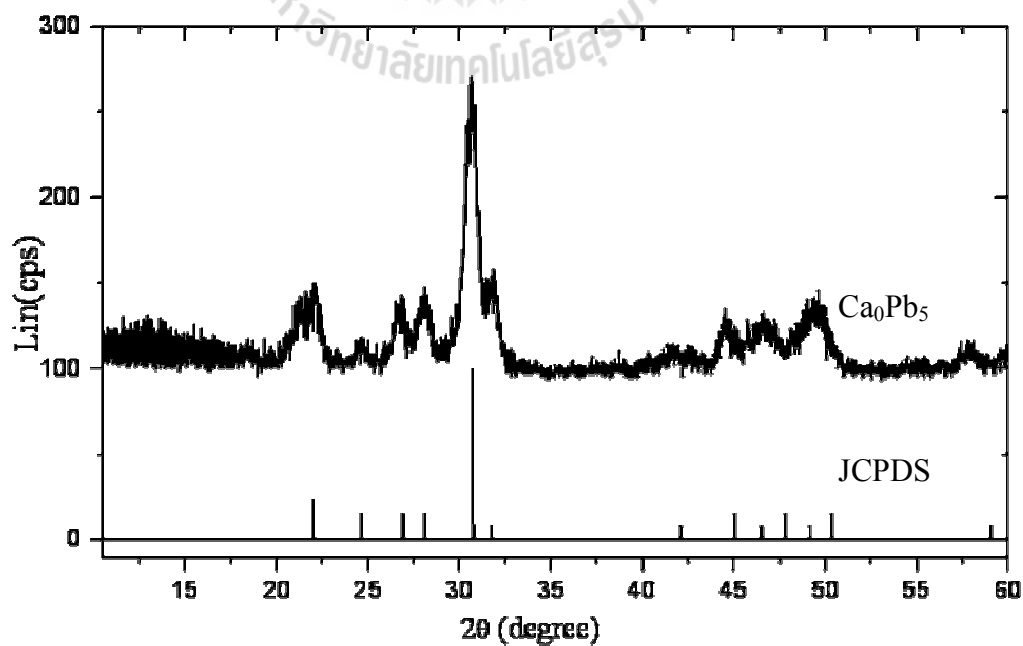
Figure 3.3 XRD patterns of Ca_0Pb_5 compared with PbHAp in the JCPDS database.

Apatite materials from the precipitation method exhibit pure apatite phase at high temperature (LeGeros, 1991), therefore, all solid products were heated at 600 °C for 4 h and their phases characterized by XRD. After heating, the XRD result of 5Ca shows shaper peak of CaHAp phase (Figure 3.4(a)), however, the XRD peaks of other products (Figure 3.4(b-f)) show higher intensity and sharper peak but do not match with CaHAp or PbHAp peak pattern in the JCPDS database and several extra peaks appear. These results could suggest multiple product phases occur in the system.

Figure 3.4 XRD patterns of solid products from precipitation of Ca-PbHAp after heating at 600 °C for 4 h. Molar ratio of Ca/Pb was varied as a) 5Ca, b) 4Ca:1Pb, c) 3Ca:2Pb, d) 2Ca:3Pb, e) 1Ca:4Pb, and f) 5Pb.

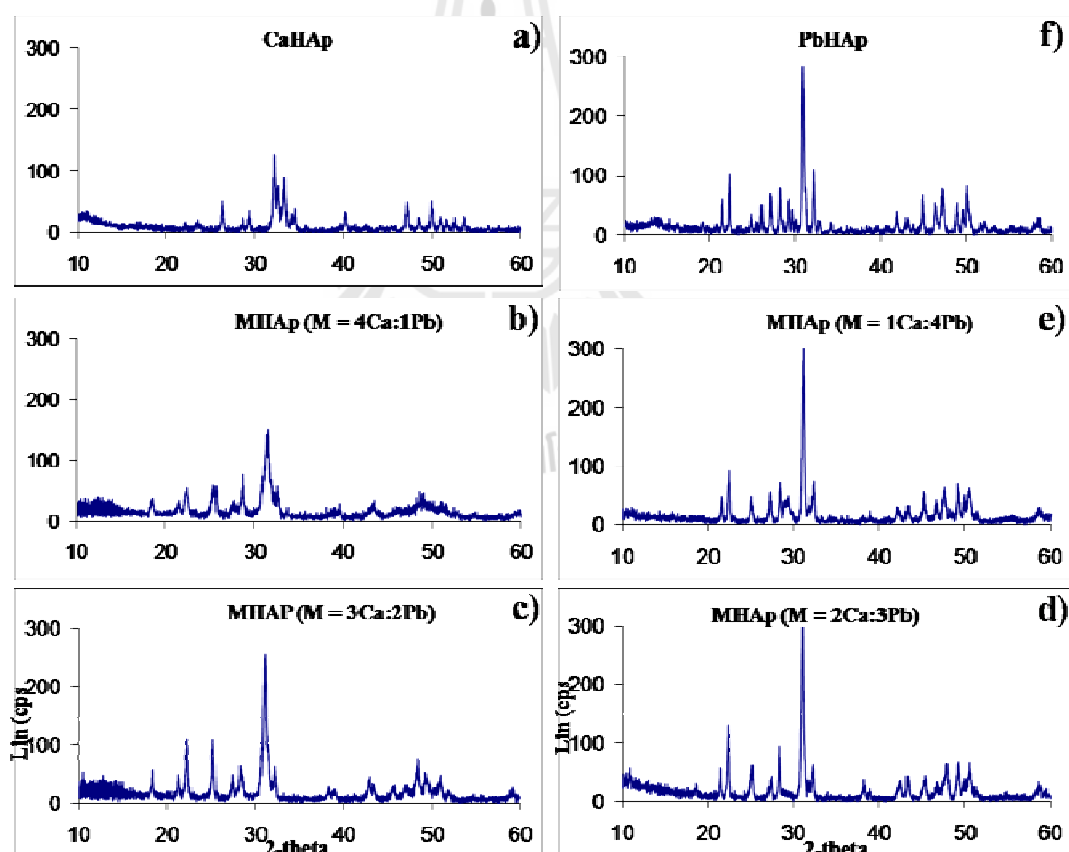The position of the dominant [211] peak near 30° 2θ from these solid products was plotted as a function of composition to study Vegard's law behavior to explore the characteristic of solid solution material. The correlation of composition and *d*-spacing of the [211] peak is shown in Figure 3.5. Result indicates these products are not Ca-PbHAp solid solution because the graph does not follow Vegard's law.
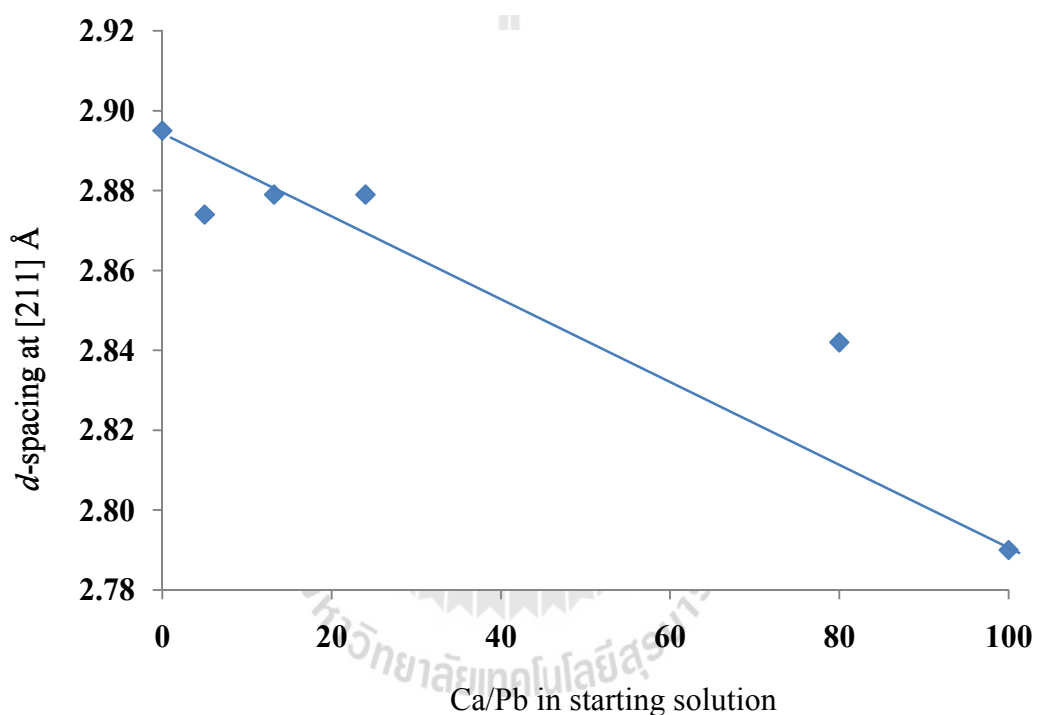
Figure 3.5 Correlation between calcium to lead ratio in starting solutions and the

expansion of *d*-spacing in solid products.

Several possible phases (positive SI value) are predicted from the PHREEQC calculation as shown in Table 3.1. These results are consistent with the XRD results, suggesting multiple products could be formed in the system.

Table 3.1 Saturation index values of Ca-P and Pb-P phases predicted from

   PHREEQC program.

Phase	SI of solid product					
	Ca_5Pb_0	Ca_4Pb_1	Ca_3Pb_2	$Ca2Pb_3$	$Ca1Pb_4$	Ca_0Pb_5
$Ca_3(PO_4)_2$	8.28	7.41	6.46	5.34	4.31	-
$Ca_4H(PO_4)_3 \cdot 3H_2O$	9.56	8.40	7.12	5.62	4.25	-
$CaHPO_4$	2.54	2.25	1.94	1.57	1.23	-
$CaHPO_4 \cdot 2H_2O$	2.19	1.90	1.58	1.21	0.86	-
$Ca_5(PO_4)_3OH$	19.72	18.26	16.66	14.78	13.07	-
$Pb_5(PO_4)_3OH$	-	15.13	14.70	14.09	12.22	12.60
$Pb_3(PO_4)_2$	-	9.04	8.78	8.42	7.30	7.54
$PbHPO_4$	-	2.45	2.37	2.25	1.88	1.97

The SI values of PbHAp and CaHAp are considerably higher than other phases, implying a higher driving force for nucleation of PbHAp and CaHAp phases resulting in reduction of the ion concentrations such that the $Pb_3(PO_4)_2$, $PbHPO_4$, $Ca_3(PO_4)_2$, $CaHPO_4$, $CaHPO_4 \cdot 2H_2O$, and $Ca_4H(PO_4)_3 \cdot 3H_2O$ phases were not formed. Several phases are predicted by PHREEQC. However, these phases do not appear clearly in the XRD pattern because they are minor products or do not form.

This work obtained unexpected results. It may cause from the pH of the solution is not suitable for the Ca-PbHAp formation. The Ca-PbHAp has been obtained at pH 12 (Verbeeck, Lassuyt, Heijligers, Driessens, and Vrojijk, 1981). However, this material also has been reported the formation at low pH of 3.92-5.22 (Yasukawa, Kamiuchi, Yokoyama, and Ishikawa, 2002) but the pH in this work is much lower than that (pH 2-3). This because we cannot adjust pH of metal solutions

in the experimental step due to the rapidly precipitate of $Pb(NO_3)_2$ with NaOH to form $Pb_6O_3(NO_3)_2(OH)_4$ (XRD peaks as shown in Appendix B, pp. 116). Adjusting pH of $Pb(NO_3)_2$ with $C_2H_4(NH_2)_2$ also shows the precipitation of solid phase ($Pb(OH)_2$) in the system (Narasaraju, Singh, and Lao, 1972). Therefore, the pH of solution is may an important factor for the formation of this material.

3.4 Conclusions

PHREEQC calculations show several Ca-P and Pb-P phases are supersaturated, suggesting multiple products could be formed. XRD results suggest the CaHAp and PbHAp phases are formed but Ca-PbHAp is not formed in this system. These results are agreement with the solid solution study that show the graph does not follow Vegard's law. The pH of solution in the system is may an important factor for the formation of this material.
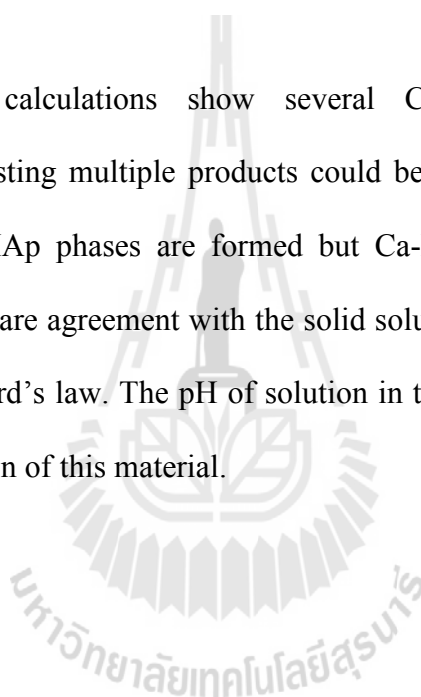
3.5 References

Bruker axs (2011). **XRD Commander Executable,** version 2.4.1.0, Bruker axs, Karlsruhe: Germany.

Dungkaew, W., Saisa-ard, O., and Haller, K. J. (2010). Phase characterization and saturation modeling of the calcium phosphate-arsenate apatite system. **Proceeding of the 14th International Annual Symposium on Computational Science and Engineering**, pp. 318-323. <http://www.mfu.ac.th/ anscse14/doc/ANSCSE14_proceedings_Eversion.pdf>, accessed on 16 May 2012.

LeGeros, R. Z. (1991). **Calcium Phosphates in Oral Biology and Medicine** (1st ed.). San Francisco, USA: Karger.

Narasaraju, T. S. B., Singh, R. P., and Rao, V. L. N. (1972). A new method of preparation of solid solutions of calcium and lead hydroxyapatites. **J. Inorg. Nucl. Chem.** 34: 2072-2074.

Parkhurst, D. L. and Appelo, C. A. J. (1999). **PHREEQC (version 2)-A computer program for speciation, batch-reaction, one-dimensional transport, and inverse geochemical calculations**. U.S. Department of the Interior and U.S. Geological Survey. <http://appt.home.xs4all.nl/index.html. The minteq.v4 database accessed with the PHREEQC software from http://www.phreeplot.org/ppihtml/minteq.v4.dat.html>, 16 May 2012.

Rajagopal, A., Dhanabalan, A., Major, S.S., and Kulkarni, S. K. (1998). The effect of different metal cation incorporation in arachidic acid Langmuir-Blodgett (LB) monolayer films. **Appl. Surf. Sci.** 125: 178-186.

Verbeeck, R. M. H., Lassuyt, C. J., Heijligers, H. J. M., Driessens, F. C. M., and Vrojijk, J. W. G. A. (1981). Lattice parameters and cation distribution of solid solutions of calcium and lead hydroxyapatite. **Calcif. Tissue Int.** 33: 243-247.

Yasukawa, A., Kamiuchi, K., Yokoyama, T., and Ishikawa, T. (2002). Preparation of lead-calcium hydroxyapatite solid solutions by a wet method using acetamide. **J. Solid State Chem.** 163: 27-32.

Yasukawa, A., Higashijima, M., Kandori, K., and Ishikawa, T. (2005). Preparation and characterization of cadmium-calcium hydroxyapatite solid solution particles. **Colloids and Surfaces, Section A** 268: 111-117.

Zhu, K., Yanagisawa, K., Shimanouchi, R., Onda, A., and Kajiyoshi, K. (2006). Preferential occupancy of metal ions in the hydroxyapatite solid solutions synthesized by hydrothermal method. **J. Eur. Ceram. Soc.** 26: 509-513.

Zhu, K., Yanagisawa, K., Shimanouchi, R., Onda, A., Kajiyoshi, K., and Qiu, J. (2009). Synthesis and crystallographic study of Pb-Sr hydroxyapatite solid solutions by high temperature mixing method under hydrothermal conditions. **Mater. Res. Bull.** 44: 1392-1396.

CHAPTER IV

GEL CRYSTALLIZATION OF LEAD-PHOSPHATE

MATERIALS[1]

4.1 Introduction

Gel crystallization is an interesting technique because of its simplicity and effectiveness in growing single crystals, especially of low solubility materials. This technique has been applied to the study of crystal formation of materials occurring in the human-related system, such as cholesterol stones, gall stones, and urinary calculi. Furthermore, it provides an ideal technique to study crystal deposition diseases, which could lead to better understanding of the cause of disease (Kalkura and Natarajan, 2010; Ramachandran and Natarajan, 2002; Girija, Yokogawa, and Nagata, 2004).

The two methods used most often to grow crystals in gel media are single diffusion and double diffusion methods (Santhana Raghavan and Ramasamy, 2000)

Single diffusion method

This method is a suitable method for highly soluble compounds which do not react chemically with the gel medium. The "inner reactant" is set with the gel

---

medium in the bottom layer of the container. After gel setting, the other reactant solution called the "outer reactant", is poured on top of the gel layer. The chemical reaction occurs as the two reactants meet and crystals are obtained. The setting of this method is shown in Figure 4.1.
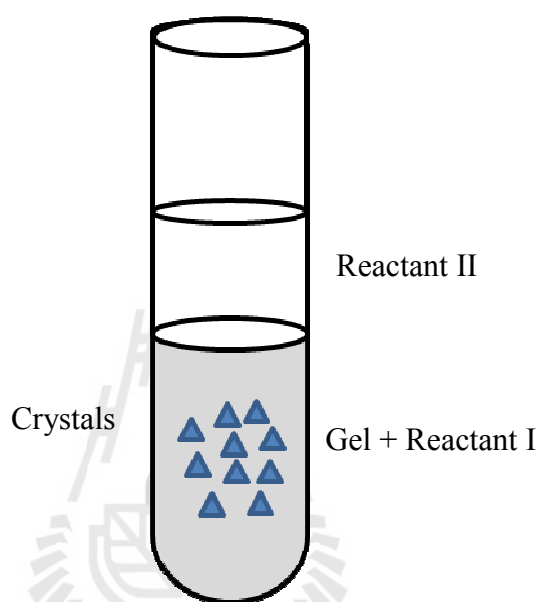
Figure 4.1 Schematic illustration of the single diffusion method.

Double diffusion method

This method is more suitable for insoluble compounds or materials that react with the gel medium. The reactant solutions are separated in the side arms of a U-tube (Figure 4.2) by placing the two reactant solutions on top of the gel medium in the opposing tubes after gel setting. Reactants diffuse through the gel medium and the reaction occurs at the point they meet.
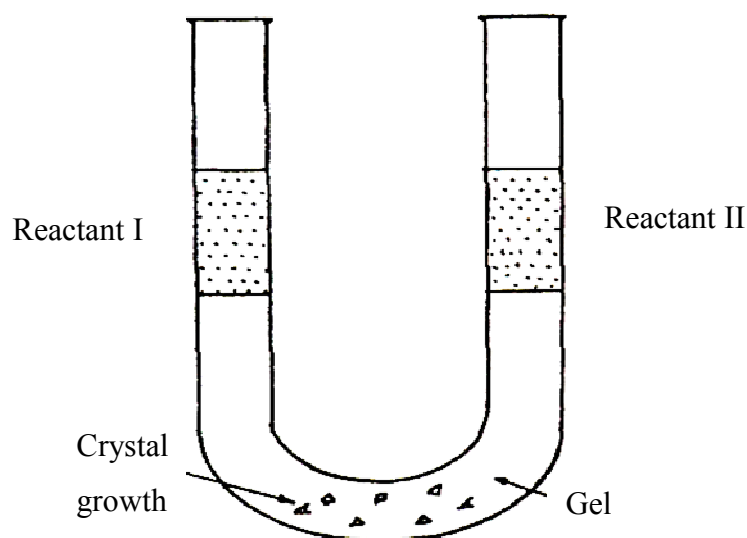
Figure 4.2 Schematic illustration of the double diffusion method.

Importance of gel technique

      Growth of crystals in gel is a good technique not only for preparation of large single crystals but also for control of defect formation. If the formation of crystals is not perfect, it leads to imperfect determination of the physical properties such as optical, electrical, and mechanical properties of the crystals (Santhana Raghavan and Ramasamy, 2000). Some important features of this technique are listed below:

- The rate of reaction and nucleation can be controlled by varying the density of the gel medium.

- The gel medium holds the crystals in fixed positions, minimizing external disturbances.

- Fewer defects occur during the formation of crystals because of the slow controlled rate of reaction.

- The crystals can be harvested easily

- The growth of crystals at each stage can be observed in the glass reaction vessel.

Crystallization of lead-phosphate materials in gel systems

Lead-phosphate (Pb-P) materials are interesting materials due to their properties. Lead hydrogen phosphate ($PbHPO_4$) and lead nitrate phosphate ($Pb_2(NO_3)(PO_4)$) show dielectric, piezoelectric, and optical properties which are useful in transducers and memory devices. Lead phosphate ($Pb_3(PO_4)_2$) is known as a ferroelastic material with a phase transition near 180 °C. The phase changes from α-phase ($C2/c$ ferroelastic phase) below 180 °C to β-phase ($R\bar{3}m$ prototypic phase) above 180 °C (Guimaraes, 1979; Decker, Petersen, and Debray, 1979). Several researchers have reported growth of $PbHPO_4$ and $Pb_2(NO_3)(PO_4)$ in silica hydrogel, tetramethoxysilane gel, cross-linked polyacylamide gel, agar gel, and gelatin, (Desai and Ramana,1990; Desai and Ramana, 1998; Robert and Lefaucheux, 1988; Březina, Havránková, and Dušek, 1976). The appearance of small crystals of lead hydroxyapatite, $Pb_5(PO_4)_3(OH)$, (PbHAp), in the gel layers or on the surfaces of other Pb-P products has not been reported. PbHAp is a material of biological interest because of the similarity to calcium hydroxyapatite, $Ca_5(PO_4)_3(OH)$, (CaHAp), the dominant component in mammalian hard tissues such as bones and teeth; about 69 wt % and 95 wt %, respectively (LeGeros, 1991). The relationship of PbHAp to CaHAp and its link to bone diseases like osteoporosis make the crystallization and growth of these materials of interest.

This chapter presents results of Pb-P material growth in agarose gel with varied density of the gel medium. The PHREEQC speciation program (Parkhurst and

Appelo, 1999) is used in this work to calculate possible phases in the Pb-P system supporting formation of PbHAp and other Pb-P phases. The relationship between synthesis conditions and crystal phases of products, including the formation of PbHAp, are discussed based on the results obtained.

4.2 Experimental

Reagents

Reagents for preparation of gel medium

- Agarose powder (Vivantis, molecular biology grade)

Reagents for preparation of lead phosphate material

- Diammonium hydrogen phosphate, $(NH_4)_2HPO_4$ (Ajax Finechem, AR grade)

- Lead(II) nitrate, $Pb(NO_3)$ (Ajax Finechem, AR grade)

Reagents for adjusting pH

- Sodium hydroxide, NaOH (Eka Chemicals AB, AR grade)

All solutions in this experiment were prepared from deionized water.

Sample preparation

Diffusion of two soluble compounds through the agarose gel was set for the crystal growth in tubes as illustrated schematically in Figure 4.3. Crystalline products are obtained in the gel when the two reactants meet. $(NH_4)_2HPO_4$ and $Pb(NO_3)_2$ were used as PO_4^{3-} and Pb^{2+} sources, respectively. Varied densities of phosphate gel (1.0, 1.3, 1.5, 1.7, and 2.0 % w/v of agarose) were prepared by dissolving agarose powder in 20 mL water with stirring for 10 min at 100 °C to give clear solutions.

Crystallization experiments were set in small test tubes (1.5 x 10 cm) by adding 3.0 mL of the appropriate hot gel solution to 2.5 mL of warm 0.6 M phosphate solution, adjusting pH to 10 with NaOH, and allowing the mixture to stand 20 min to cool to room temperature to gel. A second layer of pure gel (1.0, 1.5, and 2.0 % w/v) was created by adding 1.5 mL of pure gel solution on top of the PO_4^{3-} gel layer and allowing 20 min to set the pure gel layer, after which 2.5 mL of 1.0 M lead nitrate solution at natural pH was added on top of the gel layers. All reactions were kept at room temperature for two weeks. CO_2 was purged from the lead solution by passing Ar gas through the solution for 5 min before transfer.

After two weeks the remaining solution was removed and the gel layers separated. Each gel layer was warmed to melt the gel and the solid products filtered off. The three solutions were combined and pH measured. The solids were washed with cold water and dried at 100 °C for 24 h.
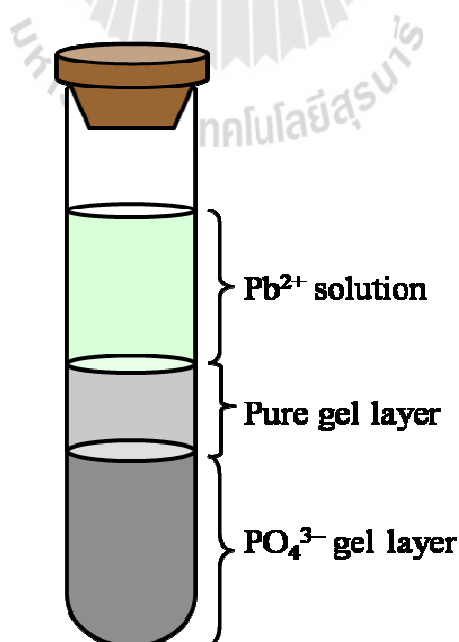
Figure 4.3 Experimental set up for gel crystallization of lead-phosphate phases.

Characterization

Crystal morphologies were observed by optical microscopy using an Olympus SZ40 microscope (Olympus, Japan) and scanning electron microscopy (SEM) using a JSM 6400 electron microscope (JEOL, Japan). IR spectra were acquired on a Perkin-Elmer model Spectrum GX Fourier transform infrared spectrophotometer (FTIR) in wave number range 400-4000 cm^{-1} from KBr pellets. Powder X-ray diffraction (XRD) scans were used for phase identification, 2θ range 10-60° using a D5005 diffractometer equipped with a Cu Kα X-ray source operating at 40 kV and 40 mA and the XRD Commander Executable analysis software (Bruker axs, 2011). The speciation program, PHREEQC V2 with the MinteqV4 database (Parkhurst and Appelo, 1999) was used to calculate potential phase formation in the system assuming complete instantaneous mixing of the reactants.

4.3 Results and discussion

Crystalline products were obtained inside both pure and PO_4^{3-} gel layers for all reactions as observed after two weeks reaction time. A typical result (density of phosphate and pure gel of 1.7 and 2.0 % w/v, respectively) is shown in Figure 4.4.
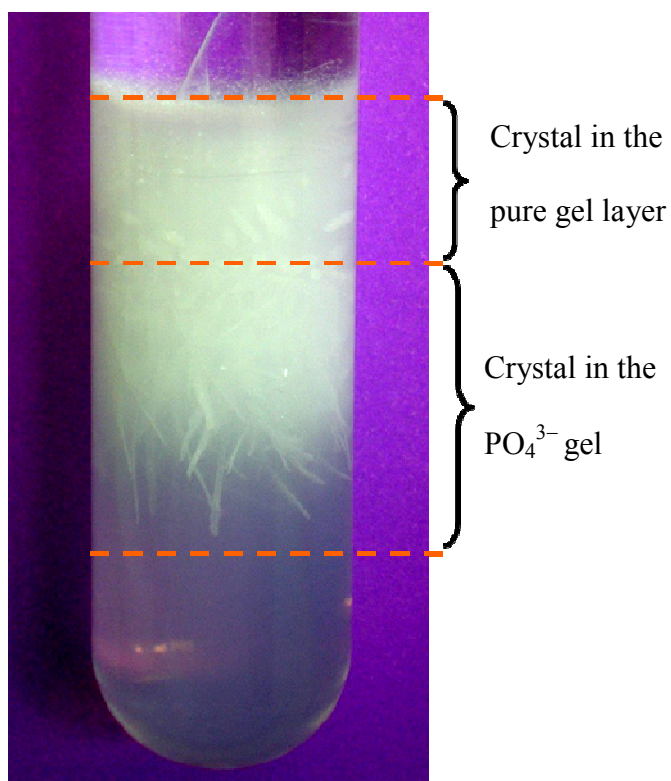
Figure 4.4 Crystalline products in pure and PO_4^{3-} gel layers for a typical reaction.

Microscopic crystalline products were accompanied by a decrease in pH to 3 for all reactions studied. Their morphologies were observed by optical microscopy and SEM. The crystal morphologies of products formed in the pure gel and PO_4^{3-} gel layers are illustrated in Figure. 4.5 and 4.6, respectively.
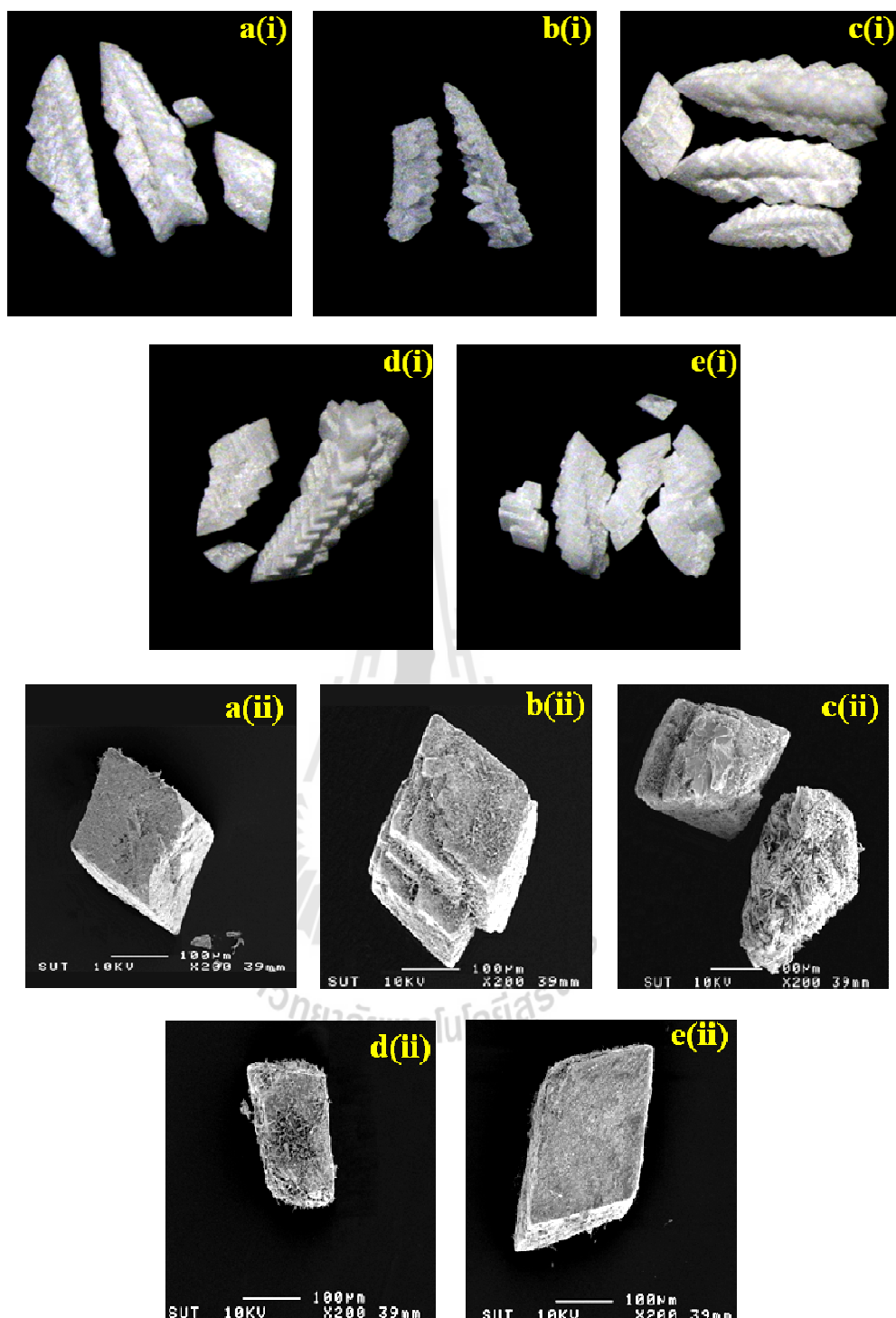
Figure 4.5 Optical and SEM images of products formed in the pure gel layer. i) Optical (2.5X) and ii) SEM images. Density of pure gel layer is 2.0 % w/v but different density of PO_4^{3-} gel: (a) 1.0, (b) 1.3, (c) 1.5, (d) 1.7, (e) 2.0 % w/v.
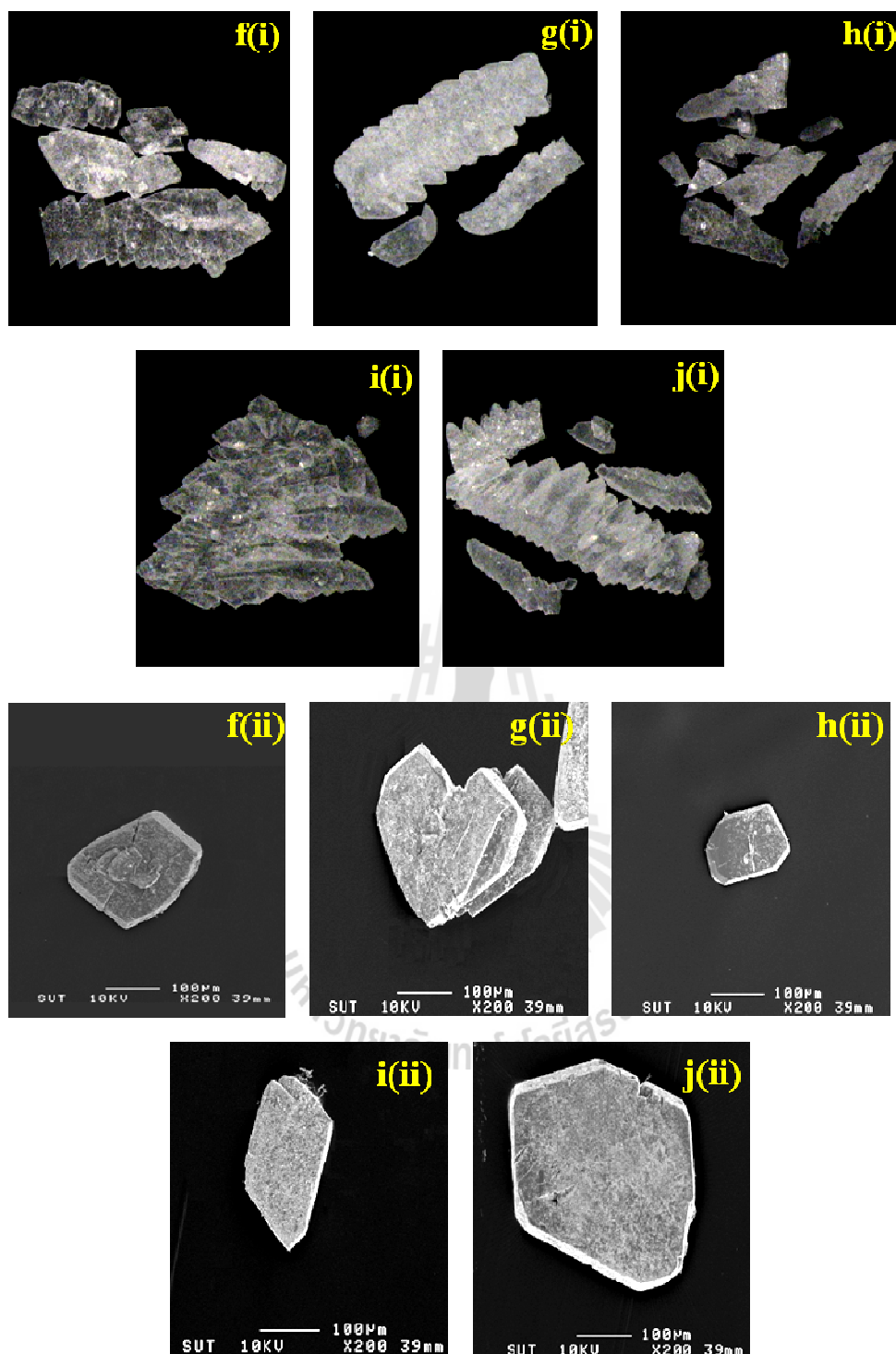
Figure 4.6 Optical and SEM images of products formed in the PO_4^{3-} gel layer. i) Optical (2.5X) and ii) SEM images. Density of pure gel layer is 2.0 % w/v but different density of PO_4^{3-} gel: (a) 1.0, (b) 1.3, (c) 1.5, (d) 1.7, (e) 2.0 % w/v.

Products appear as aggregates under optical microscopy in the pure gel layer (Figure 4.5a(i)-e(i)) and in the PO_4^{3-} gel layer (Figure 4.6f(i)-j(i)). Individual crystallites from the pure gel layer show equant habit (Figure 4.5a(ii)-e(ii)), and those from the PO_4^{3-} gel layer show plate-like habit (Figure 4.6f(ii)-j(ii)) as seen in low magnification SEM images.

Needle-like crystals with dimension about 2.5 x 10 μm are deposited on the surfaces of crystal products formed in the pure gel layer as can be seen in SEM images at higher magnification as shown in Figure 4.7. These crystals have similar morphology to those reported for PbHAp (Mavropoulos, Rocha, Moreira, Rossi, and Soares, 2004). This observation further confirms that multiple product phases occur in this system, and indicates that they occur in sequential fashion. These small crystallites observed only in the pure gel layer occur for all the different densities of PO_4^{3-} gel layer.

IR wave number and assignments for the products are given in Table 4.1. All products give almost identical spectra that show characteristic bands of PO_4^{3-} group; bands in the regions 955-1046 cm^{-1}, 923-924 cm^{-1}, and 519-601 cm^{-1} reveal the asymmetric P–O stretching (υ_3), symmetric P–O stretching (υ_1), and O–P–O bending (υ_4), respectively.

An ideal PO_4^{3-} anion has tetrahedral point symmetry. Only absorptions corresponding to the υ_3 (955-1046 cm^{-1}) and υ_4 (519-601 cm^{-1}) vibrations should be observed. The υ_1 (923-924 cm^{-1}) and υ_2 (388-449 cm^{-1}) vibrations would be allowed in lower symmetry groups. The appearance of υ_1 and υ_2 in the IR spectra of both

products from pure and PO_4^{3-} gel layers indicates the lower symmetry of PO_4^{3-} in the structure (Bhatnagar, 1970; Ternane, Ferid, Trabelsi-Ayedi, and Piriou, 1999).

Figure 4.7 SEM images of products obtained in the pure gel layer. Density of pure gel layer is 2.0 % w/v but different density of PO_4^{3-} gel: (a) 1.0, (b) 1.3, (c) 1.5, (d) 1.7, (e) 2.0 % w/v.
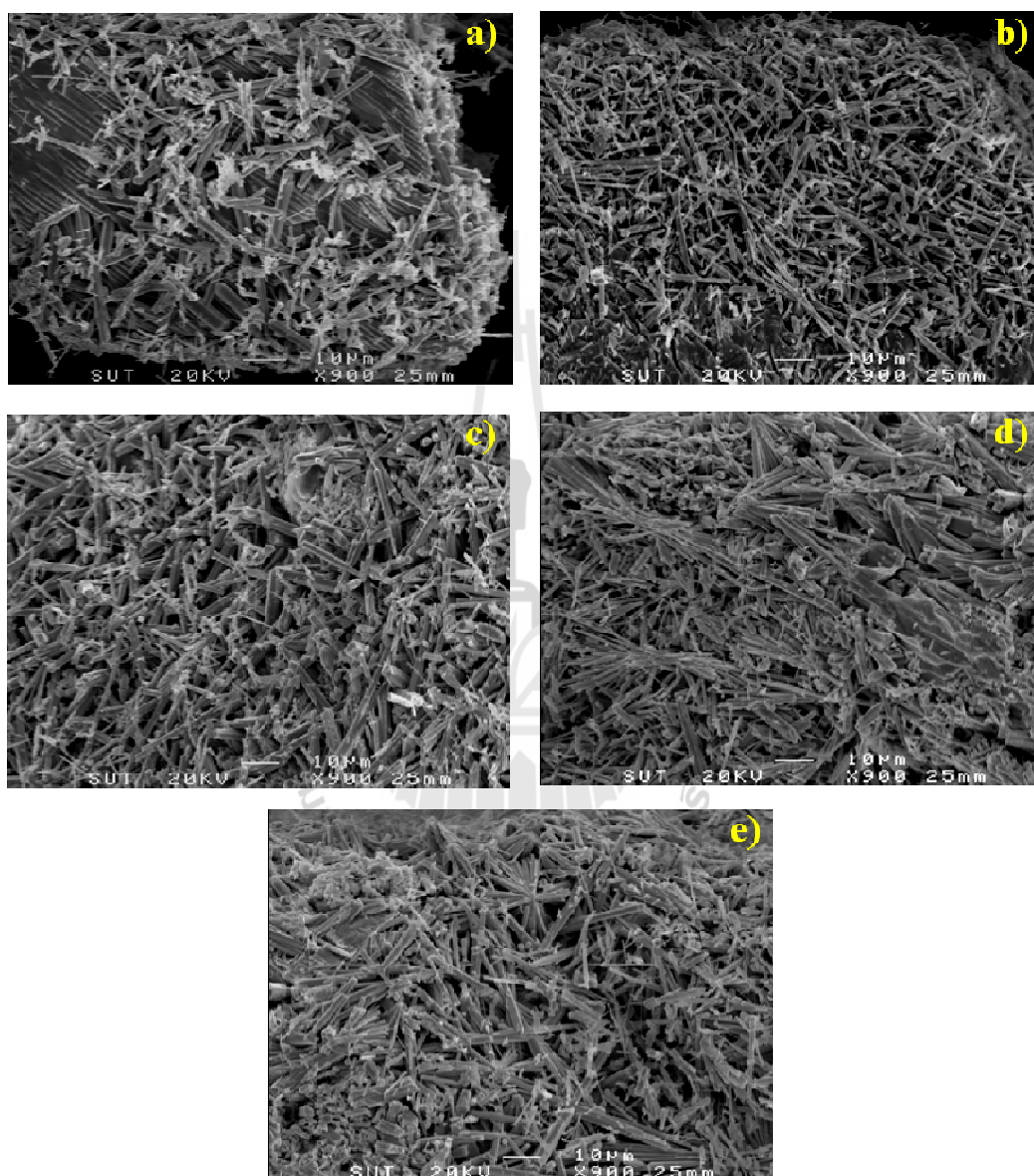
Table 4.1 IR frequencies and vibrational assignments of crystal products from pure and phosphate gel layers.

Crystal in the pure gel layer (cm^{-1})	Crystal in the PO_4^{3-} gel layer (cm^{-1})	Assignment
~3555 w, b		$(\upsilon_1 + \upsilon_3)$ H_2O stretch
~1604 m		$\upsilon_2 H_2O$ bend
1384 vs		$(\upsilon_1 + \upsilon_3)$ NO_3 stretch
1348 vs		
1046 sh	~1100 s,b	$\upsilon_3 PO_4$ stretch
1004-1005 vs		
955-956 vs		$\upsilon_1 PO_4$, $\upsilon_1 HPO_4$
923-924 vs		stretch
813-814 vw		$\upsilon_2 NO_3$ bend
715-716 vw		H_2O libration
705-706 vw		
600-601 m		
539 m	548 s	$\upsilon_4 PO_4$ bend
519-520 m		
398 sh	449 w	$\upsilon_2 PO_4$ bend,
	388 vw	$\upsilon_2 HPO_4$ bend

Abbreviations: w = weak, m = medium, s = strong, v = very, sh = shoulder, b = broad. Assignments: υ_1 = symmetric stretching, υ_2 = bending, υ_3 = asymmetric stretching, υ_4 = bending.

Water bending mode (1604 cm^{-1}) and O–H stretching mode (3555 cm^{-1}) are observed for the products obtained inside the pure gel layer but not for products obtained inside the PO$_4^{3-}$ gel layer. IR spectra of products formed in the pure gel layer also show nitrate bands at 1348-1384 and 813-814 cm^{-1} which, along with the water bands, disappear after heating at 600 °C (Figure 4.8). These bands may be due to residual nitrate from starting compound as suggested in previous work (Stepuk, Veresov, Putlyaev, and Tret'yakov, 2007). It is also possible that the nitrate and water bands represent an additional unidentified phase.
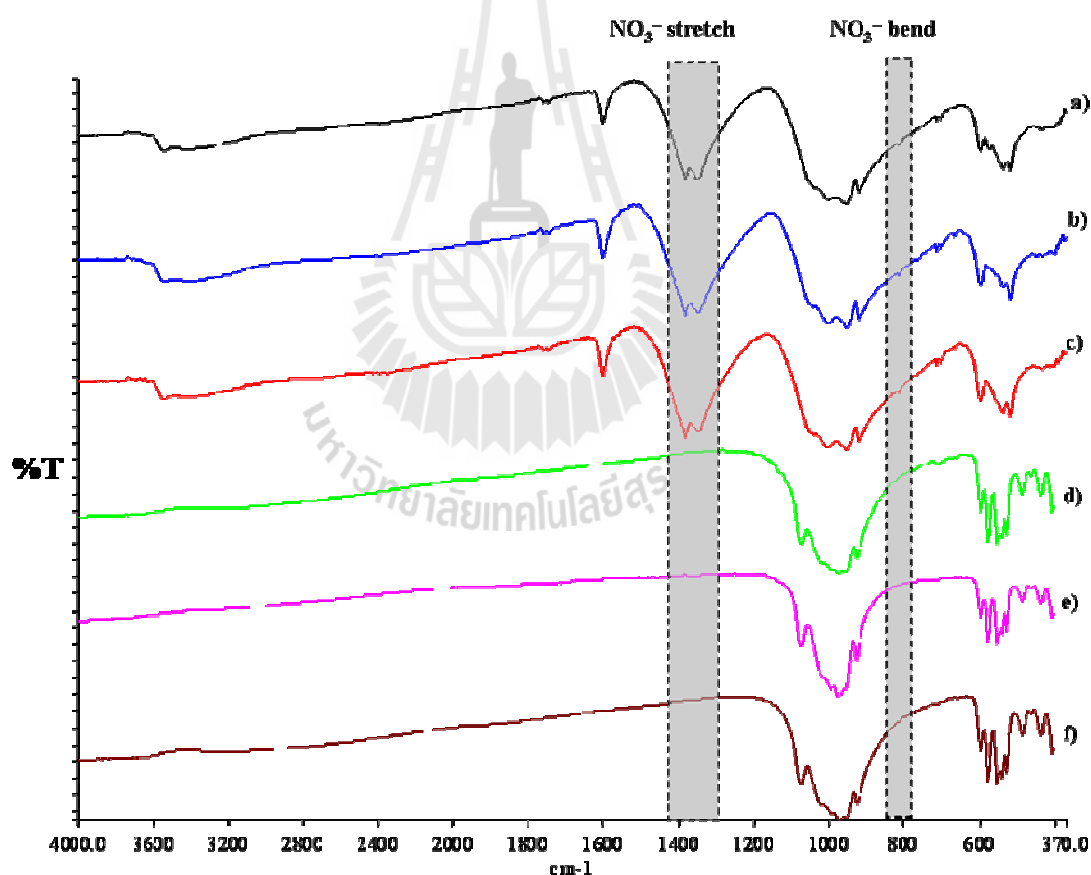
Figure 4.8 IR spectra of products formed in the pure gel layer. (a-c) before heating and (d-f) after heating at 600 °C. Density of pure gel layer is 2.0 % w/v but different density of PO$_4^{3-}$ gel: (a, d) 1.0, (b,e) 1.5, (c, f) 2.0 % w/v.

Products obtained in the pure gel layer exhibit a mixture of three phases including PbHAp (JCPDS 1-0924), PbHPO$_4$ (JCPDS 6-0274), and Pb$_3$(PO$_4$)$_2$ (JCPDS 13-0278) as shown in Figure 4.9 while products formed in the PO$_4^{3-}$ gel layer show only peaks due to PbHPO$_4$ and Pb$_3$(PO$_4$)$_2$ (Figure 4.10).

Peaks due to PbHAp and Pb$_3$(PO$_4$)$_2$ phases are difficult to see because they are minor products. Small needle-like PbHAp crystals on the surface of products separated from the pure gel layer can be seen in the SEM images in Figure 4.7.
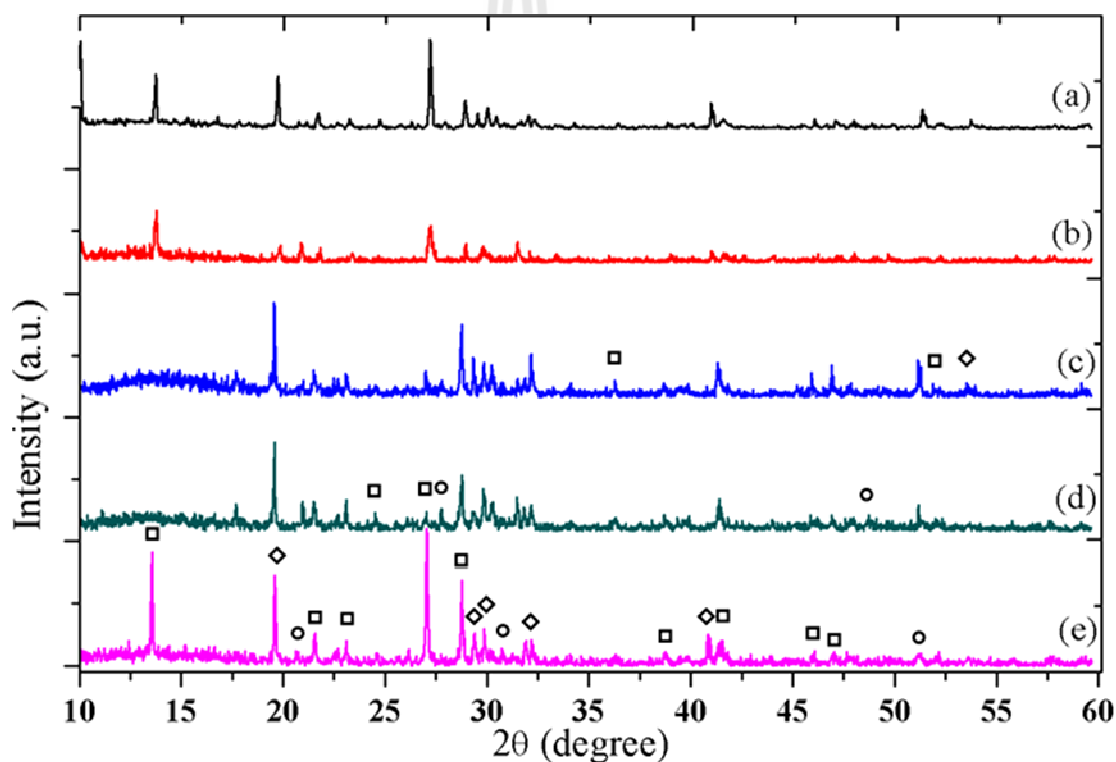
Figure 4.9 XRD patterns of products obtained in the pure gel layer. Density of pure gel layer is 2.0 % w/v but different density of PO$_4^{3-}$ gel: (a) 1.0, (b) 1.3, (c) 1.5, (d) 1.7, and (e) 2.0 % w/v; (□) PbHPO$_4$, (◊) Pb$_3$(PO$_4$)$_2$, and (○) PbHAp.
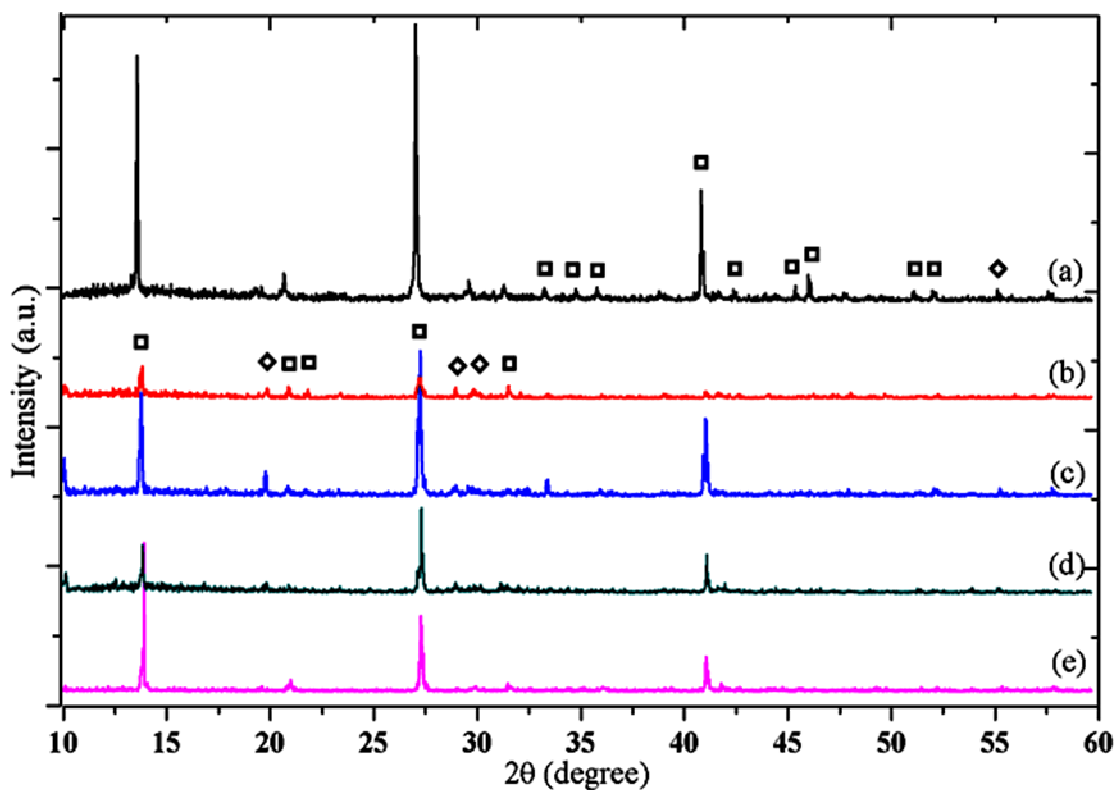
Figure 4.10 XRD patterns of products obtained in the PO_4^{3-} gel layer. Density of
pure gel layer is 2.0 % w/v but different density of PO_4^{3-} gel: (a) 1.0, (b)
1.3, (c) 1.5, (d) 1.7, and (e) 2.0 % w/v; ($\square$) $PbHPO_4$, ($\lozenge$) $Pb_3(PO_4)_2$, and
($\circ$) PbHAp.

These results are consistent with predictions (assuming instantaneous mixing
of all reactants in an aqueous solution) obtained from the PHREEQC program that
calculates saturation indices based on aqueous solution activities for all species
involved. A description of the PHREEQC program methodology is given in the
Chapter I (pp. 25-26).

Calculation of saturation index (SI) requires detailed knowledge of the
speciation of phosphate, lead compounds, and other related ions in the system.

Speciation of relevant phosphate and lead compounds in the system is given in Table 4.2.

Table 4.2 Acid dissociation constants (K_a) for H_3PO_4 speciation, and solubility product constants (K_{sp}) and SI for various lead compounds.

H_3PO_4 speciation	K_a[1]	
$H_3PO_4 \rightleftharpoons H_2PO_4^- + H^+$	6.309×10^{-3}	
$H_2PO_4^- \rightleftharpoons HPO_4^{2-} + H^+$	6.760×10^{-8}	
$HPO_4^{2-} \rightleftharpoons PO_4^{3-} + H^+$	4.466×10^{-13}	
Relevant lead compounds	K_{sp}[2]	SI[3]
$Pb_5(PO_4)_3OH + 7H^+ \rightleftharpoons 5Pb^{2+} + 3H_2PO_4^- + H_2O$	1.621×10^{-63}	13.17
$Pb_3(PO_4)_2 + 4H^+ \rightleftharpoons 3Pb^{2+} + 2H_2PO_4^-$	2.951×10^{-44}	7.88
$PbHPO_4 \rightleftharpoons Pb^{2+} + HPO_4^{2-}$	1.584×10^{-24}	2.08
$Pb(OH)_2 + 2H^+ \rightleftharpoons Pb^{2+} + 2H_2O$	1.606×10^{-9}	−0.46

[1]Values from reference (Ure and Davidson, 1995)

[2]Values from minteq.v4 database in reference (Parkhurst and Appelo, 1999)

[3]This work for the system described in the text.

An initial pH = 10 in the PO_4^{3-} gel and initial pH of 6 in the 1 M $Pb(NO_3)_2$ solution, imply a pH gradient through the "pure" gel layer from 10 to 6 as the reactants diffuse together (if all three layers were instantaneously mixed as an aqueous solution the pH would be 8). At pH = 10 the phosphate speciation (Figure 4.11) predicts a small PO_4^{3-} concentration and HPO_4^{2-} as the dominant species. At pH

= 6 $H_2PO_4^-$ is the dominant species with only a few percent HPO_4^{2-} and even less PO_4^{3-}. PHREEQC calculations based on the total initial concentrations of species in all layers combined indicate that $PbHPO_4$, $Pb_3(PO_4)_2$, and PbHAp would be supersaturated (pH = 8, and SI = 2.08, 7.88, and 13.17, respectively). The larger SI for the PO_4^{3-} containing species in spite of the low PO_4^{3-} concentration is a result of their solubilities being considerably lower than that of the HPO_4^{2-} containing species, and suggests they may nucleate first.
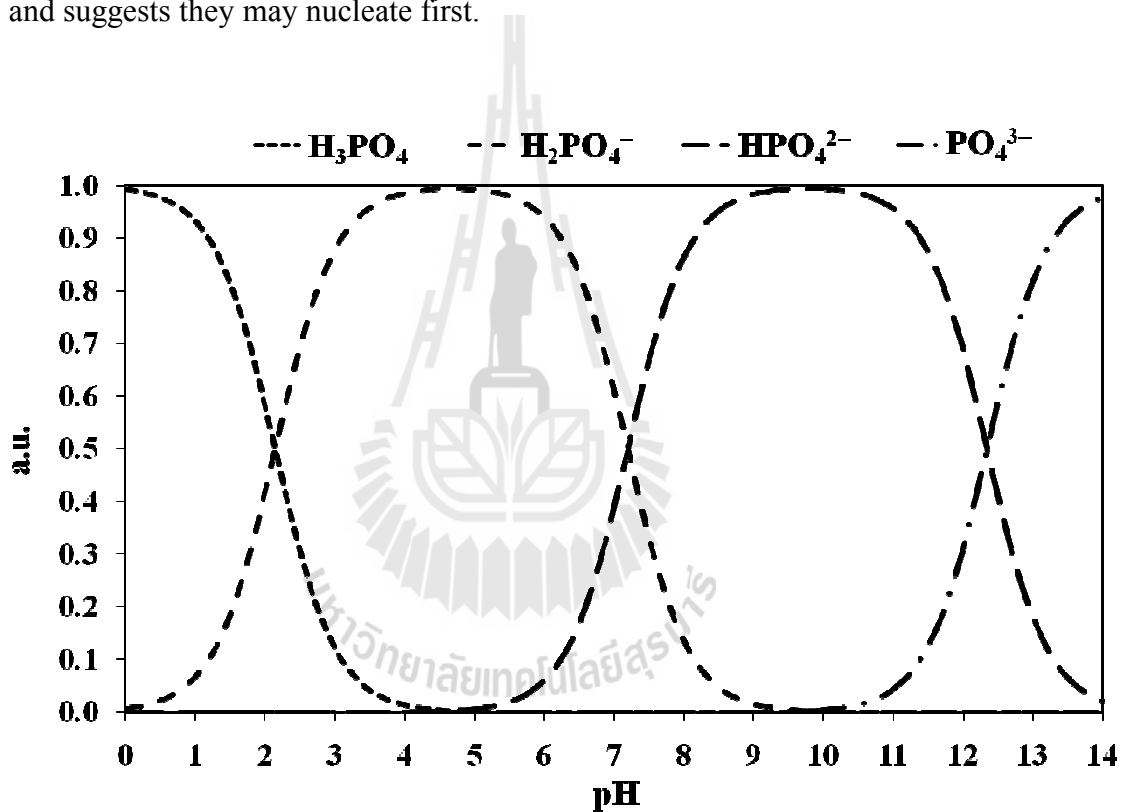
Figure 4.11 pH variation of ionic concentrations in the tripotic equilibrium for phosphoric acid solutions.

As phosphate ion is removed from the gel by precipitation, the speciation equilibrium will convert HPO_4^{2-} to H^+ and PO_4^{3-}, lowering the pH and at the same time adjusting the relative ion concentrations to favor HPO_4^{2-} until the hydrogen

phosphate species nucleates. Of course if the hydrogen phosphate species nucleates first, the opposite logic applies until the phosphate compounds nucleate, but this would require two separate phosphate compounds to reach supersaturation and nucleate, which seems less probable. As growth proceeds, the trajectory of the pH will be determined by the relative sequestering of either or both phosphate or hydrogen phosphate in the solid phases

At the beginning of the experiment, the pH gradient in the pure gel layer is predisposed to higher pH by the procedure of placing the pure gel solution on the phosphate gel layer. Diffusion of ions from the phosphate layer will commence immediately, and a small amount of the phosphate gel will dissolve before the "pure" gel sets. Both effects favor increased PO_4^{3-} ion concentration near the lead solution, favouring initial precipitation of the phosphate phases in the pure gel layer. The presence of PbHAp in the pure gel layer but not in the phosphate layer can be understood based on the higher $Pb^{2+}:PO_4^{3-}$ ratio (5:3 vs 3:2) required for the PbHAp phase relative to the $Pb_3(PO_4)_2$ phase.

4.4 Conclusions

Speciation calculations indicate the possibility of forming mixed phases of $PbHPO_4$, $Pb_3(PO_4)_2$, and PbHAp in this system. XRD results confirm their formation, including the previously unreported gel precipitation of PbHAp. IR spectra of the crystalline products exhibit υ_1 and υ_2 vibrational bands indicating the point symmetry of PO_4^{3-} is lower than tetrahedral. Formation of the microscopic crystalline products was accompanied by a decrease in pH from 8 (theoretical for all layers mixed) to 3 for all reactions studied, consistent with PbHPO4 being the major product. Formation

of $PbHPO_4$, $Pb_3(PO_4)_2$, and PbHAp phases with changing pH may be an important key for better understanding of the precipitation of biological hard tissues and the environmental geology of lead and phosphorus.

4.5 References

Březina, B., Havránková, M., and Dušek, K. (1976). The growth of $PbHPO_4$ and $Pb_4(NO_3)_2(PO_4)_2 \cdot 2H_2O$ in gels. **J. Cryst. Growth** 34: 248-252.

Bhatnagar, V. M. (1970). The preparation, X-ray and infrared spectra of lead apatites. **Archs. Oral Biol.** 15: 469-480.

Bruker axs (2011). **XRD Commander Executable,** version 2.4.1.0, Bruker axs, Karlsruhe: Germany.

Decker, D. L., Petersen, S., and Debray, D. (1979). Pressure-induced ferroelastic phase transition in $Pb_3(PO_4)_2$: A neutron-diffraction study. **Phys. Rev., Section B** 19: 3552-3555.

Desai, C. C. and Ramana, M. S. V. (1990). Nucleation density and electrolytic growth of lead hydrogen phosphate single crystals in silica gels. **J. Cryst. Growth** 102: 191-196.

Desai, C. C. and Ramana, M. S. V. (1998). Growth and properties of ferroelectric lead hydrogen phosphate and lead nitrate phosphate single crystals. **J. Cryst. Growth** 91: 126-134.

Girija, E. K., Yokogawa, Y., and Nagata, F. (2004). Apatite formation on collagen fibrils in the presence of polyacrylic acid. **J. Mater. Sci. Mater. Med.** 15: 593-599.

Guimaraes, D. M. C. (1979). Ferroelastic Transformations in lead orthophosphate and its structure as a function of temperature. **Acta Crystallogr., Section A** 35: 108-114.

Kalkura, S. N. and Natarajan, S. (2010). **Springer Handbook of Crystal Growth**, Part H, DOI: 10.1007/978-3-540-74761-1_48.

LeGeros, R. Z. (1991). **Calcium Phosphates in Oral Biology and Medicine** (1st ed.). San Francisco, USA: Karger.

Mavropoulos, E., Rocha, C. C. N., Moreira, C. J., Rossi, M. A., and Soares, A. G. (2004). Characterization of phase evolution during lead immobilization by synthetic hydroxyapatite. **Mater. Charact.** 53: 71-78.

Parkhurst, D. L. and Appelo, C. A. J. (1999). **PHREEQC (version 2)-A computer program for speciation, batch-reaction, one-dimensional transport, and inverse geochemical calculations**. U.S. Department of the Interior and U.S. Geological Survey. <http://appt.home.xs4all.nl/index.html. The minteq.v4 database accessed with the PHREEQC software from http://www.phreeplot.org/ppihtml/minteq.v4.dat.html>, 16 May 2012.

Ramachandran, E. and Natarajan, S. (2002). Crystal growth of some urinary stone constituents: II. In-vitro crystallization of hippuric acid. **Cryst. Res. Technol.** 37: 1274-1279.

Robert, M. C. and Lefaucheux, F. (1988). A comparative study of gel grown and space grown lead hydrogen phosphate crystals. **J. Cryst. Growth** 88: 499-510.

Saisa-ard, O. and Haller, K. J. (2012). Crystallization of lead phosphate in gel systems. **Eng. J.** Accepted for publication 8 May 2012. DOI: 10.4186/ej.2012.

Santhana Raghavan, P. and Ramasamy, P. (2000). **Crystal Growth: Processes and Methods**. Chennai: Hi-Tech Offset.

Stepuk, A. A., Veresov, A. G., Putlyaev, V. I., and Tret'yakov, Y. D. (2007). The influence of NO_3^-, CH_3COO^-, and Cl^- ions on the morphology of calcium hydroxyapatite crystals. **Dokl. Akad. Nauk.** 412: 11-14.

Ternane, R., Ferid, M., Trabelsi-Ayedi, M., and Piriou, B. (1999). Vibrational spectra of lead alkali apatites $Pb_8M_2(PO_4)_6$ with M = Ag and Na. **Spectrochim. Acta, Section A** 55: 1793-1797.

Ure, A. M. and Davidson, C. M. (1995). **Chemical Speciation in the Environment** (1st ed.). Glasgow, UK: Chapman and Hall.

CHAPTER V

CRYSTALLIZATION OF LEAD HYDROXYAPATITE

BY USING REFLUX METHOD[1]

5.1 Introduction

Reflux method

Reflux allows a mixture to be heated constantly without monitoring and without loss of material. A reflux vessel such as a round bottom flask is attached to a water cooled condenser which prevents vapors from escaping during the heating process.

The advantage of this technique is that it can be left for a long period of time without the need to add more solvent or fear of the reaction vessel boiling dry as any vapor is immediately condensed and returned to the reaction vessel. In addition as a given solvent will always boil at a certain temperature, one can be sure that the reaction will proceed at a constant temperature. By careful choice of solvent, one can control the temperature within a very narrow range. The constant boiling action also serves to continuously mix the solution, although a magnetic stirring rod mechanism is often used to assist achievement of a uniform solution. This technique is useful for performing chemical reactions under controlled conditions that require substantial time for completion.

---

[1]This work has been submitted for publication (Saisa-ard and Haller, 2012).
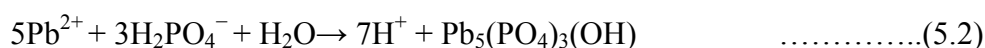
Crystallization of lead hydroxyapatite by calcium hydroxyapatite dissolution

Calcium hydroxyapatite, $Ca_5(PO_4)_3(OH)$, (CaHAp) is of interest because of its occurrence in biological hard tissues such as bones and teeth (LeGeros, 1991). Divalent cations such as Pb^{2+} can substitute for Ca^{2+} ions in the CaHAp structure. Complete substitution of Pb^{2+} ions into CaHAp structure results in isostructural lead hydroxyapatite, $Pb_5(PO_4)_3(OH)$, (PbHAp). PbHAp has been studied including its structure (Brückner, Lusvardi, Menabue, and Saladini, 1995; Kim, Fenton, Hunter, and Kennedy, 2000) and solubility properties (Valsami-Jones, Ragnarsdottir, Putnis, Bosbach, and Kemp, 1998) partly because the accumulation of Pb^{2+} in bones can lead to bone diseases like osteoporosis. Therefore, the relationship between CaHAp and PbHAp in terms of their structure and properties might be an important key for understanding the accumulation of Pb^{2+} in bone. Studies of Pb^{2+} immobilization by synthetic CaHAp have been reported (Mavropoulos, Rossi, and Costa, 2002; Mavropoulos, Rocha, Moreira, Rossi, and Soares, 2004), and show dissolution of CaHAp in Pb^{2+} solution and then concomitant crystallization of PbHAp in the system. The mechanism in acidic conditions has been proposed (Dong, Zhu, Qiu, and Zhao, 2010) as

Dissolution:

$$Ca_5(PO_4)_3(OH) + 7H^+ \rightarrow 5Ca^{2+} + 3H_2PO_4^- + H_2O \qquad \text{…………..(5.1)}$$

Precipitation:

$$5Pb^{2+} + 3H_2PO_4^- + H_2O \rightarrow 7H^+ + Pb_5(PO_4)_3(OH) \qquad \text{…………..(5.2)}$$

This chapter reports preparation of larger PbHAp crystals for studies of their structure and solubility properties. A reflux method was used to increase CaHAp dissolution rate, and thus, PbHAp crystallization rate in the system. The relationship between reaction times and crystal morphologies of products is discussed.

5.2 Experimental

Reagents

Reagents for preparation of CaHAp and PbHAp materials

- Diammonium hydrogen phosphate, $(NH_4)_2HPO_4$ (Ajax Finechem, AR grade)

- Calcium nitrate tetrahydrate, $Ca(NO_3)_2 \cdot 4H_2O$ (Ajax Finechem, AR grade)

- Lead(II) nitrate, $Pb(NO_3)_2$ (Ajax Finechem, AR grade)

Reagents for adjusting pH

- Sodium hydroxide, NaOH (Eka Chemicals AB, AR grade)

All solutions in this experiment were prepared from deionized (DI) water.

Preparation of CaHAp material

CaHAp was prepared by dropwise addition of 100 mL of 0.6 M $(NH_4)_2HPO_4$ solution into 100 mL of 1.0 M calcium nitrate solution prepared from $Ca(NO_3)_2 \cdot 4H_2O$, while stirring at room temperature and maintaining pH of the solution at 11 with 1.0 M NaOH. After addition of the phosphate solution, the suspension was stirred continuously 30 min. The precipitate was separated by filtration, washed with water three times, and dried at 100 °C for 24 h.

Crystallization of PbHAp by reflux method

Ground CaHAp, 0.2 g, was added into 80 mL of 917 mg/L Pb^{2+} solution

(0.1172 g of $Pb(NO_3)_2$) and refluxed for 24 h or 48 h. The precipitates were separated

by filtration, washed with water three times, and dried at 100 °C for 24 h.

Characterization

Crystal morphologies were observed by scanning electron microscopy (SEM)

using a JSM 6400 electron microscope (JEOL, Japan) equipped with energy

dispersive X-ray fluorescence (EDX). IR spectra were acquired on a Perkin-Elmer

model Spectrum GX Fourier transform infrared spectrophotometer (FTIR) in

wavenumber range 400-4000 cm^{-1} from KBr pellets. Powder X-ray diffraction

(XRD) scans were acquired for the 2θ range 10-55° on a Bruker axs D5005

diffractometer equipped with a Cu Kα X-ray source operating at 40 kV and 40 mA,

and the XRD Commander Executable analysis software (Bruker axs, 2011) for phase

identification of products.

5.3 Results and discussion

The SEM images of CaHAp before and after refluxing are shown in Figure

5.1. Crystalline product after refluxing for 24 h exhibits needle-like crystal

morphology (Figure 5.1b), while crystalline product after refluxing for 48 h shows

hexagonal-rod crystal morphology (Figure 5.1c). The product crystal size increased

with increasing reaction time; the largest crystal size is about 10 x 10 x 40 μm.
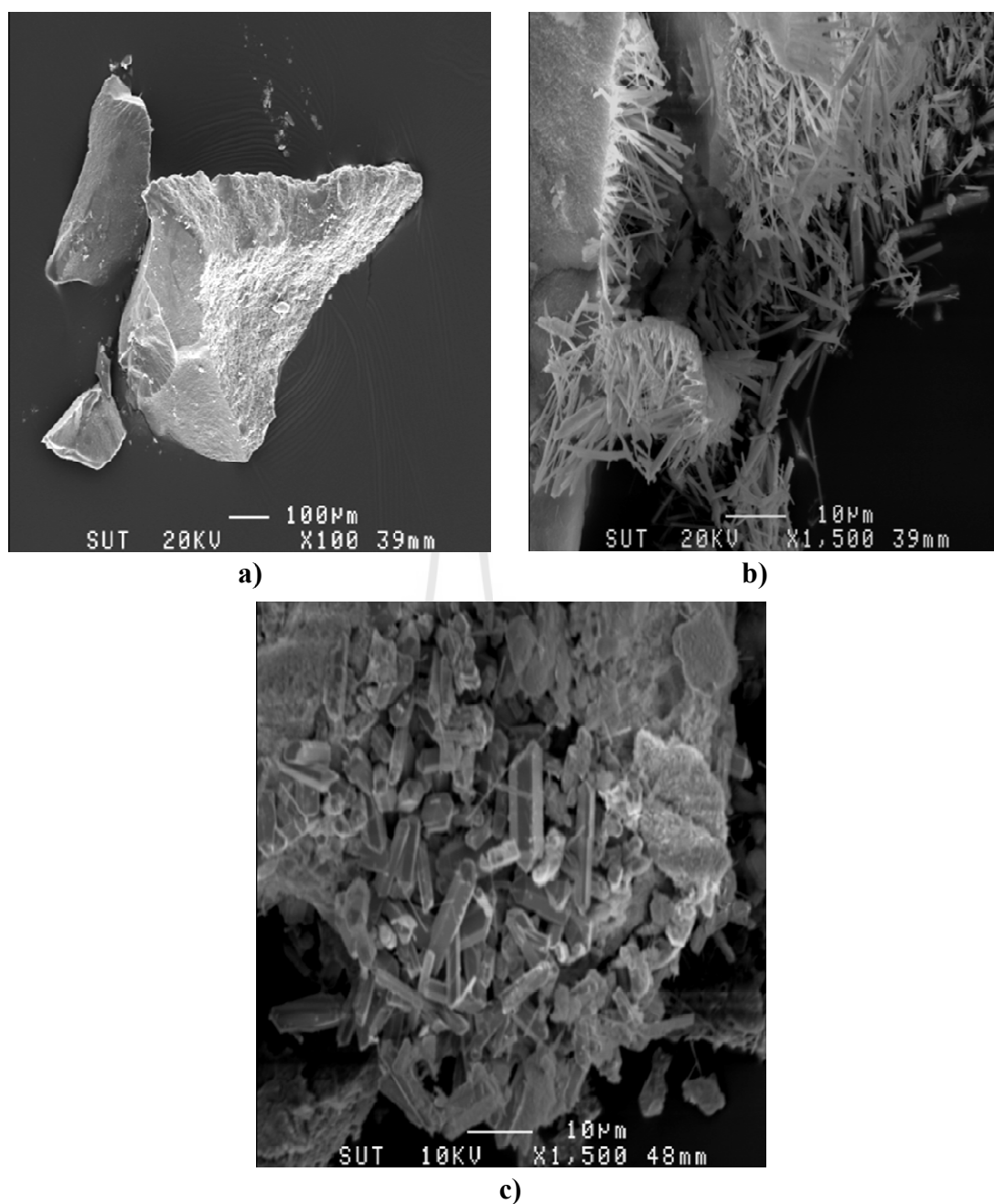
Figure 5.1 SEM images of CaHAp. a) Before refluxing, and after refluxing in Pb^{2+} solution (917 mg/L) for b) 24 h and c) 48 h.

The EDX spectrum of CaHAp substrate (Figure 5.2a) shows high intensity Ca peaks with calcium to phosphorous ratio of about 5:3 as expected for CaHAp. The EDX spectrum of the crystalline products after refluxing 24 h in lead solution show

high intensity Pb peaks with lead to phosphorous ratio of 5:3 as expected for PbHAp
(Figure 5.2b). The Pb peaks of the EDX spectrum of product after 24 h reflux are
indistinguishable from Figure 5.2b. Low intensity Ca peaks are also observed in both
product spectra, consistent with CaHAp impurity due to the growth substrate. This
result is consistent with the XRD result that shows mixed phases of CaHAp and
PbHAp.
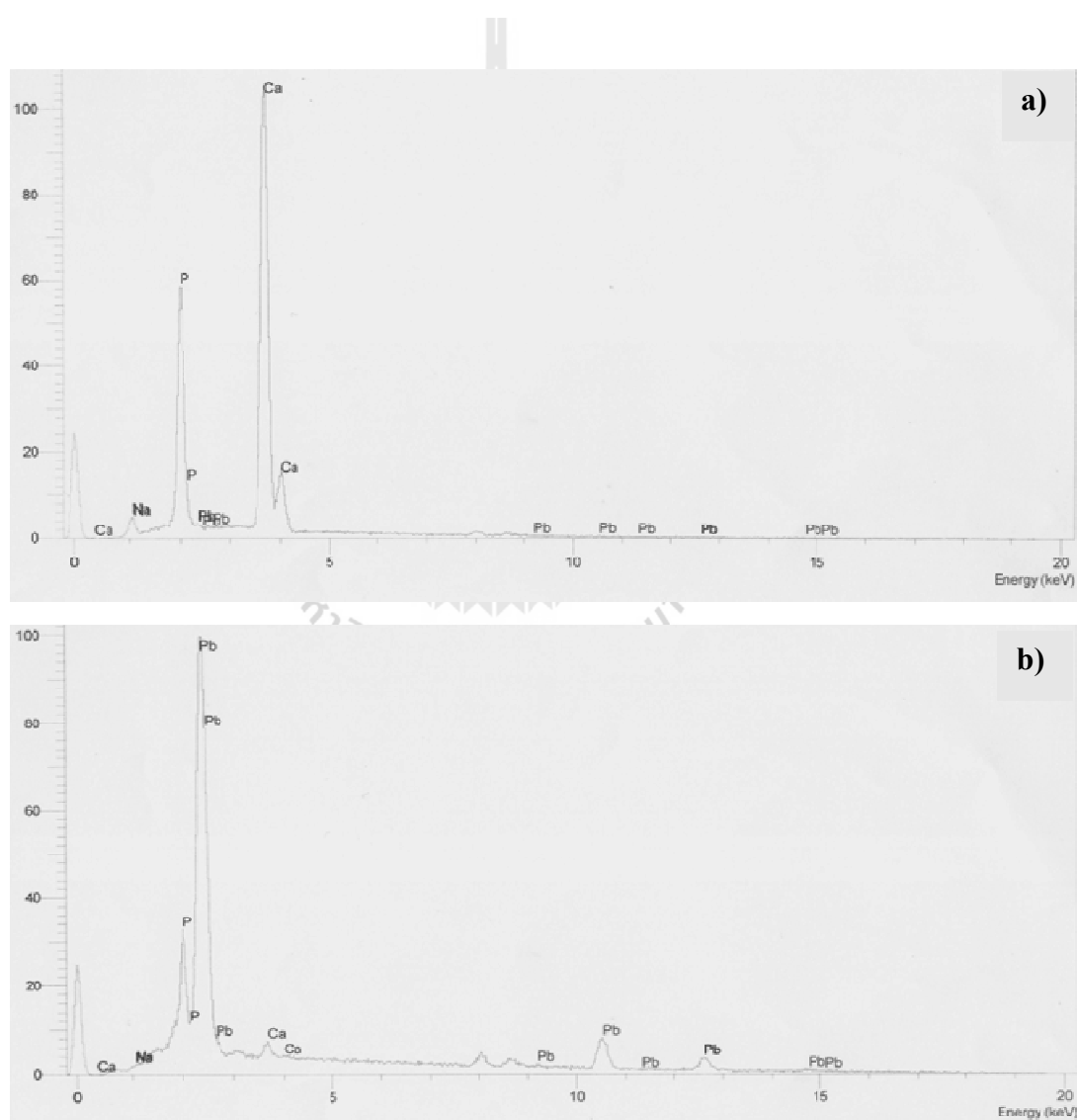
Figure 5.2 EDX spectra of a) CaHAp substrate before refluxing and b) products after
refluxing in Pb^{2+} solution (917 mg/L) for 24 h.

PbHAp and CaHAp phases were identified after 24 h and 48 h of reaction and the results are shown in Figure 5.3. XRD patterns of products after refluxing show mixed phases containing PbHAp (JCPDS 08-0259) and CaHAp (JCPDS 09-0432) due to difficulty in separating the PbHAp from the CaHAp substrate. The presence of PbHAp after 24 h is confirmed by peaks corresponding to PbHAp in the JCPDS database (International Center for Diffraction Data, 2004). Needle-like crystals of this phase were observed by SEM (Figure 5.1b) on the surface of the CaHAp substrate. After 48 h, the XRD pattern of the product clearly shows the PbHAp phase as the major phase with the intensity of PbHAp peaks considerably increased. This result indicates that the phase formation of PbHAp increased with increased reaction time in agreement with previous work (Mavropoulos, Rossi, and Costa, 2002). PbHAp crystal product is present as hexagonal-rod shaped crystals as shown in Figure 5.1c.
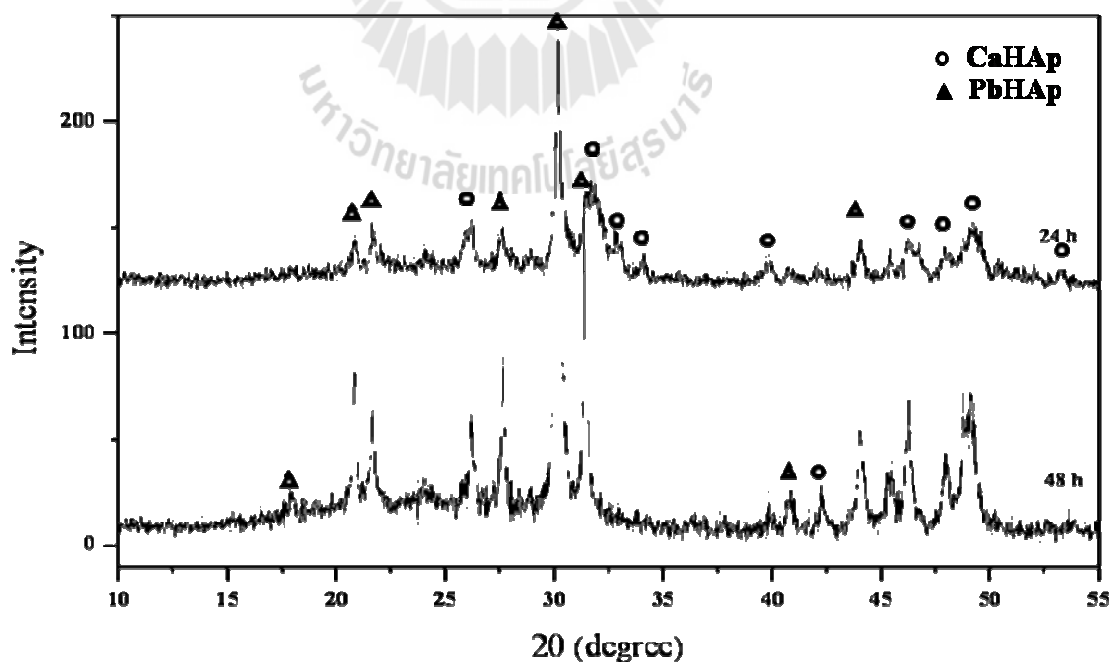
Figure 5.3 XRD patterns of products after refluxing in Pb^{2+} solution (917 mg/L) for
24 h and 48 h.

IR spectra of CaHAp and products (Figure 5.4) show PO_4^{3-} vibrational bands in the 961-1092 cm^{-1} and 562-632 cm^{-1} regions corresponding to P–O stretching and O–P–O bending modes, respectively. Water O–H stretching vibrational bands are present at about 3468 cm^{-1} in the CaHAp spectrum and 3571 cm^{-1} in the product spectra. A broad band in the 3000-3700 cm^{-1} region and a weak peak at 1639 cm^{-1} in the CaHAp spectrum consistent with O–H stretching and H–O–H bending of water. The same spectrum also exhibits the nitrate stretching noted in a previous chapter in the 1348-1384 and 813-814 cm^{-1} regions. The IR spectrum of CaHAp shows bands of NO_3^- stretching at 1384 cm^{-1} and NO_3^- bending at 873 cm^{-1} in agreement with previous work (Stepuk, Veresov, Putlyaev, and Tret'yakov, 2007). The nitrate may come from the incorporation of residual nitrate from starting compound. The adventitious ion appears to be a minor impurity that does not appear to carry over into the PbHAp product crystals. As such, further attempts to identify it were not carried out.
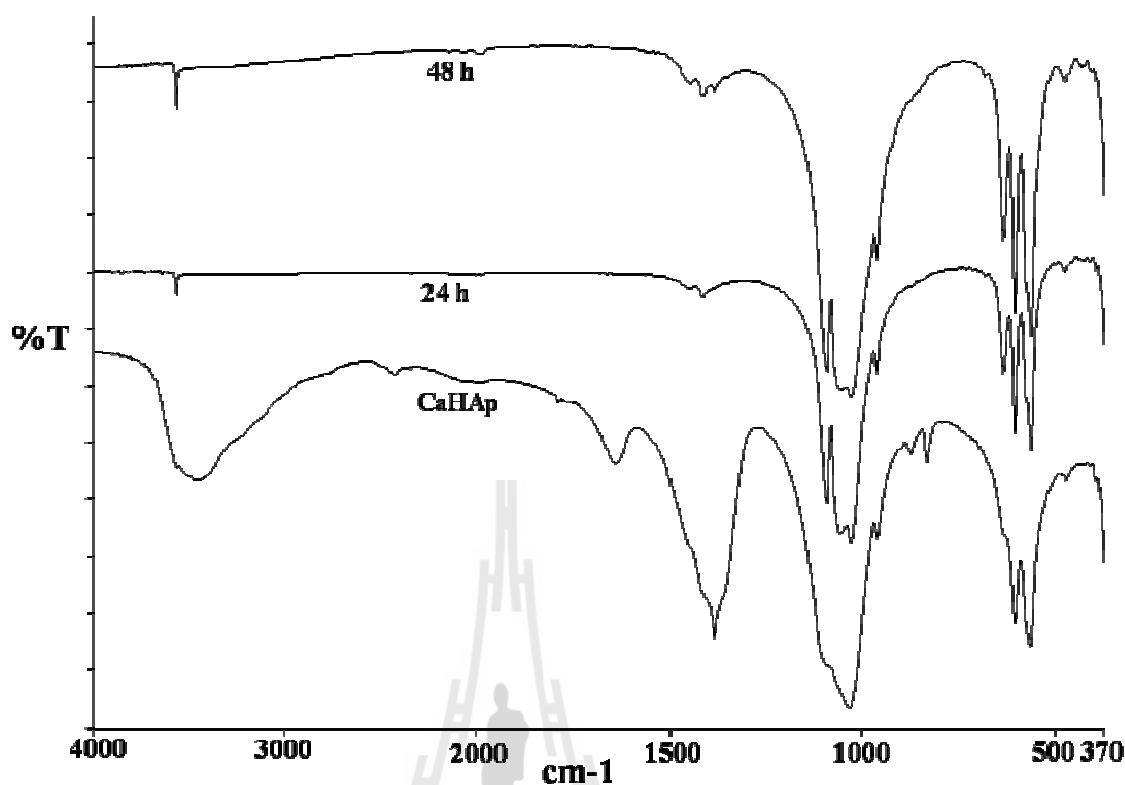
Figure 5.4 IR spectra of CaHAp before refluxing and the products after refluxing in

Pb^{2+} solution (917 mg/L) for 24 h and 48 h.

5.4 Conclusions

The reflux method of CaHAp dissolution to provide phosphate anion in the presence of lead cation succeeds for producing larger sized crystals of the less soluble PbHAp from the aqueous solution. Product crystal size increased with increasing reaction time. EDX results are consistent with the XRD results and show mixed phases of CaHAp and PbHAp due to difficulty in separating the PbHAp from the CaHAp substrate. IR results indicate the incorporation of nitrate in the CaHAp substrate, however, this ion does not appear to carry over into the PbHAp product crystals. As such, further attempts to identify it were not carried out.

5.5 References

Brückner, S., Lusvardi, G., Menabue, L., and Saladini, M. (1995). Crystal structure of lead hydroxyapatite from powder X-ray diffraction data. **Inorg. Chim. Acta** 236: 209-212.

Bruker axs (2011). **XRD Commander Executable,** version 2.4.1.0, Bruker axs. Karlsruhe: Germany.

Dong, L., Zhu, Z., Qiu, Y., and Zhao, J. (2010). Removal of lead from aqueous solution by hydroxyapatite/magnetite composite adsorbent. **Chem. Eng. J.** 165: 827-834.

International Center for Diffraction Data (2004). **Diffract Plus Basic Evaluation Package: PDFMaint**, version 10.0, Bruker axs. Karlsruhe: Germany.

Kim, J. Y., Fenton, R. R., Hunter, B. A., and Kennedy, B. J. (2000). Powder diffraction studies of synthetic calcium and lead apatite. **Aust. J. Chem.** 53: 679-686.

LeGeros, R. Z. (1991). **Calcium Phosphates in Oral Biology and Medicine** (1st ed.). San Francisco, USA: Karger.

Mavropoulos, E., Rossi, A. M., and Costa, A. M. (2002). Studies on the mechanisms of lead immobilization by hydroxyapatite. **Environ. Sci. Technol.** 36: 1625-1629.

Mavropoulos, E., Rocha, N. C. C., Moreira, J. C., Rossi, A. M., and Soares, G. A. (2004). Characterization of phase evolution during lead immobilization by synthetic hydroxyapatite. **Mater. Charact.** 53: 71-78.

Saisa-ard, O. and Haller, K. J. (2012). Crystallization of lead hydroxyapatite from calcium hydroxyapatite dissolution. **J. Microscopy Soc. Thailand** Submitted for publication.

Stepuk, A. A., Veresov, A. G., Putlyaev, V. I., and Tret'yakov, Yu. D. (2007). The influence of NO_3^-, CH_3COO^-, and Cl^- ions on the morphology of calcium hydroxyapatite crystals. **Dokl. Phys. Chem.** 412: 11-14.

Valsami-Jones, E., Ragnarsdottir, K. V., Putnis, A., Bosbach, D., and Kemp, A. J. (1998). The dissolution of apatite in the presence of aqueous metal cations at pH 2-7. **Chem. Geol.** 151: 215-233.

CHAPTER VI

CONCLUSIONS

Apatite and related materials including calcium hydroxyapatite (CaHAp), lead hydroxyapatite (PbHAp), and other calcium-phosphate, lead-phosphate, and calcium-lead-phosphate materials were studied in this work. Precipitation, gel crystallization, and reflux methods were utilized to prepare apatite and related materials. Bond valence calculations were analyzed for the published PbHAp structure. The PHREEQC speciation calculation program was used to predict possible product phases in the system.

Bond valence calculation results demonstrate discrepancy in the expected bond valence sum values of P, Pb(2), and O(4) atoms in the PbHAp structure. The O(3) atoms were adjusted to improve bond valence sums of P and Pb(2) atoms, but the bond valence sum of Pb(2) was still below its expected oxidation state value. The O(4) atom was moved from (0, 0, 0) to (0, 0, 0.1200) to improve the bond valence sum of the O(4) and Pb(2) atoms. Results after modification of O(3) and O(4) improved the bond valence sums over the published structure but they are still not optimal. These results suggest there is probable error in the published PbHAp structure model.

Results from a gel crystallization method show crystalline products formed inside both pure and PO_4^{3-} gel layers after two weeks reaction time. Crystalline product formed in the pure gel layer shows equant crystal morphology while product

formed in the PO_4^{3-} gel layer shows plate-like crystal morphology. Products in the pure gel show needle-like crystals on the surface of larger crystalline product indicating multiple product phases in this system consistent with XRD and PHREEQC results. XRD patterns of products obtained in the pure gel layer exhibit mixed phases containing PbHAp, $PbHPO_4$, and $Pb_3(PO_4)_2$ while products formed in the PO_4^{3-} gel layer show only peaks due to $PbHPO_4$ and $Pb_3(PO_4)_2$ phases. These results are in agreement with PHREEQC results which indicate, PbHAp, $Pb_3(PO_4)_2$, and $PbHPO_4$ are supersaturated. IR spectra of products from both pure and PO_4^{3-} gel layers exhibit the υ_1 and υ_2 vibrations indicating the PO_4^{3-} group in the structure has lower than T_d symmetry. The decrease in pH from 8 (theoretical for all layers mixed) to 3 for all reactions studied is due to the speciation equilibrium converting HPO_4^{2-} to H^+ and PO_4^{3-} as PO_4^{3-} containing species are precipitated. The presence of PbHAp in the pure gel layer but not in the PO_4^{3-} layer can be understood based on the higher $Pb^{2+}:PO_4^{3-}$ ratio (5:3 vs 3:2) required for the PbHAp phase relative to the $Pb_3(PO_4)_2$ phase and the increment of PO_4^{3-} ion concentrations near the lead solution from placing pure gel solution on the PO_4^{3-} gel layer in the gel preparation step.

Results from a reflux method show needle-like and hexagonal-rod crystal morphologies of products after refluxing for 24 h and 48 h, respectively. The crystal size increased with increasing reaction time. The EDX spectra of CaHAp substrate and crystalline product show Ca/P or Pb/P ratio of about 5:3 as expected for the respective apatite materials. Low intensity Ca peaks are also observed in the product spectra, consistent with CaHAp impurity due to the growth substrate. This result is consistent with the XRD result that shows mixed phases of CaHAp and PbHAp. The intensity of the PbHAp peaks of the product increased greatly with time and clearly

show PbHAp as the major product phase. IR spectra of CaHAp and products show vibrational bands of PO_4^{3-}, H_2O, and NO_3^-.

Vibrational bands of nitrate were observed in products from both gel crystallization and reflux methods. Nitrate may come from the incorporation of residual nitrate from starting compound. However, the nitrate ion does not appear to carry over into the PbHAp product crystals.

Ca-PbHAp materials were also studied in this work. A precipitation method was utilized for preparation of apatite materials. XRD results suggest the CaHAp and PbHAp phases are formed but Ca-PbHAp solid solution is not formed in this system. PHREEQC calculation results show several calcium-phosphate and lead-phosphate phases are supersaturated suggesting multiple products may be formed in this system. However, these phases do not appear clearly in the XRD pattern because they are minor products.

Studies of the formation of apatite and related materials may be an important key for understanding of the precipitation of biological hard tissues and the environmental geology of lead and phosphorus.

APPENDICES

APPENDIX A

SUPPORTING INFORMATION FOR CHAPTER I

A.1 K_{sp} with the double formula of CaHAp

A discrepancy in the K_{sp} values of CaHAp has been reported (McDowell, Gregory, and Brown, 1997; Valsami-Jones, Ragnarsdottir, Putnis, Bosbach, Kemp, and Cressey, 1998; Tanaka, Miyajima, Nakagaki, and Shimabayashi, 1991; Zhu et al., 2009). The K_{sp} value of CaHAp calculated from its double formula is 58 orders of magnitude (10^{-58}) lower than that calculated from its empirical formula as shown, based on literature reports, in Table A.1. Throughout this thesis the conventional empirical formula has been used for CaHAp and all other ionic compounds.

Table A.2 The K_{sp} values of CaHAp materials.

Formula	K_{sp}	Author and year
$Ca_5(PO_4)_3(OH)$	$10^{-58.3}$	McDowell et al., 1977
	10^{-57} - 10^{-59}	Valsami-Jones et al., 1998
	$10^{-53.02}$ - $10^{-53.51}$	Zhu et al., 2009
$Ca_{10}(PO_4)_6(OH)_2$	$10^{-115.8}$	Tanaka et al., 1991

A.2 References

McDowell, H., Gregory, T. M., and Brown, W. E. (1997). Solubility of $Ca_5(PO_4)_3OH$ in the system $Ca(OH)_2$-H_3PO_4-H_2O at 5, 15, 25, and 37 °C. **J. Res. Natl. Bur. Stand.**, **Section A** 81: 2-3.

Tanaka, H., Miyajima, K., Nakagaki, M., and Shimabayashi, S. (1991). Incongruent dissolution of hydroxyapatite in the presence of phosphoserine. **Colloid Polym. Sci.** 269: 161-165.

Valsami-Jones, E., Ragnarsdottir, K. V., Putnis, A., Bosbach, D., Kemp, A. J., and Cressey, G. (1998). The dissolution of apatite in the presence of aqueous metal cations at pH 2-7. **Chem. Geol.** 151: 215-233.

Zhu, Y., Zhang, X., Chen, Y., Xie, Q., Lan, J., Qian, M., and He, N. (2009). A comparative study on the dissolution and solubility of hydroxylapatite and fluorapatite at 25 °C and 45 °C. **Chem. Geol.** 268: 89-96.
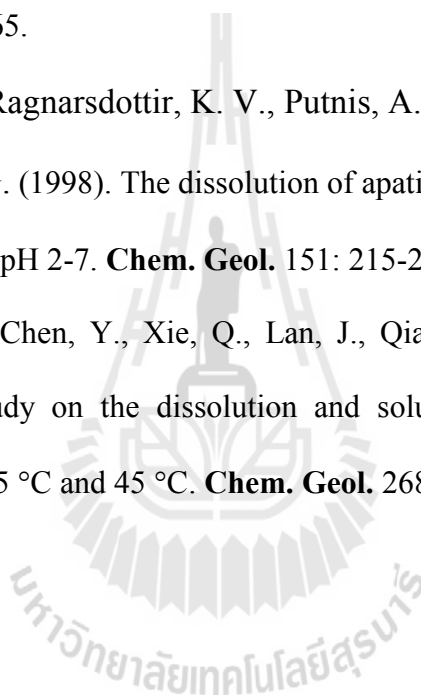
APPENDIX B

SUPPORTING INFORMATION FOR CHAPTER III

B.1 PHREEQC input

PHREEQC input of 5Ca

```
                        060412_CaHap pure
   Input file: C:\DOCUME~1\sut\LOCALS~1\Temp\phrq0000.tmp
  Output file: C:\Documents and Settings\sut\Desktop\060412_Ca-Pb
apatite.out
Database file: C:\Program Files\Phreeqc\Databases\minteq.v4.dat

------------------
Reading data base.
------------------

        SOLUTION_MASTER_SPECIES
        SOLUTION_SPECIES
        SOLUTION_SPECIES
        PHASES
        PHASES
        SURFACE_MASTER_SPECIES
        SURFACE_SPECIES
        END
------------------------------------
Reading input data for simulation 1.
------------------------------------

        TITLE CALCIUM-LEAD HYDROXYAPATITE
        SOLUTION 1
                units    ppm
                pH       8
                temp     24.0
        Ca      40000
        P                18586
        N       44803
        Na      1838
          END
-----
```

PHREEQC input of 5Pb

```
                        060412_PbHap pure
    Input file: C:\DOCUME~1\sut\LOCALS~1\Temp\phrq0000.tmp
   Output file: C:\Documents and Settings\sut\Desktop\060412_Ca-Pb
apatite.out
Database file: C:\Program Files\Phreeqc\Databases\minteq.v4.dat

------------------
Reading data base.
------------------

        SOLUTION_MASTER_SPECIES
        SOLUTION_SPECIES
        SOLUTION_SPECIES
        PHASES
        PHASES
        SURFACE_MASTER_SPECIES
        SURFACE_SPECIES
        END
-------------------------------------
Reading input data for simulation 1.
-------------------------------------

        TITLE CALCIUM-LEAD HYDROXYAPATITE
        SOLUTION 1
                units    ppm
                pH       8
                temp     24.0
        Pb               220720
        P                18586
        N       44803
        Na      1838
         END
-----
```

PHREEQC input of 4Ca:1Pb

```
                            060412 4Ca1Pb apatite
    Input file: C:\DOCUME~1\sut\LOCALS~1\Temp\phrq0000.tmp
    Output file: C:\Documents and Settings\sut\Desktop\Ca-Pb apatite solid
solution\060412 Ca-Pb apatite.out
Database file: C:\Program Files\Phreeqc\Databases\minteq.v4.dat

------------------
Reading data base.
------------------

        SOLUTION_MASTER_SPECIES
        SOLUTION_SPECIES
        SOLUTION_SPECIES
        PHASES
        PHASES
        SURFACE_MASTER_SPECIES
        SURFACE_SPECIES
        END
--------------------------------------
Reading input data for simulation 1.
--------------------------------------

        TITLE CALCIUM-LEAD HYDROXYAPATITE
        SOLUTION 1
                units    ppm
                pH       8
                temp     24.0
        Pb      44144
        Ca      32000
        P                18586
        N       44803
        Na      1838
         END
-----
```

มหาวิทยาลัยเทคโนโลยีสุรนารี

B.2 PHREEQC output

PHREEQC output of 5Ca

```
Phase                 SI  log IAP  log KT

Ca3(PO4)2(beta)     8.28  -20.67  -28.95  Ca3(PO4)2
Ca4H(PO4)3:3H2O     9.56  -37.52  -47.08  Ca4H(PO4)3:3H2O
CaHPO4              2.54  -16.76  -19.29  CaHPO4
CaHPO4:2H2O         2.19   16.82   19.01  CaHPO4:2H2O
Hydroxylapatite    19.72  -24.61  -44.33  Ca5(PO4)3OH
Lime              -20.00   12.81   32.81  CaO
O2(g)             -35.49   47.93   83.43  O2
Portlandite       -10.10   12.78   22.88  Ca(OH)2
```

PHREEQC output of 4Ca:1Pb

```
Phase                 SI  log IAP  log KT

Ca3(PO4)2(beta)     7.41  -21.54  -28.95  Ca3(PO4)2
Ca4H(PO4)3:3H2O     8.40  -38.68  -47.08  Ca4H(PO4)3:3H2O
CaHPO4              2.25  -17.04  -19.29  CaHPO4
CaHPO4:2H2O         1.90  -17.11  -19.01  CaHPO4:2H2O
Hydroxylapatite    18.26  -26.07  -44.33  Ca5(PO4)3OH
Hydroxylpyromorphite  15.13  -47.66  -62.79  Pb5(PO4)3OH
Lime              -20.31   12.51   32.81  CaO
Litharge           -4.54    8.19   12.73  PbO
Massicot           -4.75    8.19   12.93  PbO
Minium            -25.24   48.53   73.77  Pb3O4
O2(g)             -35.50   47.93   83.43  O2
Pb(OH)2            -0.03    8.15    8.18  Pb(OH)2
Pb2O(OH)2          -9.85   16.34   26.19  Pb2O(OH)2
Pb2O3             -20.70   40.34   61.04  Pb2O3
Pb3(PO4)2           9.04  -34.49  -43.53  Pb3(PO4)2
PbHPO4              2.45  -21.36  -23.00  PbHPO4
Pbmetal           -20.02  -15.78    4.25  Pb
PbO:0.3H2O         -4.80    8.18   12.98  PbO:0.33H2O
Plattnerite       -17.62   32.15   49.77  PbO2
Portlandite       -10.41   12.47   22.88  Ca(OH)2
```

PHREEQC output of 3Ca:2Pb

```
Phase                  SI log IAP  log KT

Ca3(PO4)2(beta)     6.46  -22.49  -28.95  Ca3(PO4)2
Ca4H(PO4)3:3H2O     7.12  -39.96  -47.08  Ca4H(PO4)3:3H2O
CaHPO4              1.94  -17.35  -19.29  CaHPO4
CaHPO4:2H2O         1.58  -17.43  -19.01  CaHPO4:2H2O
Hydroxylapatite    16.66  -27.67  -44.33  Ca5(PO4)3OH
Hydroxylpyromorphite 14.70 -48.09 -62.79  Pb5(PO4)3OH
Lime              -20.64   12.18   32.81  CaO
Litharge           -4.64    8.09   12.73  PbO
Massicot           -4.84    8.09   12.93  PbO
Minium            -25.53   48.24   73.77  Pb3O4
O2(g)             -35.50   47.93   83.43  O2
Pb(OH)2            -0.13    8.06    8.18  Pb(OH)2
Pb2O(OH)2         -10.04   16.15   26.19  Pb2O(OH)2
Pb2O3             -20.89   40.15   61.04  Pb2O3
Pb3(PO4)2           8.78  -34.75  -43.53  Pb3(PO4)2
PbHPO4              2.37  -21.44  -23.80  PbHPO4
Pbmetal           -20.12  -15.87    4.25  Pb
PbO:0.3H2O         -4.90    8.08   12.98  PbO:0.33H2O
Plattnerite       -17.72   32.06   49.77  PbO2
Portlandite       -10.74   12.14   22.88  Ca(OH)2
```

PHREEQC output of 2Ca:3Pb

```
Phase                  SI log IAP  log KT

Ca3(PO4)2(beta)     5.34  -23.62  -28.95  Ca3(PO4)2
Ca4H(PO4)3:3H2O     5.62  -41.46  -47.08  Ca4H(PO4)3:3H2O
CaHPO4              1.57  -17.72  -19.29  CaHPO4
CaHPO4:2H2O         1.21  -17.80  -19.01  CaHPO4:2H2O
Hydroxylapatite    14.78  -29.55  -44.33  Ca5(PO4)3OH
Hydroxylpyromorphite 14.09 -48.70 -62.79  Pb5(PO4)3OH
Lime              -21.02   11.79   32.81  CaO
Litharge            4.77    7.96   12.73  PbO
Massicot           -4.97    7.96   12.93  PbO
Minium            -25.92   47.85   73.77  Pb3O4
O2(g)             -35.50   47.92   83.43  O2
Pb(OH)2            -0.26    7.92    8.18  Pb(OH)2
Pb2O(OH)2         -10.30   15.88   26.19  Pb2O(OH)2
Pb2O3             -21.16   39.88   61.04  Pb2O3
Pb3(PO4)2           8.42  -35.11  -43.53  Pb3(PO4)2
PbHPO4              2.25  -21.55  -23.80  PbHPO4
Pbmetal           -20.25  -16.00    4.25  Pb
PbO:0.3H2O         -5.03    7.95   12.98  PbO:0.33H2O
Plattnerite       -17.85   31.92   49.77  PbO2
Portlandite       -11.13   11.75   22.88  Ca(OH)2
```

PHREEQC output of 1Ca:4Pb

```
Phase                     SI log IAP  log KT

Ca3(PO4)2(beta)    4.31   -24.64   -28.95   Ca3(PO4)2
Ca4H(PO4)3:3H2O    4.25   -42.83   -47.08   Ca4H(PO4)3:3H2O
CaHPO4             1.23   -18.06   -19.29   CaHPO4
CaHPO4:2H2O        0.86   -18.15   -19.01   CaHPO4:2H2O
Hydroxylapatite   13.07   -31.27   -44.33   Ca5(PO4)3OH
Hydroxylpyromorphite  12.22  -50.57  -62.79  Pb5(PO4)3OH
Lime             -21.37    11.44    32.81   CaO
Litharge          -5.15     7.58    12.73   PbO
Massicot          -5.35     7.58    12.93   PbO
Minium           -27.07    46.70    73.77   Pb3O4
O2(g)            -35.51    47.92    83.43   O2
Pb(OH)2           -0.65     7.54     8.18   Pb(OH)2
Pb2O(OH)2        -11.07    15.12    26.19   Pb2O(OH)2
Pb2O3            -21.92    39.12    61.04   Pb2O3
Pb3(PO4)2          7.30   -36.23   -43.53   Pb3(PO4)2
PbHPO4             1.88   -21.92   -23.80   PbHPO4
Pbmetal          -20.62   -16.38     4.25   Pb
PbO:0.3H2O        -5.41     7.57    12.98   PbO:0.33H2O
Plattnerite      -18.24    31.54    49.77   PbO2
Portlandite      -11.48    11.40    22.88   Ca(OH)2
```

PHREEQC output of 5Pb

```
Phase                     SI log IAP  log KT

Hydroxylpyromorphite  12.60  -50.19  -62.79  Pb5(PO4)3OH
Litharge          -5.09     7.64    12.73   PbO
Massicot          -5.29     7.64    12.93   PbO
Minium           -26.88    46.89    73.77   Pb3O4
O2(g)            -35.52    47.91    83.43   O2
Pb(OH)2           -0.59     7.60     8.18   Pb(OH)2
Pb2O(OH)2        -10.94    15.24    26.19   Pb2O(OH)2
Pb2O3            -21.80    39.24    61.04   Pb2O3
Pb3(PO4)2          7.54   -35.99   -43.53   Pb3(PO4)2
PbHPO4             1.97   -21.84   -23.80   PbHPO4
Pbmetal          -20.56   -16.31     4.25   Pb
PbO:0.3H2O        -5.35     7.63    12.90   PbO:0.33H2O
Plattnerite      -18.18    31.60    49.77   PbO2
```
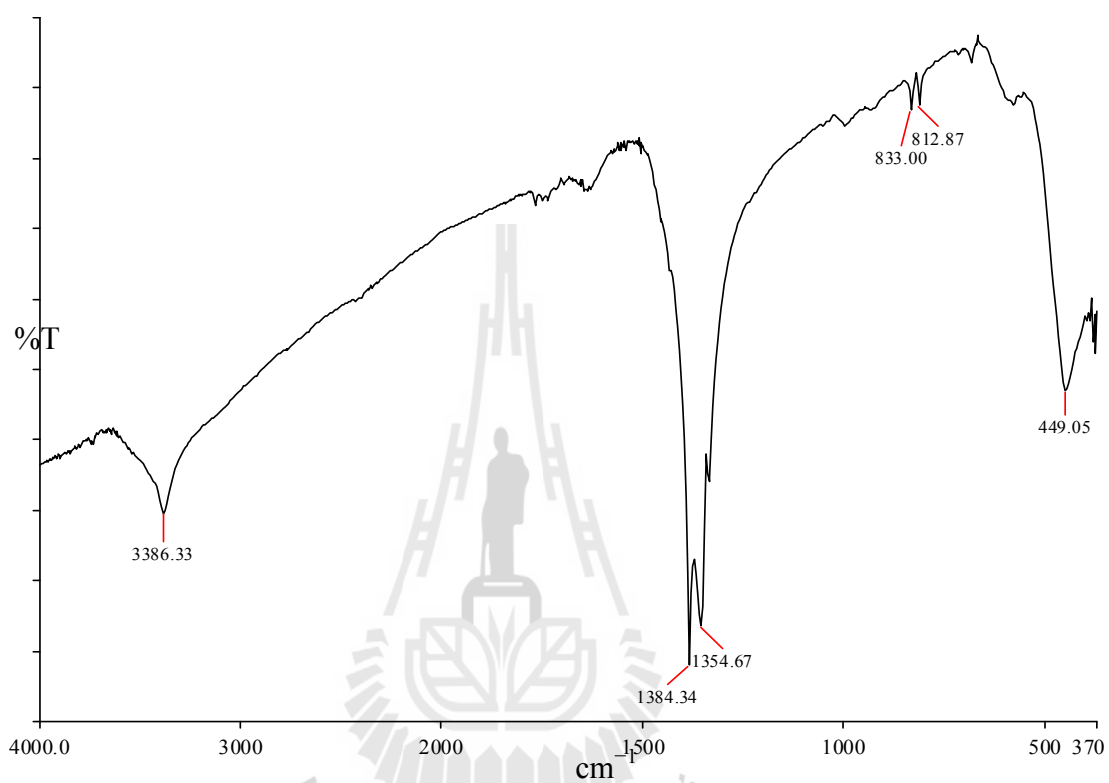
B.3 XRD peak pattern of $Pb_6O_3(NO_3)_2(OH)_4$
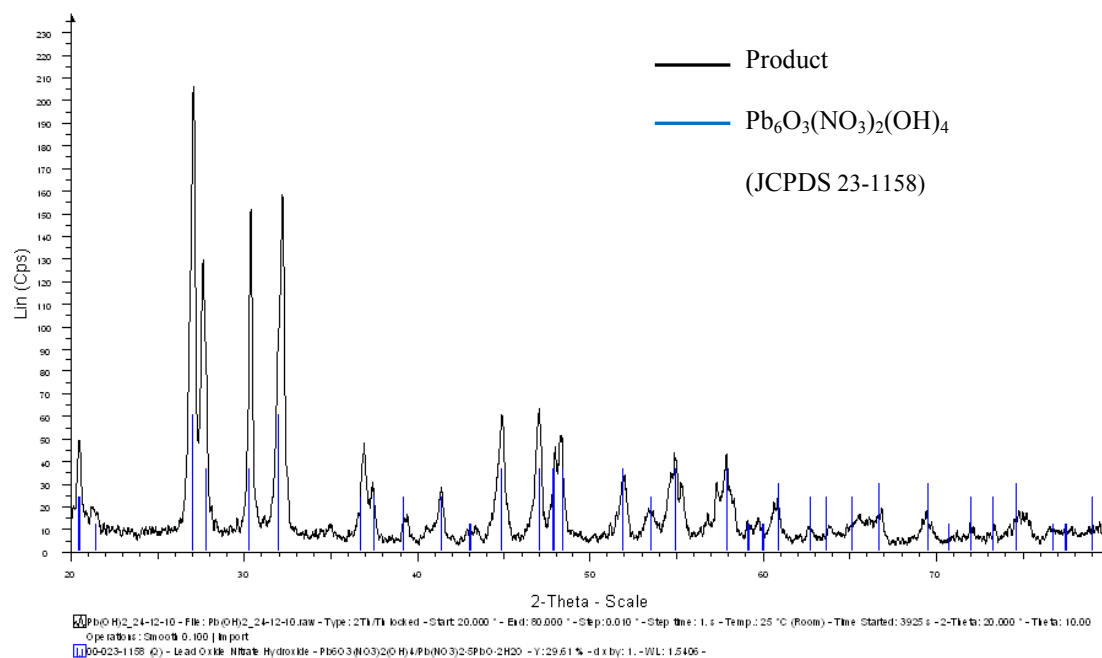
Figure B.3 XRD pattern of product from adjusting pH of $Pb(NO_3)_2$ solution with

NaOH compared with the JCPDS database.
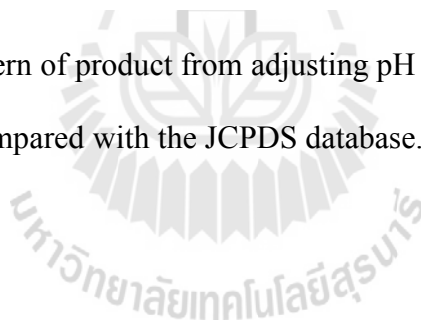
B.4 FTIR spectrum of product from adjusting pH of Pb(NO$_3$)$_2$

    solution with NaOH

Figure B.4 IR spectrum of product from adjusting pH of Pb(NO$_3$)$_2$ solution with

    NaOH.
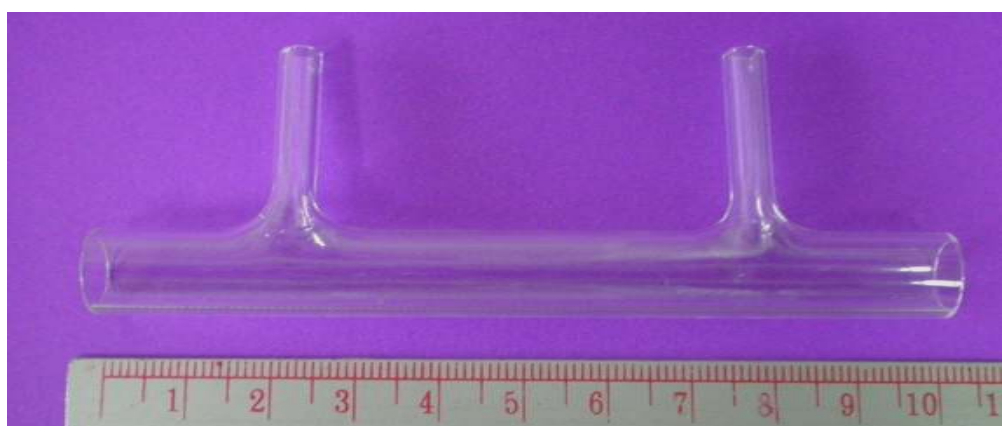
APPENDIX C

SUPPORTING INFORMATION FOR CHAPTER IV

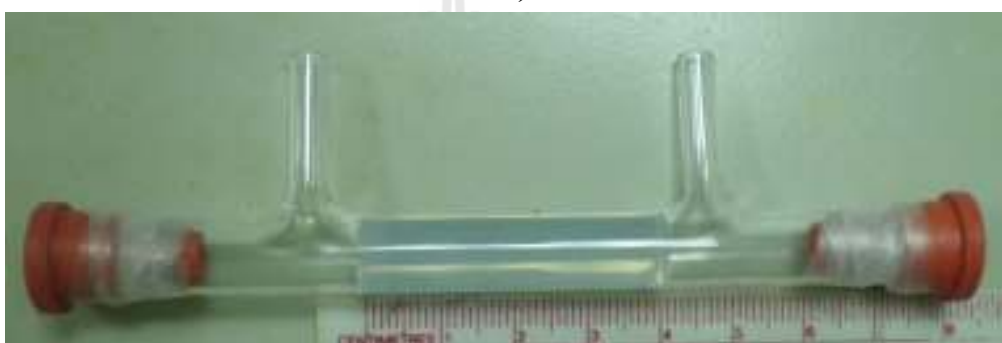## C.1 Setting gel in test tubes

Figure C.1 Microscopic pictures of crystalline products after 2 weeks of reaction. Crystalline product (a) in test tubes, (b) in the pure gel layer (2 % w/v), and (c) in the PO_4^{3-} gel (1.7 % w/v).
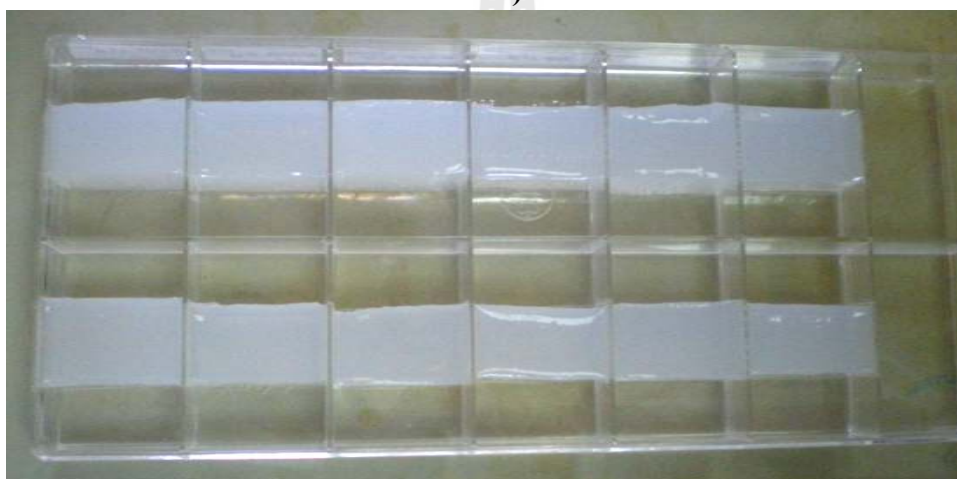
C.2 Setting gel in reactors

Figure C.2 Setting gel in the reactor. (a) reactor before setting gel, (b) after setting

gel, and (c) 2 weeks after reaction.

C.3 Setting gel in plastic boxes

Figure C.3 Setting gel in plastic boxes. (a) plastic boxes before setting gel, (b) after

setting gel, and (c) after adding reactants.

C.4 PHREEQC input

```
                        150212 PbHAP pH = 8
   Input file: C:\DOCUME~1\sut\LOCALS~1\Temp\phrq0000.tmp
  Output file: D:\PHREEQC result\150212 PbHAP pH = 8.out
Database file: C:\Program Files\Phreeqc\Databases\minteq.v4.dat


------------------
Reading data base.
------------------

        SOLUTION_MASTER_SPECIES
        SOLUTION_SPECIES
        SOLUTION_SPECIES
        PHASES
        PHASES
        SURFACE_MASTER_SPECIES
        SURFACE_SPECIES
        END
-------------------------------------
Reading input data for simulation 1.
-------------------------------------

        TITLE LEAD HYDROXYAPATITE
        SOLUTION 1
                units    ppm
                pH       8.0
                temp     24.0
        Pb      207200
        P       18400
        Na      1842
        N       44757
        PHASES
          END
-----
```

C.5 PHREEQC output

```
Phase                    SI log IAP  log KT

Hydroxylpyromorphite  13.17  -49.62  -62.79   Pb5(PO4)3OH
Litharge              -4.97    7.76   12.73   PbO
Massicot              -5.17    7.76   12.93   PbO
Minium                26.53   47.25   73.77   Pb3O4
O2(g)                -35.51   47.91   83.43   O2
Pb(OH)2               -0.46    7.72    8.18   Pb(OH)2
Pb2O(OH)2            -10.71   15.48   26.19   Pb2O(OH)2
Pb2O3               -21.56   39.48   61.04   Pb2O3
Pb3(PO4)2             7.88   -35.65  -43.53   Pb3(PO4)2
PbHPO4                2.08   -21.73  -23.80   PbHPO4
Pbmetal             -20.44   -16.19    4.25   Pb
PbO:0.3H2O           -5.23    7.75   12.98   PbO:0.33H2O
Plattnerite         -18.06   31.72   49.77   PbO2
```
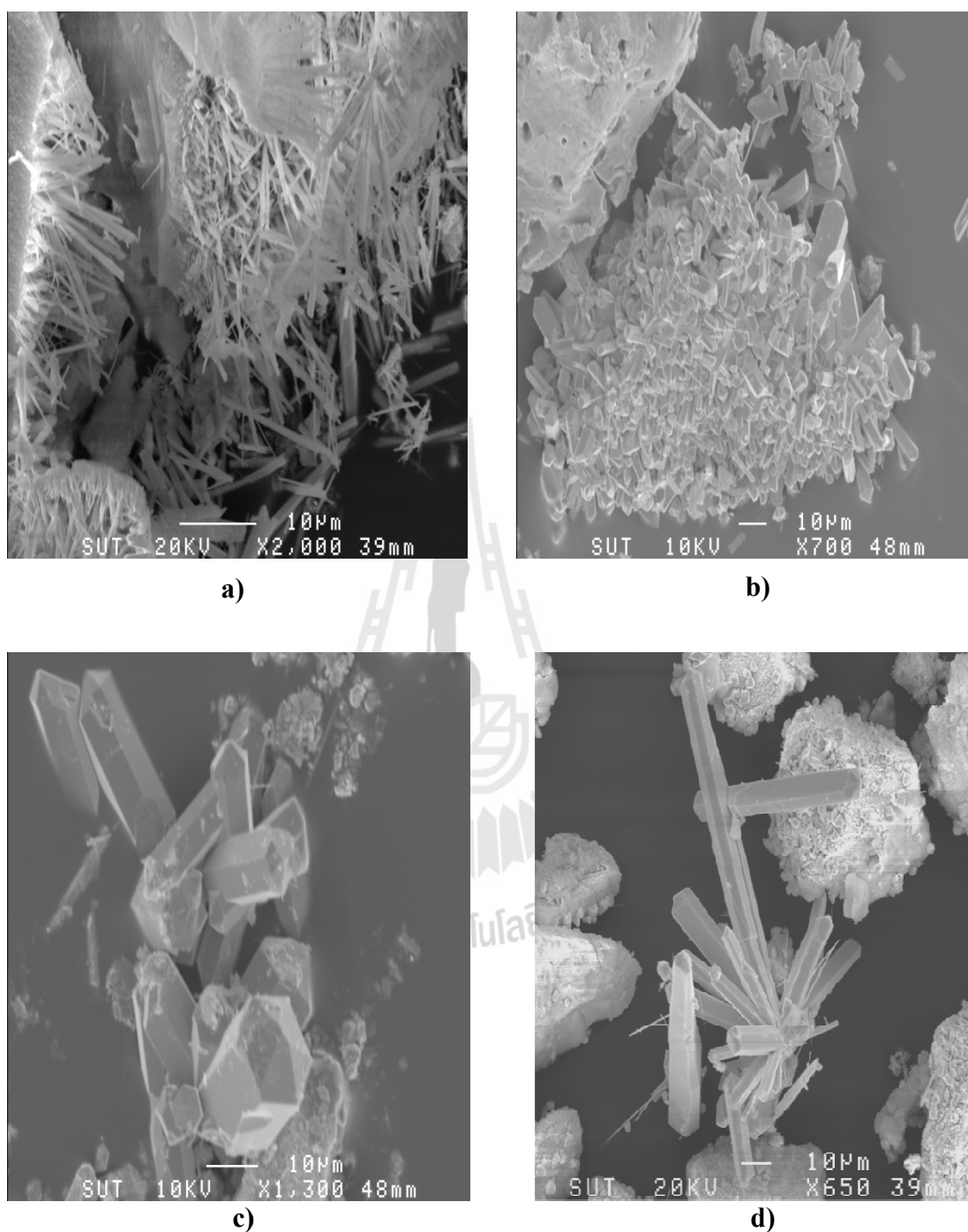
APPENDIX D

SUPPORTING INFORMATION FOR CHAPTER V

D.1 Microscopic images of CaHAp
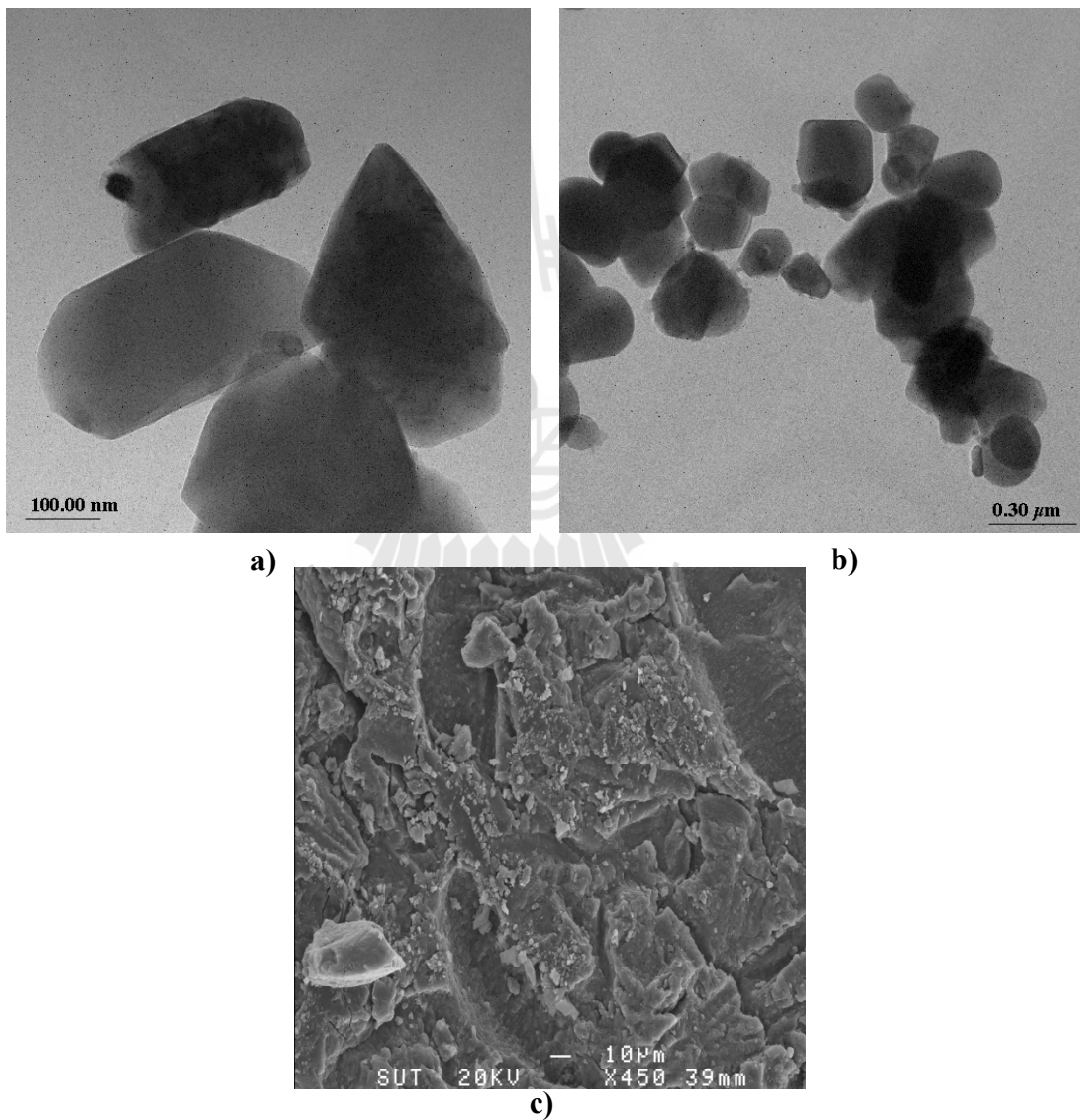
Figure D.1 Microscopic images of CaHAp. a-b)TEM and c) SEM.

D.2 SEM images of products after refluxing in lead solution

a)

b)

c)

d)

Figure D.2 SEM images of products after refluxing in Pb^{2+} solution (917 mg/L). The reaction times are a) 24 h and b-d) 48 h.

APPENDIX E

THESIS RELEVANT PRESENTATIONS AND PROCEEDINGS

E.1 Conferences presentations

Oral presentations

- **Oratai Saisa-ard**, Navarat Sodesiri, and Kenneth J. Haller. Cocrystalization and Characterizaion of an Ethylenediamine and Cyanuric Acid Adduct, *the 1ˢᵗ Suranaree University of Technology Graduate Conference (SUT-GRAD 1)*. 1-2 November 2007. Nakhon Ratchasima, Thailand.

- **Oratai Saisa-ard** and Kenneth J. Haller**.** Phase Characterization and Saturation Modeling of the Calcium-lead Phosphate Apatite System, *the 14ᵗʰ International ANnual Symposium on Computational Science and Engineering (ANSCSE14)*. 23-26 March 2010. Chiang Rai, Thailand.

- **Oratai Saisa-ard** and Kenneth J. Haller. Gel Crystallization and Physical Characterization of Lead Hydroxyapatite, *International Conference on Materials for Advanced Technologies (ICMAT2011),* 26 June-1 July 2011. Suntec, Singapore.

Poster presentations

- **Oratai Saisa-ard**, Winya Dungkaew, Weenawan Somphon, and Kenneth J. Haller. Divalent Cation Incorporation into Calcium Phosphate Hydroxyapatite, *the 8ᵗʰ conference of the Asian Crystallographic Association (AsCA'07)*. 4-7 November 2007. Taipei, Taiwan.

- **Oratai Saisa-ard** and Kenneth J. Haller. Study of Synthetic Calcium Phosphate Hydroxyapatite Modified with Pyrophosphate, *the CHE-Congress 2008*. 5-7 September 2008. Chon Buri, Thailand.

- **Oratai Saisa-ard**, Winya Dungkaew, Weenawan Somphon, and Kenneth J. Haller. Structural Study of Lead Incorporation into Calcium Phosphate Hydroxyapatite, *the 33nd Congress on Science and Technology of Thailand (STT'33)*. 18-20 October 2007. Nakhon Si Thammarat, Thailand.

- **Oratai Saisa-ard** and Kenneth J. Haller. Interaction of Pyrophosphate with Synthetic Calcium Phosphate Hydroxyapatite: Formation of a Surface Complex, *the 34th Congress on Science and Technology of Thailand (STT'34)*. 31 October-2 November 2008. Bangkok, Thailand.

- **Oratai Saisa-ard** and Kenneth J. Haller. Lead Incorporation into Hydroxyapatite Structure, *German-Thai Symposium on Nanoscience and Nanotechnology (GTSNN'09)*. 21-22 September 2009. Chiang Mai, Thailand.

- **Oratai Saisa-ard** and Kenneth J. Haller**.** Lead Incorporation into Hydroxyapatite Structure, *Pure and Applied Chemistry International Conferen*ce *(PACCON2010)*. 21-23 January 2010. Ubon Ratchathani, Thailand.

- **Oratai Saisa-ard** and Kenneth J. Haller. Gel Crystallization of Calcium-Lead Hydroxyapatite, MHAP (M = Ca^{2+} and/or Pb^{2+}), *the 10th conference of the Asian Crystallographic Association 2010 (AsCA'10)*, 31 October-3 November 2010. Busan, Korea.

- **Oratai Saisa-ard** and Kenneth J. Haller. Structure of Calcium-Lead Hydroxyapatite, MHAP (M = Ca^{2+} and/or Pb^{2+}), *NanoThailand 2010.* 18-20 November 2010. Pathum Thani, Thailand.

- **Oratai Saisa-ard** and Kenneth J. Haller. Synthesis and Characterization of Nitrate Containing Lead Hydroxyapatite, *the 3rd Suranaree University of Technology Graduate Conference (SUT-GRAD 3).* 21-23 November 2010. Nakhon Ratchasima, Thailand.

- **Oratai Saisa-ard** and Kenneth J. Haller. Transformation of Synthetic Calcium Phosphate Materials in Lead Solution, *Chiang Mai International Conference on Biomaterials and Applications (CMICBA2011)*, 9-10 August 2011. Chiang Mai, Thailand.

- **Oratai Saisa-ard** and Kenneth J. Haller. Single Crystal Growth and Characterization of Lead Hydroxyapatite, *International Union of Crystallography (IUCr2011),* 22-23 August 2011. Madrid, Spain.

- **Oratai Saisa-ard** and Kenneth J. Haller. Crystallization and Characterization of Lead Phosphate Materials, *Pure and Applied Chemistry International Conferen*ce *(PACCON2012)*, 11-13 January 2012. Chiang Mai, Thailand.

- **Oratai Saisa-ard** and Kenneth J. Haller. Crystallization of Lead Hydroxyapatite from Calcium Hydroxyapatite Dissolution, *the Microscopy Society of Thailand (MST29)*. 31 January-1 February 2012. Phetchaburi, Thailand.

- **Oratai Saisa-ard** and Kenneth J. Haller. Study of Calcium-lead Phosphate Apatite System, *the 4ᵗʰ HOPE Meeting*. 7-11 March 2012. Ibaraki, Japan.

E.2 Conference proceedings

Conference proceedings

- **Oratai Saisa-ard**, Navarat Sodesiri, and Kenneth J. Haller**. Cocrystallization and Characterization of an Ethylenediamine and Cyanuric Acid, *the 1ˢᵗ Suranaree University of Technology Graduate Conference (SUT-GRAD 1)*. 1-2 November 2007. Nakhon Ratchasima, Thailand.

- **Oratai Saisa-ard** and Kenneth J. Haller. Structural Analysis of Calcium and Lead Hydroxyapatite, *the 35ᵗʰ Congress on Science and Technology of Thailand (STT'35)*. 15-17 October 2009. Chon Buri, Thailand.

- **Oratai Saisa-ard** and Kenneth J. Haller. Crystallization of Lead Phosphate in Gel Systems, *German-Thai Symposium on Nanoscience and Nanotechnology (GTSNN2011)*. 13-16 September 2011. Nakhon Ratchasaima, Thailand.

- **Sunaree Choknud**, Oratai Saisa-ard, and Kenneth J. Haller. Preparation and Characterization of Carboxylic Acid Adducts of Gabapentin, *German-Thai Symposium on Nanoscience and Nanotechnology (GTSNN2011)*, 13-16 September 2011. Nakhon Ratchasaima, Thailand.

- **Oratai Saisa-ard** and Kenneth J. Haller. Crystallization of Lead Hydroxyapatite from Calcium Hydroxyapatite Dissolution, *the Microscopy Society of Thailand (MST29)*, 31 January-1 February 2012. Phetchaburi, Thailand (submitted).

CURRICULUM VITAE

Personal Information:

Name: Oratai   Saisa-ard

Date of Birth: March 6, 1983

Place of Birth: 84 Moo 1, Tumbon Sangthonoi, Hua Taphan, Amnat Charoen,

                  37240, Thailand

Education:

2005   B.Sc. in Chemistry, Ubon Ratchathani University, Thailand

2011   Ph.D. in Chemistry, Suranaree University of Technology,

                  Thailand

Scholarship:

2007-2010   The Commission on Higher Education (CHE), Thailand

Publications:

1. Oratai Saisa-ard and Kenneth J. Haller. Crystallization of Lead Phosphate in Gel Systems, Engineering Journal (accepted for publication).

2. Sunaree Choknud, Oratai Saisa-ard, and Kenneth J. Haller. Preparation and Characterization of Carboxylic Acid Adducts of Gabapentin, Engineering Journal (accepted for publication).

3. Oratai Saisa-ard and Kenneth J. Haller. Crystallization of Lead Hydroxyapatite from Calcium Hydroxyapatite Dissolution, Journal of the Microscopy Society of Thailand (manuscript submitted for publication).